Development of a Modular Antibody-Degrader Conjugate Platform for Targeted Delivery of a Pan-LMO Degrader



Qingqing Ye

Supervisor: Prof. Angela Russell

Department of Chemistry

Wolfson College

Thesis

October 2026

This report entitled ‘Development of a Modular Antibody-Degrader Conjugate Platform for Targeted Delivery of a Pan-LMO Degrader’ submitted on Monday 5th October 2026 by Qingqing Ye contains material of a confidential nature, specifically the disclosure of a novel structure of LMO2 degrader. This report should therefore be withheld from consultation and prevented from being reproduced until appropriate IP protection has been filed.

Declaration of authorship

Qingqing Ye

I acknowledge the use of generative AI tools specified below for the following task:

- Language and grammar improvement

  I used ChatGPT5 Edu to refine written text. This included improving clarity, grammar, and structure of sections of the thesis.

Acknowledgement

First and foremost, I would like to express my sincere gratitude to Professor Angela Russell for her invaluable guidance, encouragement, and support throughout this project. Her expertise, insightful discussions, and continual encouragement have been instrumental in shaping this work and enabling me to explore the project in depth. I am truly grateful for her mentorship and the opportunities she has provided during my time in her research group.

I would also like to thank Dr Jacob Hiles for his continuous support both inside and outside the laboratory. His technical expertise, patience, and willingness to discuss ideas have been invaluable in helping me overcome the many challenges encountered throughout this project.

I am deeply grateful to all members of the AJR Group for creating such a supportive and collaborative research environment. Their encouragement, helpful discussions, and willingness to share their knowledge have made my time in the laboratory both enjoyable and rewarding.

I would like to thank the Mass Spectrometry Service for their continued support with analytical characterization. In particular, I am especially grateful to Dr Victor Mikhailov for his advice and expertise in the characterization of the antibody-drug conjugates, which were invaluable to this work.

Finally, I would like to thank Vanessa and Damjan from the Tate Group at Imperial College London for generously sharing their expertise in antibody-drug conjugation and for taking the time to answer my many questions throughout the project.

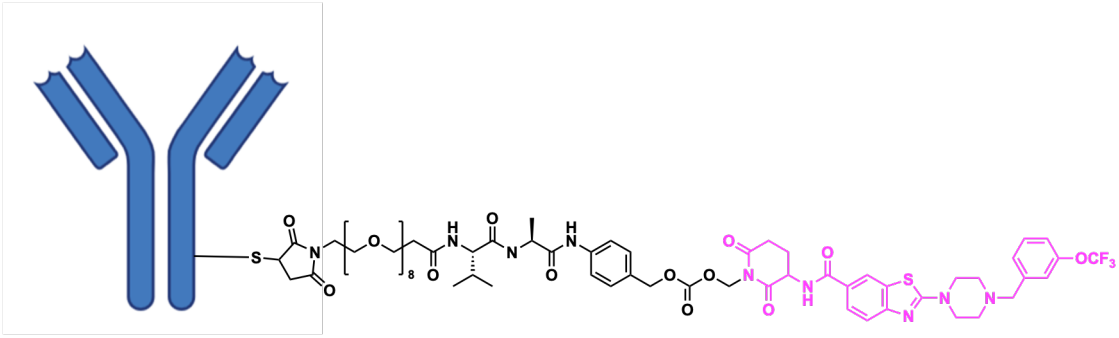
Abstract

The LIM-domain-only (LMO) family of proteins play crucial roles in transcriptional regulation and cell differentiation through mediating protein-protein interactions. Dysregulation of LMO proteins has been implicated in multiple human malignancies, including LMO2 in T-cell acute lymphoblastic leukaemia (T-ALL), LMO3 in neuroblastoma, and LMO4 in breast cancer. Despite their therapeutic significance, LMO proteins have long been considered challenging drug targets due to their intrinsically disordered structures.

Previous work in the Russell group led to the discovery of a series of targeted protein degraders targeting LMO2 and resulted in the development of a highly potent small molecule degrader capable of targeting all LMO family members. This provides an opportunity to extend targeted protein degradation beyond T-ALL and investigate the therapeutic potential of degrading LMO4 in breast cancer.

This project aimed to establish a modular antibody-drug conjugate (ADC) platform for the targeted delivery of a pan-LMO degrader to tumour cells. By varying the targeting antibody, this platform has the potential to deliver the same degrader selectively to different cancer types expressing distinct cell-surface antigens. As a proof of concept, trastuzumab was selected to target HER2-overexpressing breast cancer cells and enable the intracellular delivery of the pan-LMO degrader to degrade LMO4.

In this study, four pre-conjugated payloads were successfully designed and synthesised. One payload was subsequently conjugated to trastuzumab to generate a proof-of-concept ADC with an average drug-to-antibody ratio (DAR) of approximately 1. The ADC will be tested in HER2-positive BT474 and SKBR3 breast cancer cell lines. More broadly, this work establishes a versatile ADC platform in which the targeting specificity can be readily altered by exchanging the antibody component, enabling selective delivery of the pan-LMO degrader to different tumour types while retaining the same degradation mechanism.



Abbreviation

Abbreviation	Definition
°C	Degree Celsius
Abd	Antibody derived
Ala	Alanine
Alloc	allyloxycarbonyl
ca.	*Circa* (approximately)
Cit	Citrulline
DIPEA	*N, N*-Diisopropylethylamine
DMAP	4-Dimethylaminopyridine
DMF	Dimethylformamide
DMSO	Dimethyl sulfoxide
equiv.	Equivalents
Fmoc	fluorenylmethoxycarbonyl
g	Grams
h	Hour
HC	Heavy chain
IR	Infrared
LC	Light chain
LC-MS	Liquid chromatography-mass spectrometry
m/z	Mass-to-charge ratio
MG	Molecular glue
min	Minute(s)
mL	Millilitre(s)
mmol	Millimole(s)
MS	mass spectrometry
NMR	Nuclear magnetic resonance

PAB	Para-aminobenzyl
POI	Protein of interest
PPI	Protein-Protein interaction
PROTAC	Proteolysis Targeting Chimera
r.t.	Room temperature
TBME	Methyl *tert*-butyl ether
TCEP	Tris(2-carboxyethyl)phosphine
THF	Tetrahydrofuran
Val	Valine
µM	Micromolar

Table of Contents

Declaration of authorship 3

Abstract 5

Abbreviation 7

Table of Contents 9

Introduction 10

Target protein degradation 12

Target protein - LIM-domain-only proteins 15

LMO2 16

LMO4 17

Antibody-drug-conjugates 19

Previous work 25

Aims and Objectives 28

Result and Discussion 30

Payload synthesis 30

Disulfide-based linker 31

Cathepsin B linker - Val-Cit/Val-Ala 34

Phosphate modified Cathepsin B linker 40

GSH assay 48

Bioconjugation 52

Conclusion 64

Future work 65

Bioconjugation optimisation 65

Phosphate chemistry optimisation 66

Carbonate linkage optimisation 67

Cell testing with breast cancer cells 68

Bioconjugation with anti-CD7 antibody and testing *in vitro* 69

References 71

Experimental 76

Synthesis of Intermediates 77

Biological testing 102

Introduction

Cancer has become one of the most challenging issues in global public health in the 21st century. In 2019, the World Health Organization (WHO), ranked cancer as the first or second leading cause of death before the age of 70 years in 112 of 183 countries.[1] Efforts to improve patient survival through the development of effective anticancer therapies date back approximately 170 years. Since then, substantial advances in cancer research and drug development have transformed treatment approaches, shifting from traditional small molecule cytotoxic chemotherapies, such as *cis*-platin, towards increasingly precise and individualised strategies tailored to the characteristics of both the patient and their disease.[2]

The development of small-molecule therapeutics has remained a cornerstone of cancer treatment. Early advances focused on compounds that broadly inhibited tumour growth, whereas more recent efforts have targeted specific oncogenic signalling pathways. A major milestone was the FDA approval of imatinib in 2001, the first kinase inhibitor, which revolutionised the treatment of chronic myeloid leukaemia and gastrointestinal stromal tumours.[3] More recently, sotorasib became the first small-molecule inhibitor to directly target the previously "undruggable" KRAS G12C mutation in non-small cell lung cancer (NSCLC), demonstrating that challenging oncogenic targets can be therapeutically addressed.[4, 5] The emergence of targeted protein degradation has further expanded the capabilities of small-molecule therapeutics. In 2026, the FDA approved Veppanu**,** the first Proteolysis Targeting Chimera (PROTAC)-based therapy, for the treatment of oestrogen receptor-positive (ER+), HER2-negative, ESR1-mutated advanced or metastatic breast cancer, establishing targeted protein degradation as a clinically viable alternative to conventional protein inhibition.[6]

Alongside advances in small molecules, biomolecule-based therapeutics have transformed cancer treatment by exploiting the high specificity of proteins. In 1997, the FDA approved rituximab, the first targeted monoclonal antibody therapy for B-cell lymphomas.[7] This was followed by trastuzumab, which established HER2 as a clinically actionable target in HER2-positive breast cancer.[8] Additional antibody-based therapies, including bevacizumab, the first anti-angiogenic monoclonal antibody targeting vascular endothelial growth factor A (VEGFA), further broadened the therapeutic applications of antibody-based medicines.[9]

The convergence of these therapeutic modalities has led to the development of antibody-drug conjugates (ADCs), which combine the tumour specificity of monoclonal antibodies with the potency of highly active small-molecule payloads. A major milestone was the FDA approval of gemtuzumab ozogamicin in 2000, the first ADC, in which a CD33-targeting monoclonal antibody was conjugated to the cytotoxic antibiotic calicheamicin for the treatment of acute myeloid leukaemia (AML).[10] Since then, ADCs have emerged as one of the fastest-growing classes of targeted cancer therapeutics by integrating the advantages of antibody-mediated tumour targeting with increasingly diverse payload technologies.

Collectively, these advances illustrate a fundamental shift in cancer drug discovery from broadly acting cytotoxic agents towards increasingly selective, mechanism-based therapeutic modalities. Despite these achievements, achieving sufficient tumour selectivity while maintaining therapeutic efficacy and overcoming drug resistance remains a major challenge, driving continued innovation in targeted drug delivery strategies such as antibody-drug conjugates. The following sections explore these emerging modalities in greater detail, focusing on targeted protein degradation as a means

of addressing traditionally 'undruggable' targets, specifically the LIM-domain-only (LMO) protein family, and on ADCs as a strategy for their selective delivery to tumour cells.

Target protein degradation

Target protein degradation (TPD) has attracted significant interest as a therapeutic strategy to modulate proteins that have proved difficult to target with traditional small molecules which inhibits the protein function.[11, 12] In addition, this approach could potentially minimize the off-target effects and overcome drug resistance.[13, 14] Unlike conventional small molecules that directly inhibit protein activity, TPD leverages the cell's endogenous proteolytic systems including the ubiquitin-proteasome systems (UPS) and lysosomal pathways to selectively destroy disease-causing proteins.[11, 15] Within the UPS, protein ubiquitination is mediated by an E1-E2-E3 enzymatic cascade. Ubiquitin is first activated by the E1 ubiquitin-activating enzyme with ATP and subsequently transferred to an E2 ubiquitin-conjugating enzyme. The E3 ubiquitin ligase then recognises the protein of interest (POI) and facilitates the transfer of ubiquitin from the E2 enzyme to lysine residues on the POI. This system plays an important role in regulating essential cellular processes, including cell-cycle progression, signal transduction, and gene expression.[16] UPS-based TPD approaches exploit these E3 ligases to specifically direct target proteins for recognition and degradation by proteasome.[17] Many TPD strategies have been emerged including PROteolysis TArgeting Chimeras (PROTACs)[18] and Molecular Glues (MGs)[19] (**Figure 1**), providing a clearer understanding of the mechanisms of these protein degraders.

Both PROTACs and MGs exploit UPS to induce degradation of POI. PROTACs are heterobifunctional molecules composed of three functional elements: POI-targeting

ligand, an E3 ligase ligand and a linker. PROTAC form a POI-PROTAC-E3 ternary complex by binding simultaneously with both POI and E3 ligase, activates and directs the ubiquitination of the target protein. This enables the subsequent recognition and degradation by the 26S protease.[20] To date, the most popular E3 ligase ligands are those recruiting von Hippel-Lindau (VHL) and cereblon (CRBN) proteins, which serve as substrate recognition subunits within the Cullin-RING E3 ubiquitin ligase complexes.[21] Following target degradation, PROTACs are released and can be recycled to induce the degradation of additional target proteins, making them highly efficient catalytic degraders.[22] However, their activity is limited by the Hook effect, where excessive PROTAC concentrations reduce degradation efficiency by saturating binding sites of either POI or the E3 ligase, disrupting functional ternary complex formation.[23] Although PROTACs generally violate Lipinski's Rule of Five[24], many PROTACs exhibit sufficient oral bioavailability for further development. However, their relatively large molecular weight (often 800-1000 Da) and large topological polar surface area (tPSA; 96 to 238 $Å^2$) of PROTACs can result in poor cell permeability, limiting intracellular uptake and posing a major challenge for drug development. [11, 25, 26]

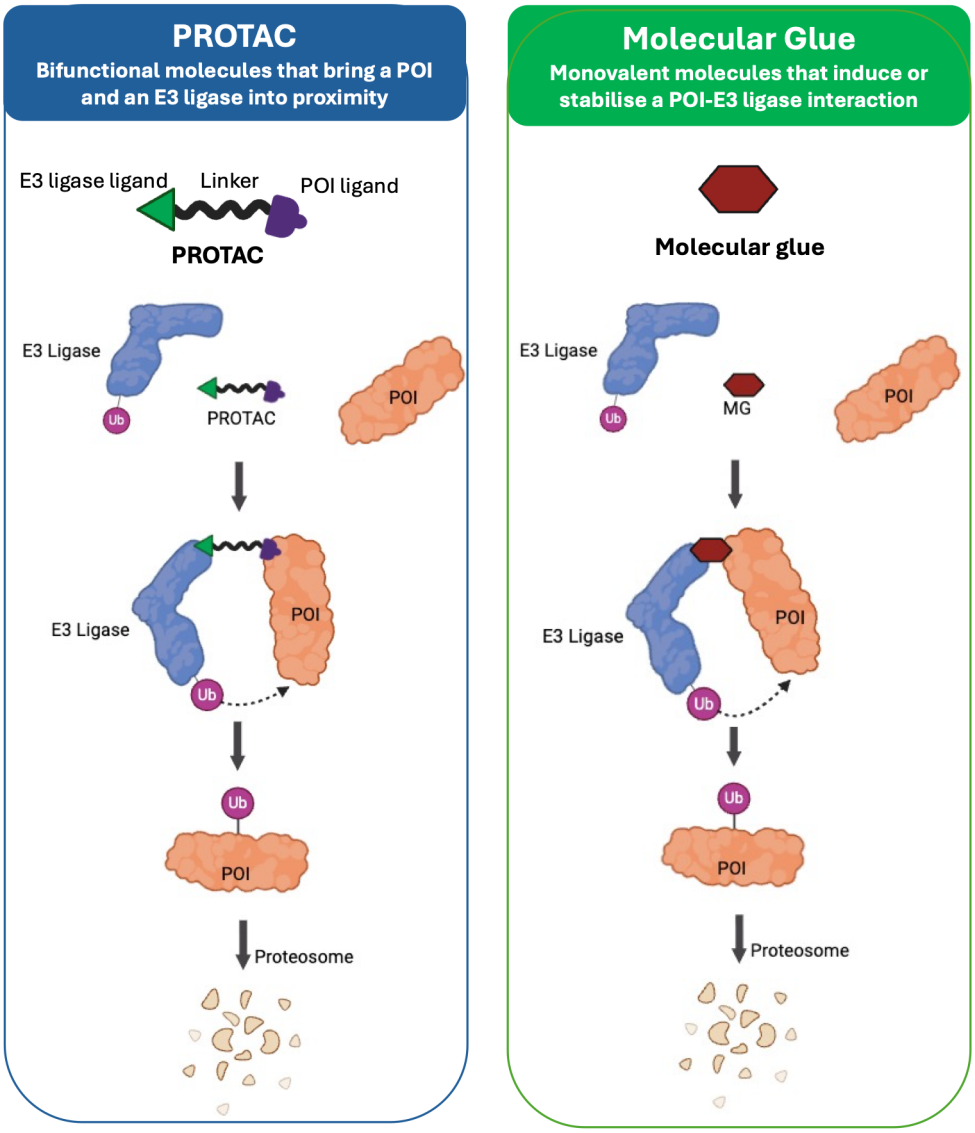


Figure 1. Schematic representation of the mode of action for PROTACs and MGs.

On the other hand, molecular glues (MGs) are monovalent small molecules that bind to an E3 ubiquitin ligase and indirectly induce or stabilise protein-protein interactions (PPIs) with a target protein, thereby promoting its ubiquitination and subsequent proteasomal degradation.[15] Unlike PROTACs, MGs do not require a chemical linker, resulting in smaller molecular weight (< 500 Da) with favourable properties, including improved oral bioavailability, membrane permeability, metabolic stability, and pharmacokinetic profiles.[11] Furthermore, because MGs stabilise naturally occurring or inducible PPIs

rather than relying on the formation of a heterobifunctional ternary complex, they are generally not susceptible to the Hook effect.[27] However, despite these advantages, the discovery of molecular glues remains challenging, as the rationale design and identification of suitable E3 ligase-POI interactions that can be stabilised by a small molecule is more difficult than designing bifunctional PROTACs.

Together, PROTACs and molecular glues represent two complementary approaches to targeted protein degradation, each offering distinct advantages and limitations. While PROTACs provide a modular platform capable of degrading a wide range of target proteins, molecular glues possess superior drug-like properties and exploit endogenous PPI to achieve selective degradation. These technologies have significantly expanded the therapeutic landscape of TPD and offer promising strategies for addressing disease-associated proteins that remain 'undruggable' to traditional small-molecule inhibitors.

Target protein - LIM-domain-only proteins

LIM-domain proteins are a large family of zinc finger proteins that play important roles in in the development and progression of a wide range of human cancers. Unlike most zinc fingers, which directly bind DNA, LIM-domain proteins only mediate protein-protein interactions, serving as scaffolds for the assembly of multiprotein complexes.[28] Based on the presence of additional functional domains, the LIM-domain protein family is further subdivided into several subfamilies. Among these, the LIM-domain-only (LMO1-4) proteins are characterised by the presence of two tandemly arranged LIM domains.[29] They regulate gene transcription by facilitating the assembly of multiprotein transcriptional complexes thereby controlling cellular processes, including cell differentiation, proliferation.[30]

All four LMO proteins have been identified as contributors to the development of cancer. LMO1 and LMO2 have been identified as a contributor to T-ALL.[31, 32] LMO3 is an oncogene associated with neuroblastoma[33] while LMO4 is reported to be an auto-antigen which facilitates the transformation of breast cancer cells in the body.[34, 35]

LMO2

LMO2 (LIM domain only 2) is a cysteine-rich protein, containing two zinc-binding LIM domains[36]. It is a transcription factor that acts as a bridge that interacts with different proteins, forming bipartite DNA-binding multi-protein complexes[37] (**Figure 2**). Owing to its intrinsically flexible structure, LMO2 adopts multiple conformations that enable it to act as a bridging transcription factor. By interacting with proteins including TAL1, E47, GATA-1, and the LIM-domain-binding protein LDB1, LMO2 assembles multiprotein transcriptional complexes that stabilise the protein and protect it from proteasomal degradation.[38] (**Figure 2a**). This DNA-binding transcription regulator complex is found to play a key role in haematopoiesis and angiogenesis.[39-41] With the replacement of GATA-1 by TAL-1 and E47 (**Figure 2b**), forming a homodimeric complex, leading to different target genes being activated which are associated with the development of T-cell acute lymphoblastic leukaemia (T-ALL).[42, 43] The expression of LMO2 is down regulated after the initial development of T-cells.[44, 45] However, LMO2 is found to be activated as a result of chromosomal translocation in T-cell acute lymphoblastic leukaemia (T-ALL)[32] and is overexpressed in more than 50% of T-ALL cases[46]. Despite its strong oncogenic potential, LMO2 remains a “undruggable” target due to the absence of classical binding pockets and its intrinsically disordered nature.

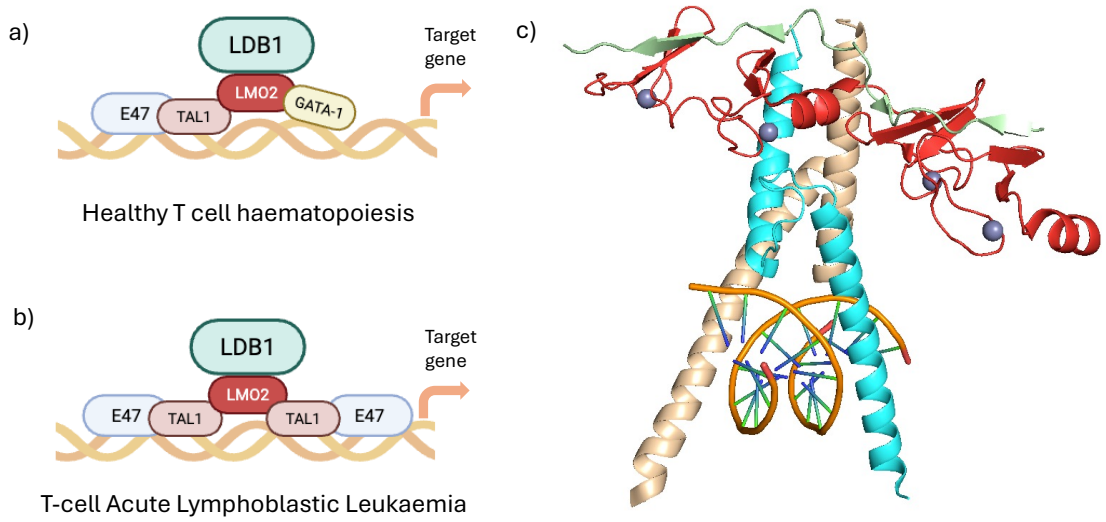


Figure 2. a) Schematic representation of the DNA-binding multi-protein complexes in healthy T cells and abnormal T-cells; b) Schematic representation of the DNA-binding multi-protein complexes in abnormal T-cells; c) crystal structure of the DNA-binding complexes in T-ALL, DNA in orange, LDB in green, LMO2 in red, TAL1 in beige and E47 in blue. (Image generated by Pymol, PDB: 2YPA[40])

LMO4

LMO4 is considered to be the most distant member of the LMO family, sharing only approximately 50% amino acid sequence identity with the rest of the family members (LMO1-3).[29] LMO4 is overexpressed in more than 50% of primary breast tumours, where elevated expression is associated with reduced differentiation of mammary epithelial cells, supporting its contribution in breast cancer. [34] Studies have demonstrated that LMO4 promotes mammary tumour development by regulating transcriptional programmes controlling cell proliferation, differentiation, cell-cycle progression, and apoptosis.[35] Mechanistically, LMO4 acts as a transcriptional adaptor, assembling multiprotein complexes that regulate signalling pathways including HER2/ErbB2[47], p53[48], and TGF-β[49].

Among these, the HER2/ErbB2 pathway is one of the best-characterised mechanisms linking LMO4 to breast cancer progression. HER2 is amplified or overexpressed in approximately 15–20%[50] of breast cancers and is associated with aggressive disease and poor clinical outcome. LMO4 has been identified as a key downstream effector of the HER2/ErbB2 signalling pathway (**Figure 3**). Activation of the HER2-PI3K-AKT signalling axis induces LMO4 expression, which in turn promotes the transcription of genes involved in cell-cycle progression, including the G1 cyclin Cyclin D1 and the G2/M-associated E3 ubiquitin ligase component Cullin-3.[47] Through regulation of these cell-cycle regulators, LMO4 promotes tumour cell proliferation and contributes to the aggressive phenotype of HER2-positive breast cancer. More recently, LMO4 has also been involved in the development of resistance to trastuzumab[51], the first-line HER2-targeted monoclonal antibody treatment for breast cancer. LMO4 has been shown to promote trastuzumab resistance by enhancing the stem cell-like properties of breast cancer cells, highlighting LMO4 as a promising therapeutic target for overcoming resistance in HER2-positive breast cancer.

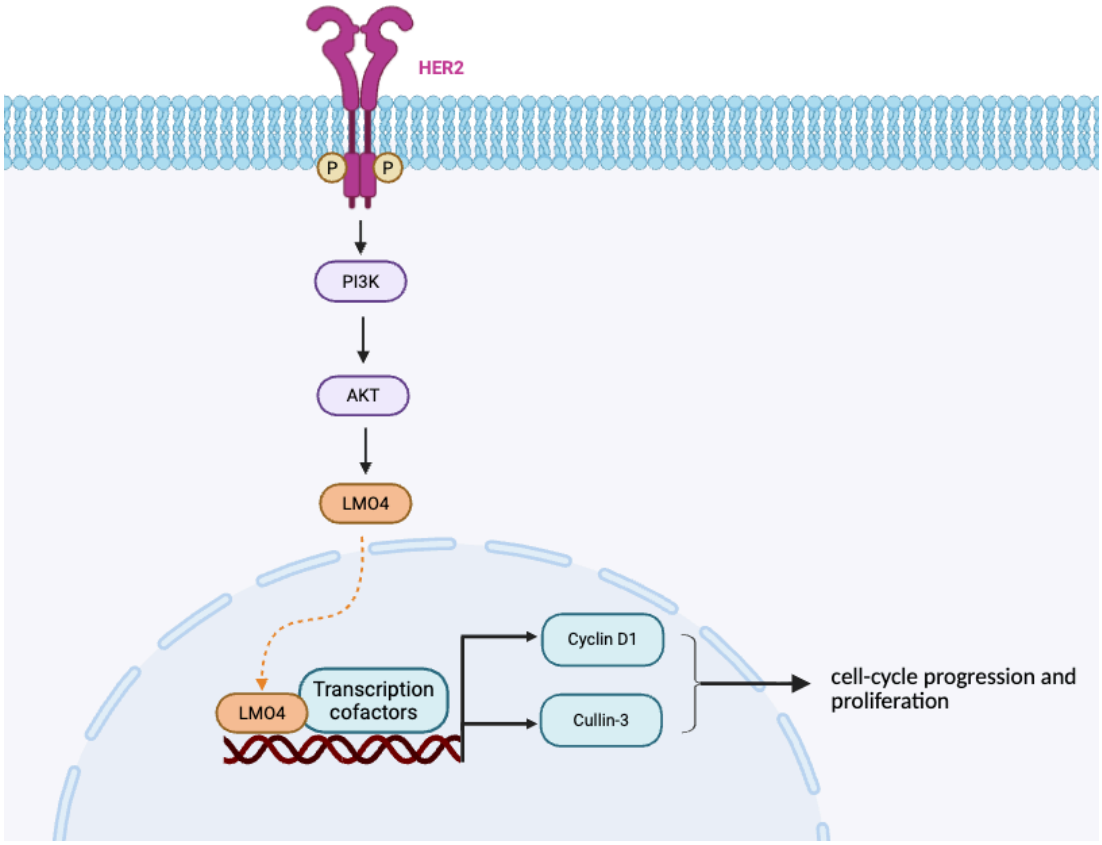


Figure 3. Role of LMO4 in HER2 signalling. LMO4 is overexpressed in a subset of breast cancers, particularly those exhibiting HER2 overexpression. LMO4 functions as a key downstream effector of the HER2 signalling pathway.

Antibody-drug-conjugates

Despite the clinical success of traditional chemotherapeutic agents, such as alkylating agents, their lack of tumour selectivity remains a major limitation.[52] Cytotoxic drugs indiscriminately affect both cancerous cells and healthy cells, resulting in dose-limiting toxicity and a narrow therapeutic window.[53] The need for strategies capable of selectively delivering highly potent therapeutics to tumour cells while minimising off-target toxicity led to the development of Antibody-Drug-Conjugates (ADCs).

ADCs were inspired by Paul Ehrlich's theory of the 'magic bullet', which envisioned a therapeutic agent capable of selectively targeting pathogens without damaging normal

human cells.[54] An ADC is typically composed of three key components: 1) a potent cytotoxic payload that becomes active upon release inside the cell; 2) a monoclonal antibody (mAb) that specifically recognizes and binds to tumour-associated antigens and 3) a chemical linker that is cleaved under intracellular conditions to release the active drug (**Figure 4a**). By recognising tumour-associated surface antigens, ADCs selectively deliver their payloads to target cells while minimising exposure to healthy tissues. Human immunoglobulin G1 (IgG1) antibodies are the predominant backbone for ADC designs because they possess favourable pharmacokinetic and biological properties, including a prolonged circulating half-life, high tumour specificity, efficient receptor-mediated internalisation, and low immunogenicity.[55, 56] In line with Ehrlich's vision, ADCs selectively recognise and bind to tumour-associated antigens on the surface of cancer cells. Following antigen binding, the ADC-antigen complex undergoes receptor-mediated endocytosis and is trafficked through the endosomal pathway to the lysosome. In the lysosomal environment, the cytotoxic payload is released through enzymatic or chemical cleavage. Once released, the payload exerts its cytotoxic activity by targeting specific intracellular mechanisms, inducing apoptosis.[57] (**Figure 4b**)

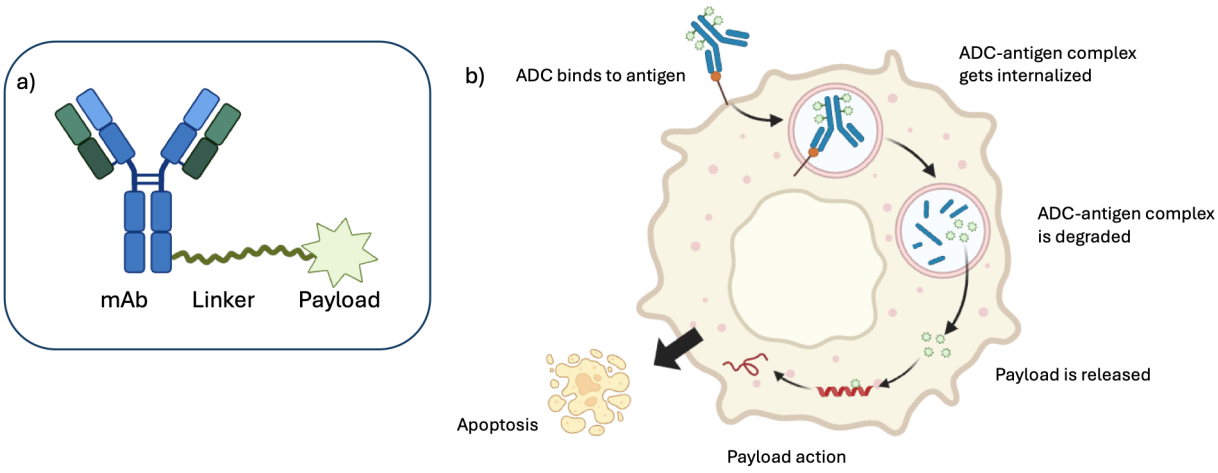


Figure 4. a) General structure of an antibody-drug conjugate. b) ADC mechanism of action.

The payloads used in ADCs are typically 1,000- to over 1,000,000-fold more potent than conventional chemotherapeutic agents, exhibiting sub-nanomolar or even picomolar *in vitro* cytotoxicity.[58, 59] One of the most important parameters of ADC is drug antibody ratio (DAR), which describes the average number of payload molecules conjugated to each antibody. A low DAR may reduce therapeutic efficacy whereas a high DAR can compromise antibody stability and antigen-binding affinity and ultimately reduce the overall activity of the ADC.[60] As highly potent small molecule drugs, many payloads possess moderate to high level of lipophilicity as a consequence of their chemical design. The lipophilicity enhances hydrophobic interactions with biological targets, contributing to high binding affinity[61] while also facilitate passive diffusion across the phospholipid bilayer, increasing membrane permeability[62]. In the context of ADCs, this lipophilicity is particularly advantageous because, following intracellular release, the payload can diffuse out of the targeted cell and into neighbouring tumour cells, producing a bystander effect that enables the elimination of antigen-negative or poorly targeted cancer cells within a heterogeneous tumour.[63] However, this same property may also result in the diffusion of the cytotoxic payload into surrounding healthy tissues, increasing the risk of off-target toxicity.[64] The bystander effect is determined not only by the lipophilicity of the payload but also by the biochemical properties of the linker, which regulate payload release within the tumour microenvironment.[65]

The linkage between the cytotoxic payload and the monoclonal antibody is a critical component of ADC design. Linkers are carefully engineered to maintain stability during systemic circulation while enabling the efficient release of the cytotoxic payload once the ADC reaches the target tumour cells.[66, 67] According to their mechanism of payload release, linkers are generally classified as either cleavable or non-cleavable. Non-

cleavable linkers are less commonly employed in ADCs and are typically selected when enhanced plasma stability and a more controlled mechanism of payload release are desired.[68] In contrast, cleavable linkers (**Figure 5**) are designed to release payload through specific intracellular conditions such as acidic pH[69], enzymatic activity[70] or reducing conditions[71]. By exploiting the unique biochemical environment of tumour cells, these linkers facilitate selective intracellular payload release while minimising premature drug release in systemic circulation, thereby maximising therapeutic efficacy and reducing off-target toxicity. Among the various cleavable linkers, cathepsin-cleavable dipeptides, such as valine–citrulline (Val–Cit) and valine–alanine (Val–Ala), are the most widely used owing to their favourable balance between plasma stability and efficient lysosomal cleavage[72]. More recently, advances in linker chemistry have led to the development of enzyme-responsive linkers with improved stability and tumour specificity, including cathepsin-cleavable GGFG tetrapeptide linkers[73] and tripeptide linkers[74] as well as linkers cleavable by β-glucuronidase[75], sulfatase[76], phosphatase[77], and legumain[78].

The payload is covalently attached to the antibody through bioconjugation. The choice of conjugation chemistry is a critical determinant of the drug-to-antibody ratio (DAR), which significantly influences the pharmacokinetic properties, stability, and therapeutic efficacy of the resulting ADC.[67]

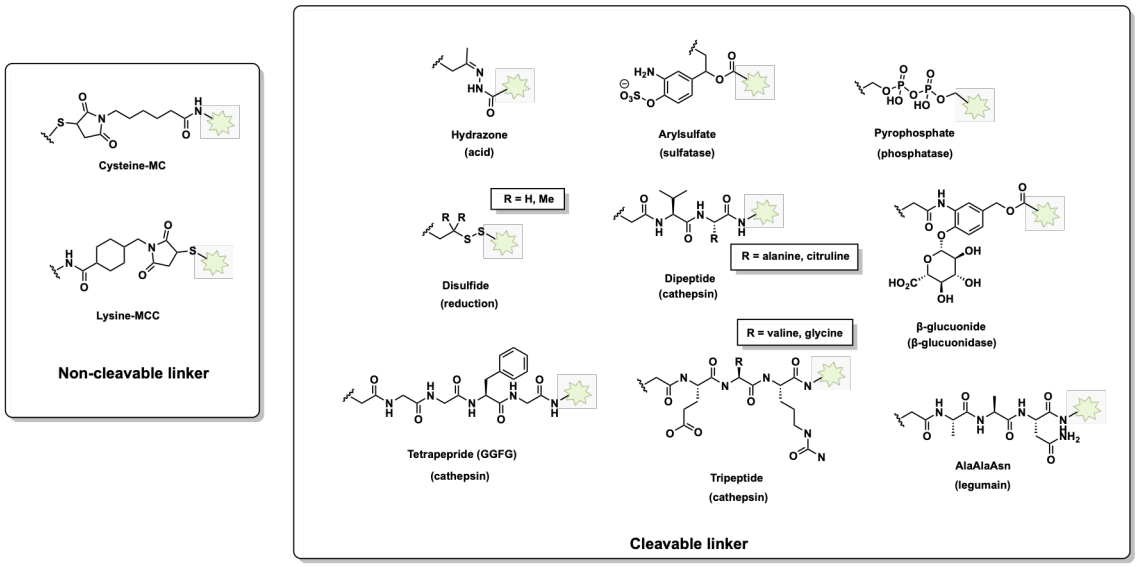


Figure 5. *Common non-cleavable and cleavable linkers used for ADC design with their cleavage method.*[56]

Most chemical conjugation strategies exploit the naturally occurring amino acid residues on antibodies, primarily lysine and cysteine, as sites for payload attachment. Lysine-based conjugation (**Figure 6a**) takes advantage of the abundance and surface accessibility of lysine residues. The chemical handle, typically an activated ester, reacts with the amino groups of surface-exposed lysine residues to form a stable amide bond.[60] However, abundant surface lysine residues results in random conjugation at multiple sites, generating a heterogeneous mixture of ADC species with variable drug-to-antibody ratios (DARs).[79] This heterogeneity can adversely affect the stability, safety, and therapeutic efficacy of the ADC.[80] On the other hand, cysteine-based conjugation (**Figure 6b**) is achieved by selectively reducing the four interchain disulfide bonds of the antibody to generate free thiol groups. These thiols subsequently react with maleimide handles to form stable thioether bonds.[81] Owing to the limited number of available conjugation sites, this strategy produces ADCs with a more controlled drug-to-antibody ratio (DAR) and lower heterogeneity than lysine-based conjugation. Consequently, cysteine-based

conjugation has become one of the most widely adopted conjugation strategies and is employed in several FDA-approved ADCs.[72]

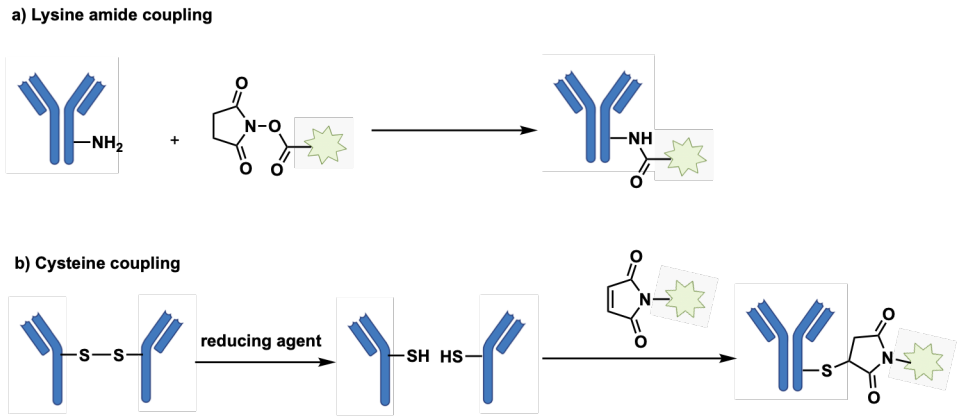


Figure 6. Two common bioconjugation methods used in ADC.

Since the introduction of the first ADC, 13 new ADCs have received FDA approval in the past 20 years.[82] Although ADCs have substantially improved the selectivity of cytotoxic drug delivery, the vast majority of clinically approved ADCs continue to employ conventional cytotoxic payloads, including the microtubule inhibitors MMAE, MMAF, DM1, and DM4, and DNA-damaging agents such as SN-38 and DXd.[83] While antibody-mediated targeting limits systemic exposure, these payloads ultimately eliminate tumour cells by disrupting fundamental cellular processes, such as mitosis or DNA replication, rather than directly modulating the molecular drivers responsible for tumour initiation and progression. Consequently, there is growing interest in expanding the range of ADC payloads beyond conventional toxins towards mechanism-based therapeutics. One promising strategy is the incorporation of targeted protein degraders as ADC payloads. PROTAC molecules have been successfully incorporated into ADCs by conjugating the antibody through the primary hydroxyl group of the VHL ligand[84, 85]. This approach temporarily masks the recruitment of VHL E3 ubiquitin ligase during systemic circulation. Following intracellular linker cleavage, the active PROTAC is

released, restoring VHL binding and enabling selective degradation of disease-causing proteins. By combining the tumour specificity of ADCs with the catalytic mechanism of targeted protein degradation, degrader-based ADCs represent a promising next-generation therapeutic strategy with the potential to improve efficacy while reducing the systemic toxicity associated with conventional cytotoxic payloads.

Previous work

Owing to the intrinsically disordered nature of LMO2 and its lack of well-defined ligand-binding pockets, the identification of high-affinity small-molecule ligands has proven particularly challenging. Previous work in the Russell group addressed this challenge by developing a cell-based screening platform using a BRET2 biosensor and a dematured (reduced-affinity) intracellular LMO2-binding antibody (iDAb) to identify small molecules capable of binding LMO2.[86] The Abd-L series of small molecules exhibit inhibition of the LMO2-iDAb interaction but limited disruption between LMO2 and its natural protein partners in LMO2-dependent tumour cells. These ligands subsequently served as the basis for the rational design of a series of bifunctional PROTAC degraders capable of inducing targeted LMO2 degradation.[87] Further optimisation led to the development of low molecular weight ('linkerless') degraders that retained potent degradation activity while exhibiting improved drug-like properties (**Figure 7a**). During optimisation of potency and selectivity across the LMO family, one degrader was identified as a highly potent pan-LMO degrader (**Figure 7b**). **JDH-06-040** was capable of targeting multiple LMO family members with similar degradation efficiency, as demonstrated using a Renilla luciferase (RLuc8) reporter assay (**Figure 7c**). In this assay, LMO1, LMO2, and LMO4 were expressed as RLuc8 fusion proteins, whereby degrader-induced loss of the LMO protein produced a corresponding reduction in luminescence,

providing a measure of degradation activity. This discovery provides the opportunity to extend targeted protein degradation beyond LMO2-driven T-cell acute lymphoblastic leukaemia (T-ALL) to other LMO-dependent cancers, including LMO4-positive breast cancer. However, systemic administration of a pan-LMO degrader would be expected to degrade LMO proteins in both tumour and healthy tissues, potentially limiting its therapeutic window. Therefore, a strategy capable of selectively delivering the degrader to tumour cells is required.

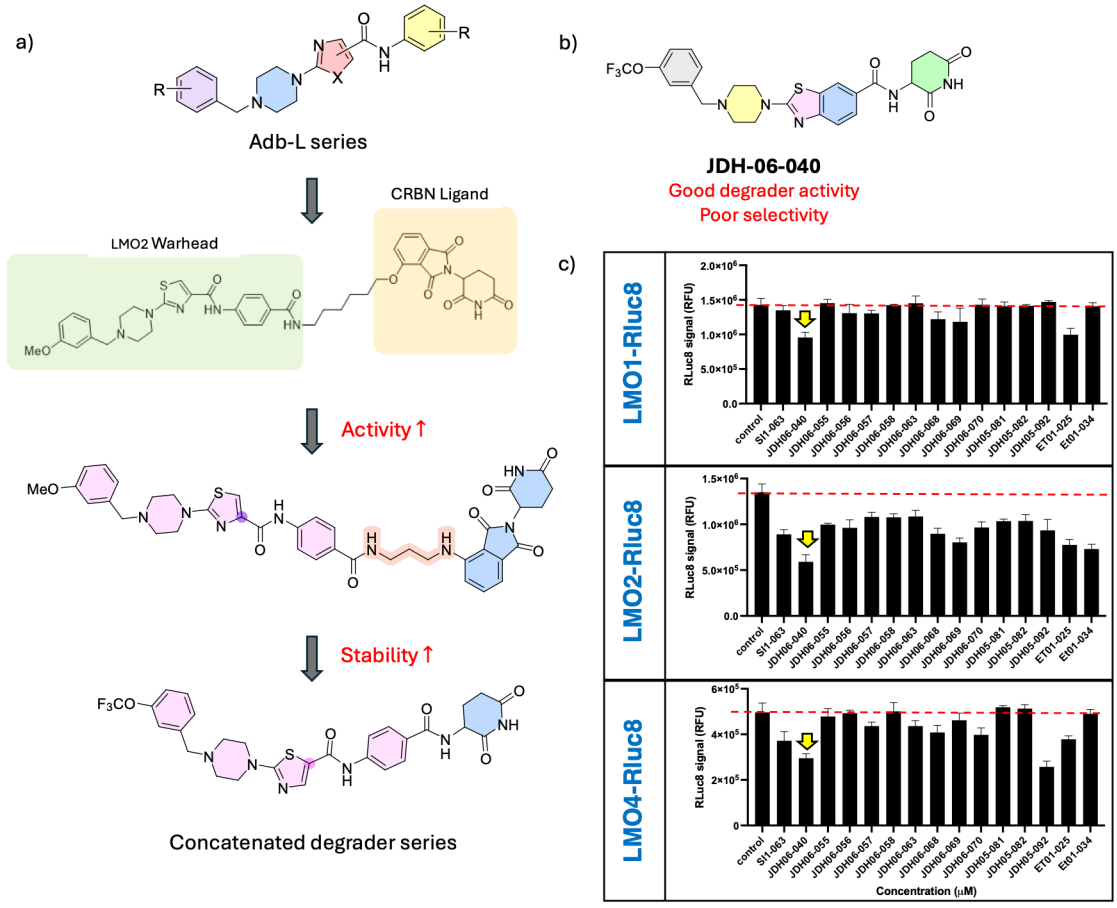


Figure 7. a) Structures and arrows showing the progression of the discovery of degraders leading to concatenated degrader series. b) the structure of the pan-LMO degrader. c) Luciferase assay at fixed concentration across the concatenated degrader series, showing good degradation activity of JDH-06-040 in LMO1, LMO2 and LMO4.

Antibody–drug conjugates (ADCs) provide an attractive solution by combining the tumour-targeting specificity of antibodies with the intracellular delivery of highly potent payloads. These studies establish the feasibility of developing a modular ADC platform for the targeted delivery of the pan-LMO degrader. By altering the antibody component, the same degrader can be selectively directed towards different tumour types expressing distinct surface antigens, enabling the therapeutic targeting of multiple LMO family members across different cancers.

Aims and Objectives

The aim of this project was to develop a proof-of-concept antibody-degrader conjugate platform for the targeted delivery of a pan-LMO degrader to tumour cells. As a proof of concept, trastuzumab was selected as the targeting antibody because it is a well-characterised anti-HER2 monoclonal antibody with established clinical efficacy in HER2-positive breast cancer and extensive use in FDA-approved antibody–drug conjugates. Furthermore, trastuzumab undergoes receptor-mediated internalisation following HER2 binding, making it an ideal vehicle for the selective intracellular delivery of therapeutic payloads.

Project objectives:

1. To design and synthesise a series of cleavable linker-payload conjugates incorporating the pan-LMO degrader and a cysteine-reactive maleimide handle.
2. To characterise the synthesised linker-payload pre-conjugates using appropriate analytical techniques to confirm their identity.
3. To conjugate the optimised linker-payload to trastuzumab via cysteine-selective bioconjugation to generate a proof-of-concept antibody-degrader conjugate.
4. To characterise the ADC, including determination of the drug-to-antibody ratio (DAR).
5. To examine the ability of targeted payload delivery and LMO4 degradation by testing the ADC in HER2-positive breast cancer cell lines BT474 and SKBR3.

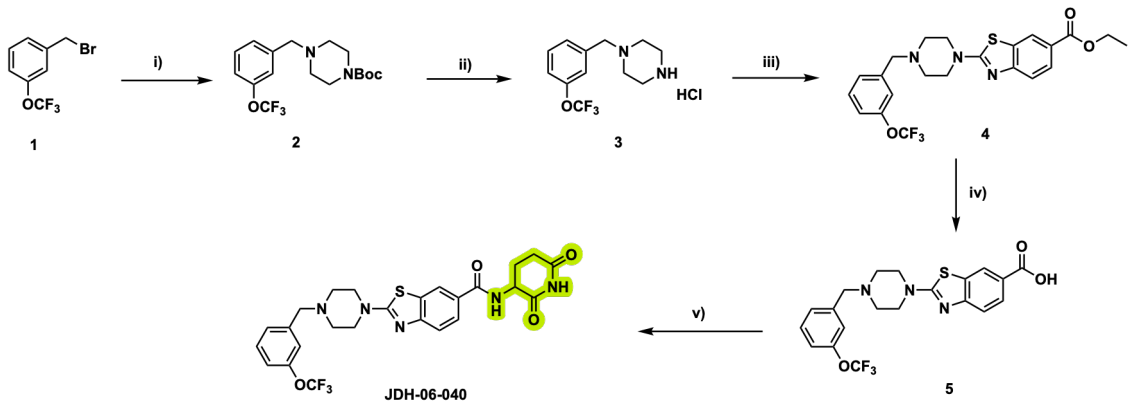
Beyond the development of a proof-of-concept HER2-targeted conjugate, this project seeks to establish a versatile antibody–degrader conjugate platform in which the targeting antibody can be readily exchanged to redirect the same pan-LMO degrader towards

different LMO-driven cancers. This strategy has the potential to extend the therapeutic application of targeted protein degradation while improving tumour selectivity and reducing systemic toxicity.

Result and Discussion

Payload synthesis

The pan-LMO degrader **JDH-06-040** was synthesized using an established protocol (**Scheme 1**). Commercially available **1** was reacted with *tert*-butyl piperazine-1-carboxylate in the presence of K_2CO_3 to afford **2**, followed by acid-mediated Boc deprotection to give **3**. Subsequent coupling of **3** with ethyl 2-chlorobenzo[d]thiazole-6-carboxylate under reflux in the presence of DIPEA afforded **4**. Hydrolysis of the ethyl ester **4** using lithium hydroxide hydrate generated the corresponding carboxylic acid **5**, which was subsequently coupled with 3-aminopiperidine-2,6-dione hydrochloride via HATU-mediated amide bond formation to afford the pan-LMO degrader **JDH-06-040**.



Scheme 1. i) *tert*-butyl piperazine-1-carboxylate, K_2CO_3, MeCN, RT, 19h, 78%; ii) 2.68M HCl in 1,4-dixoane, MeOH, RT, 18h, 99%; iii) ethyl 2-chlorobenzo[d]thiazole-6-carboxylate, DIPEA, 1,4-dioxane, 100 °C, 18h, 70%; iv) $LiOH{\cdot}H_2O$, THF/EtOH/H2O, RT, 20h, 99%; v) 3-aminopiperidine-2,6-dione hydrochloride, HATU, DIPEA, DMF, RT, 20h, 37%.

In this project, the conjugation site between the degrader and the linker was positioned on the glutarimide moiety (highlighted in green), which was critical for binding to the E3 ligase. To prevent premature activity, the degrader warhead was masked prior to cellular

internalisation, ensuring that it remained inactive until the ADC was taken up by target cells and the linker was cleaved. As the antibody used was an IgG1 monoclonal antibody, a cysteine-selective bioconjugation strategy was selected, taking advantage of the accessible interchain cysteine residues generated by controlled reduction of the antibody interchain disulfide bonds.

Disulfide-based linker

The initial synthetic strategy focused on the development of a simple linker design as proof-of-concept to bridge the pan-LMO degrader and the antibody through cysteine-selective bioconjugation. Reduction-cleavable disulfide bond has been used as bioactivatable linkers for connecting protein toxins, chemotherapeutic drugs and probes to biomolecules for around four decades.[88] Disulfide bonds generally display good stability in blood circulation and are rapidly cleaved by glutathione (GSH) intracellularly. However, the stability is influenced by steric hinderance around the bond. Unhindered disulfides undergo the most rapid reduction in the cytosol and have the lowest stability in circulation. Increasing the number and size of adjacent alkyl groups increases the stability of the disulfide bonds and leads to longer circulation half-life. Consequently, linker design requires balancing systemic stability with efficient intracellular payload release.[89] For this proof-of-concept study, an unhindered disulfide linker was selected to simplify the synthetic route.

The disulfide-containing antibody-drug conjugate was designed to undergo intracellular processing following receptor-mediated internalisation, releasing the payload through GSH-mediated reduction (**Figure 8**). Upon internalisation into the target cell, the intracellular reducing environment cleaved the disulfide bond, releasing a thiol-containing linker-drug intermediate. This intermediate subsequently underwent self-

immolation, followed by spontaneous fragmentation with the release of formaldehyde, releasing the active pan-LMO degrader.

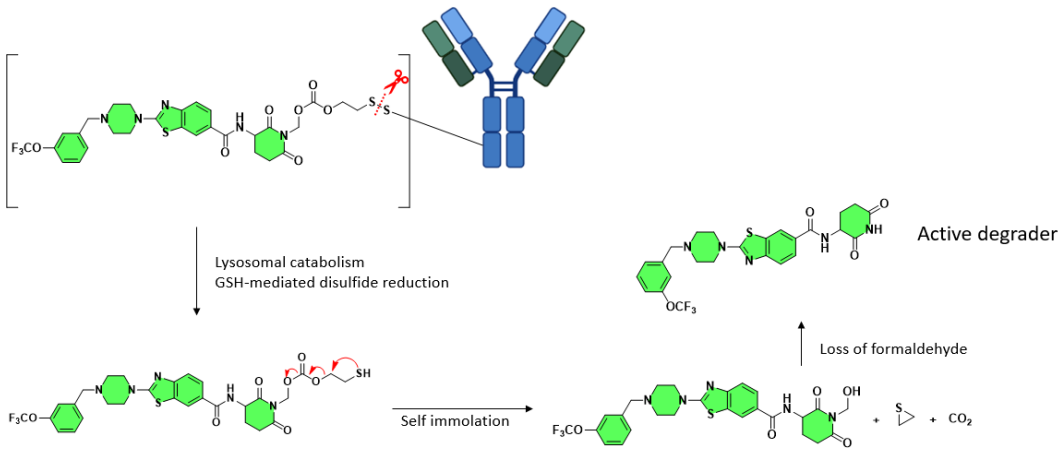


Figure 8. Proposed mechanism of cleavage for the disulfide linkage.

The overall design of the pre-conjugate **OX05156** incorporated three functional elements: the pan-LMO degrader, a carbonate linkage, and an activated pyridyl disulfide handle for cysteine-selective antibody conjugation. The linker was attached through the glutarimide region of the degrader, temporarily masking the degrader prior to intracellular release. A convergent strategy was adopted to simplify assembly of the relatively complex linker-degrader construct (**Figure 9)**, allowing the carbonate linkage and cysteine-reactive disulfide handle to be installed onto the glutarimide fragment first, followed by HATU-mediated amide coupling with carboxylic acid **5** to assemble the complete pre-conjugate **OX05156**.

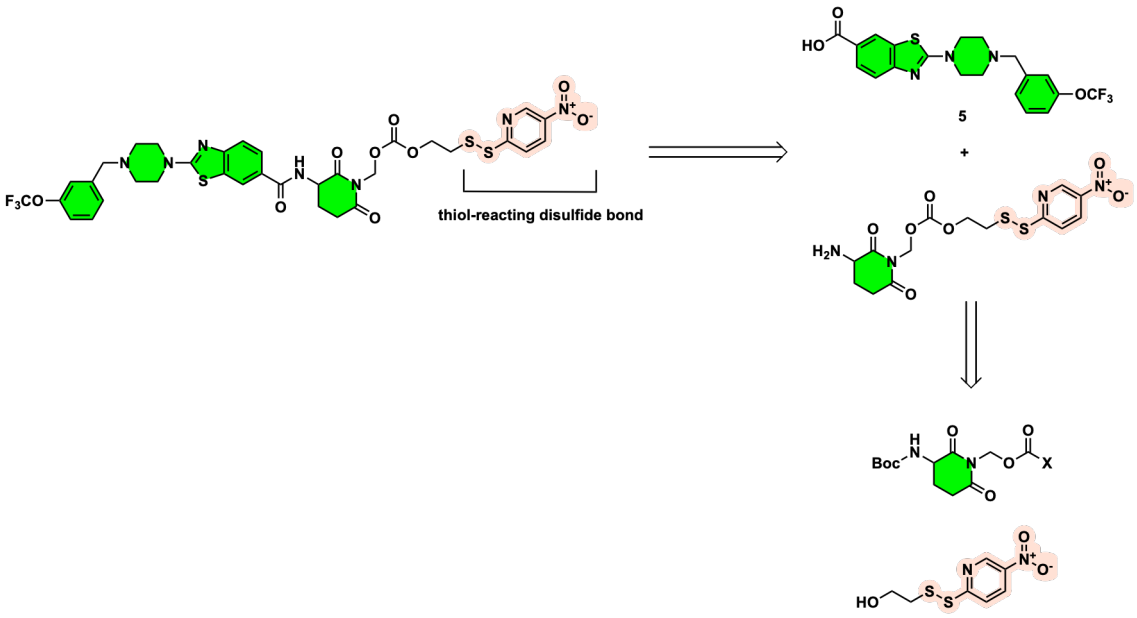
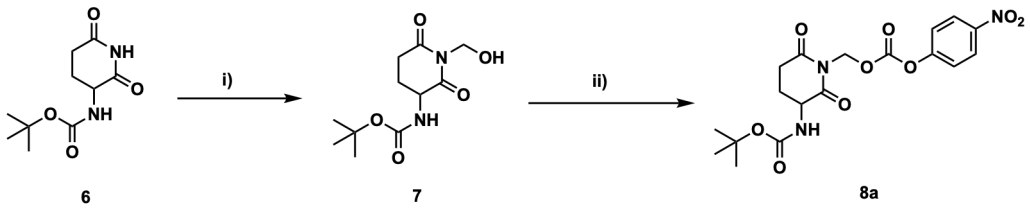


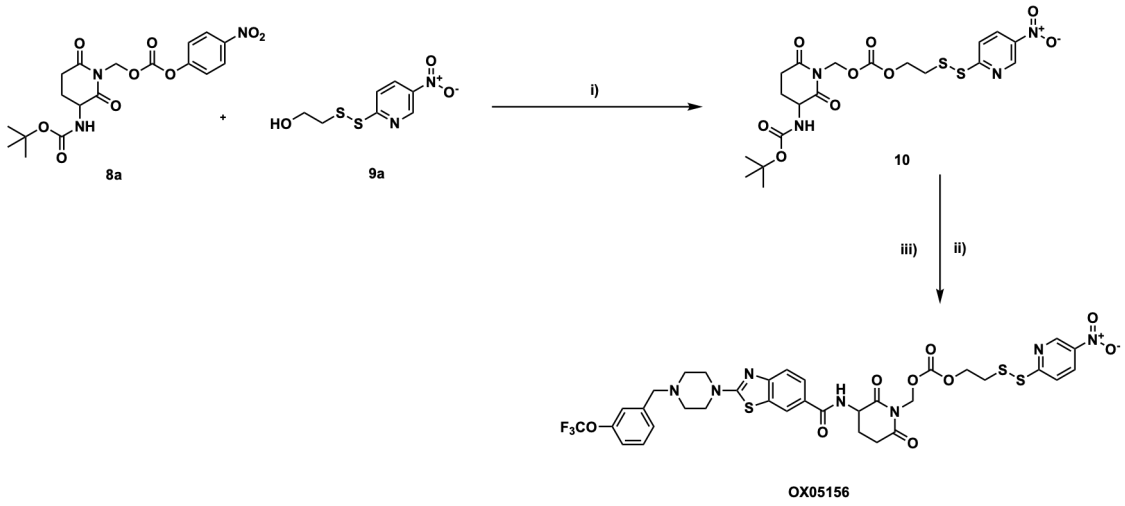
Figure 9. Retrosynthesis of disulfide-based linker containing pre-conjugate **OX05156**. The target molecule was disconnected at the amide bond to separate carboxylic acid **5** from the linker-functionalised glutarimide fragment. Further disconnection at the carbonate linkage separates the glutarimide moiety from the cysteine-reactive pyridyl disulfide handle, enabling the two components to be prepared independently.

To enable incorporation of the linker while temporarily masking the glutarimide moiety, intermediate **8a** was designed and synthesised (**Scheme 2**). A *p*-nitrophenyl carbonate was introduced as an activated leaving group[90], allowing subsequent nucleophilic substitution by the linker intermediate to form the carbonate linkage between the glutarimide-containing degrader and the linker.



Scheme 2. The synthesis of intermediate with *p*-nitrophenyl carbonate. i) formaldehyde, reflux, 30min, 54%; ii) bis(4-nitrophenyl) carbonate, DIPEA, DMF, RT, 4h, 82%.

The full payload (**OX05156**) was subsequently assembled using **8a** as the key intermediate (**Scheme 3**). The cysteine-reactive handle was first introduced by coupling **8a** with **9a**, followed by removal of the *tert*-butoxycarbonyl (Boc) protecting group. The remaining portion of the pan-LMO degrader was then coupled to the deprotected intermediate *via* HATU-mediated amide bond formation, affording the final payload. The cysteine-reactive handle contains an activated pyridyl disulfide moiety that are designed to undergo thiol-disulfide exchange with cysteine residues on the antibody, releasing one equivalent of 5-nitropyridine-2-thiol and forming the desired antibody-payload disulfide linkage.



Scheme 3. The synthesis of **OX05156**. i) DMAP, DMF, RT, 18h, 32%; ii) TFA, CH_2Cl_2, rt, 5 min; iii) **5**, HATU, DIPEA, DMF, 20h, 30%.

Cathepsin B linker - Val-Cit/Val-Ala

To further improve payload release, the linker design was optimised by replacing the reduction-cleavable disulfide linker with an enzyme-cleavable dipeptide linker, providing greater control over intracellular payload release. In particular, the Val-Cit-PAB and Val-Ala-PAB linkers were selected because they are efficiently cleaved by lysosomal cathepsins following receptor-mediated internalisation of the ADC, while

remaining stable during systemic circulation. Among these, the Val-Cit-PAB linker is one of the most extensively validated linker systems in clinically approved ADCs owing to its favourable balance between plasma stability and efficient intracellular cleavage.[91] Maleimide chemistry was chosen as the conjugation strategy due to its well-characterised reactivity and selectivity towards cysteine residues via Michael additions[92], enabling efficient and site-specific antibody modification. More than half of FDA-approved ADCs employ maleimide-based conjugation[82], highlighting its reliability and broad applicability in ADC development.

Val-Cit-PAB and Val-Ala-PAB linkers are designed to undergo intracellular cleavage by cathepsin B following receptor-mediated internalisation of the ADC in the cells (**Figure 10**). Upon lysosomal trafficking, proteolytic cleavage of the dipeptide linker will trigger self-immolation of the *para*-aminobenzyl (PAB) spacer through a 1,6-elimination mechanism. This process will generate a hydroxymethyl-substituted degrader intermediate, which will subsequently undergo spontaneous decomposition with the release of one equivalent of formaldehyde, regenerating the active pan-LMO degrader within the target cell.

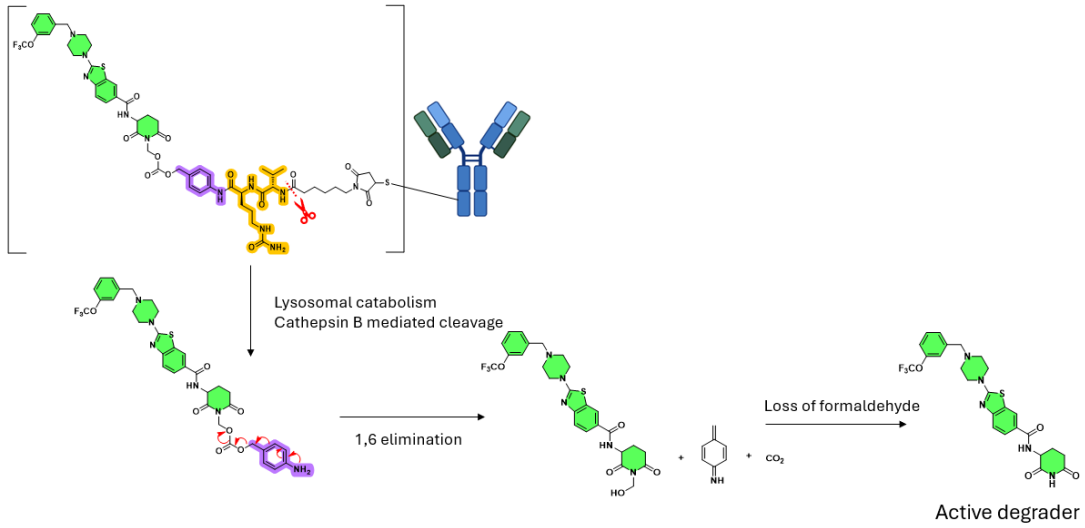


Figure 10. Proposed mechanism of cleavage for the dipeptide linkage. Val-Cit-PAB linker is shown as a representative example, with Val-Ala-PAB undergoing the same release mechanism.

Similar to **OX05156**, the dipeptide-containing pre-conjugates were designed as modular constructs with four main components: the pan-LMO degrader, a carbonate linkage, a cleavable Val-Ala-PAB or Val-Cit-PAB linker, and a maleimide-based cysteine-reactive handle incorporating either a C5 or PEG8 spacer. Structural variation within the linker was introduced to investigate how linker composition influences the physicochemical properties of the pre-conjugates. Val-Cit and Val-Ala differ in the size and polarity of their amino-acid side chains, potentially affecting properties such as hydrophobicity and steric environment. In parallel, incorporation of a PEG8 spacer in place of the C5 spacer was intended to increase linker hydrophilicity and improve aqueous solubility.

A convergent synthetic strategy was adopted for their assembly (**Figure 11**). The synthesis was designed to build from the carbonate linkage between the glutarimide fragment and the dipeptide-PAB linker, followed by installation of the maleimide handle at the terminal amine. Late-stage amide coupling with carboxylic acid **5** then completed the pan-LMO degrader scaffold to afford the final pre-conjugates.

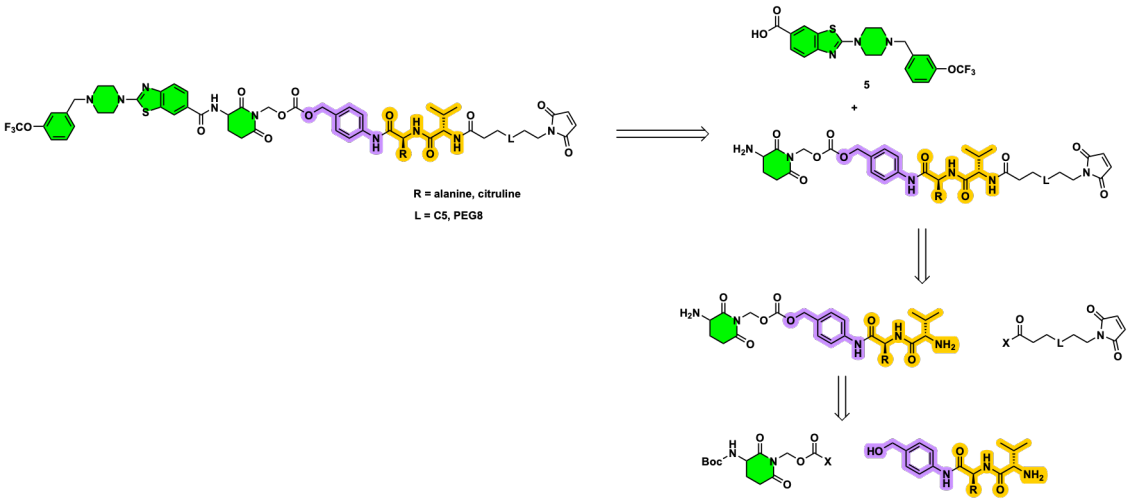
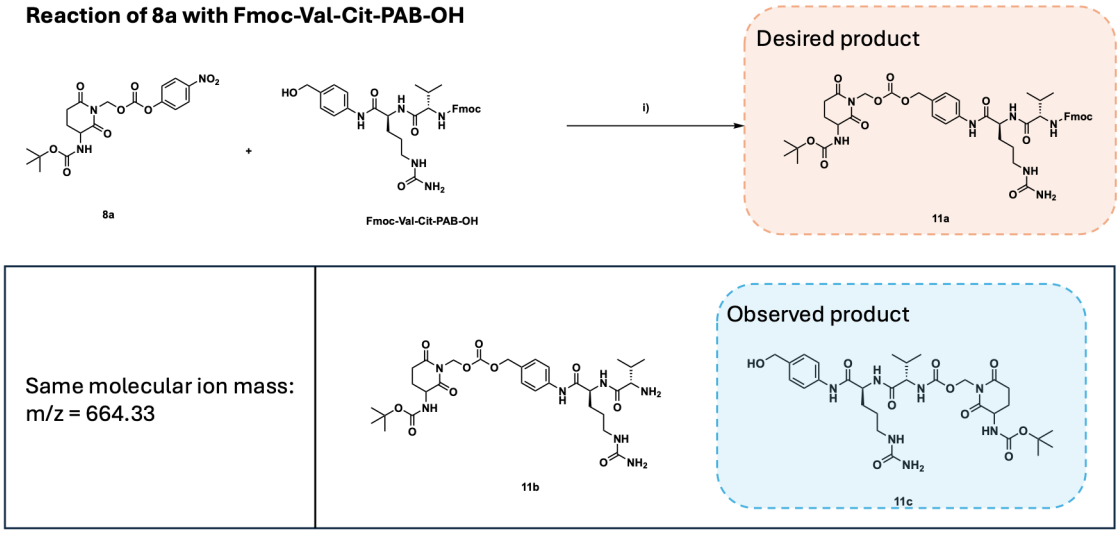


Figure 11. Retrosynthetic analysis of the dipeptide-containing pre-conjugates. The target structures were disconnected at the degrader amide bond to separate carboxylic acid **5** from the linker-functionalised glutarimide fragment. Further disconnections at the carbonate linkage and terminal maleimide amide bond enabled independent variation of the Val-Ala/Val-Cit dipeptide linker and C5/PEG8 maleimide handle prior to final assembly.

Initially, the synthesis started from directly reacting the commercially available linker precursor, Fmoc-Val-Cit-PAB-PNP, with compound **7** with the presence of DIPEA and reacted at room temperature for 24 hours. However, LC-MS analysis showed no evidence of the desired product, either with or without the Fmoc protecting group. This result suggests that the methyl hydroxyl group on the glutarimide moiety exhibits low nucleophilicity, limiting its reactivity in the substitution step.

Alternatively, intermediate **8a** was reacted with Fmoc-Val-Cit-PAB-OH following the literature protocol using DMAP as the base[90] (**Scheme 4**). LC-MS analysis revealed a new peak of *m/z* 664.33, consistent with the desired coupling product **11a** with the loss of the Fmoc protecting group. This unexpected deprotection raised concerns that the liberated primary amine could participate in competing reactions under the coupling conditions. To minimise Fmoc cleavage, DMAP was therefore replaced with DIPEA, which has a substantially slower rate of Fmoc deprotection, with a reported half-life of

10.1 h[93]. However, the desired Fmoc-protected carbonate product **11a** (*m/z* = 886.4) was not detected under the modified conditions. Instead, the *m/z* = 664.33 species remained, with an LC-MS peak area approximately equal to that of the remaining Fmoc-Val-Cit-PAB-OH, indicating substantial conversion. The *m/z* = 664.33 species was subsequently isolated in 25% yield for further characterisation.



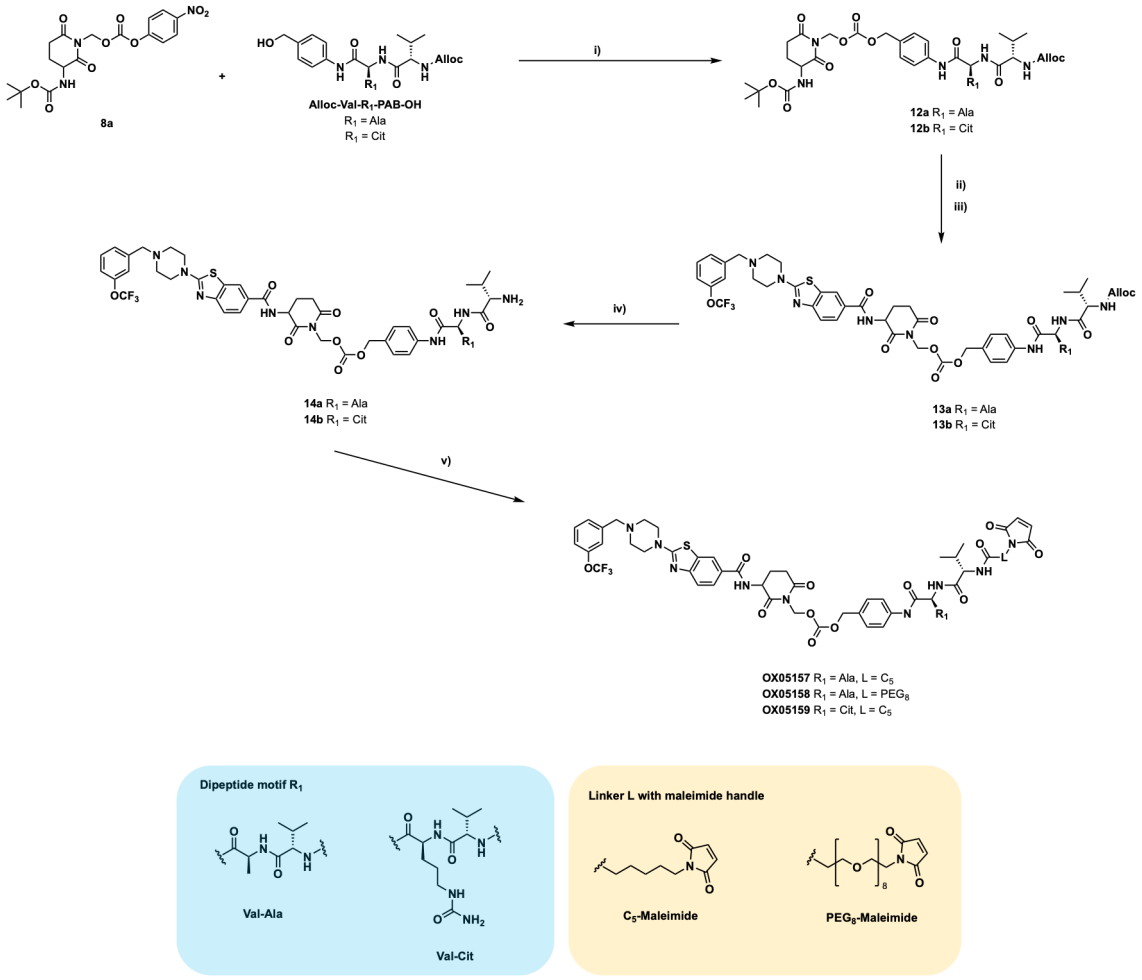
Scheme 4. The formation of the carbonate linkage between **8a** and Fmoc-Val-Cit-PAB-OH. i)DIPEA, rt, 24 h. Isolated yield of the *m/z* = 664.33 product: 25%.

The *m/z* = 664.33 species was initially proposed to be **11b**, which involved nucleophilic attack of the benzylic hydroxyl group of the linker on **8a** to form the carbonate linkage, followed by subsequent Fmoc deprotection. However, IR analysis of the isolated product revealed a strong carbamate carbonyl absorption (1702 cm^{-1}, C=O) rather than the expected carbonate band (1750 cm^{-1}, C=O). These observations support an alternative reaction pathway in which Fmoc deprotection occurs prior to nucleophilic substitution, allowing the liberated amine to react with **8a** to afford the carbamate product **11c** (**Scheme 5**). This result indicates that the Fmoc protecting group is incompatible with the

basic reaction conditions employed and highlights the need for an alternative amine protecting group.

An allyloxycarbonyl (Alloc) group was then used to replace the Fmoc group. It can be selectively removed using a palladium(0) catalyst in the presence of a nucleophilic allyl cation scavenger while remaining stable under both acidic and basic reaction conditions. This orthogonal protecting group strategy was particularly advantageous, as the downstream synthesis required basic conditions for carbonate formation and acidic conditions for Boc deprotection.

8a was successfully coupled with Alloc-Val-Cit-PAB-OH in the presence of DMAP to afford the desired carbonate-linked intermediate **12b**. Subsequent Boc deprotection using 2.68 M HCl in 1,4-dioxane generated the corresponding free amine, which was coupled to **5** *via* HATU-mediated amide bond formation to afford the complete degrader construct **13b**. Finally, the Alloc protecting group was removed under $Pd(PPh_3)_4/PhSiH_3$ conditions, and the liberated amine on the terminal of the dipeptide linker **14b** was reacted with the corresponding maleimide *N*-hydroxysuccinimide (NHS) ester produce **OX05159** (**Scheme 5**). Using the established synthesis route, three dipeptide-containing pre-conjugates (**OX05157, OX05158, OX05159**) were successfully synthesized for subsequent antibody bioconjugation.



Scheme 5. The synthesis of degrader with dipeptide linker and maleimide handle. i) DMAP, DMF, RT, 24h, 41%; ii) 2.68M HCl in 1,4-dioxane, RT, 3.5h, 99%; iii) 5, HATU, DIPEA, DMF, 20h, 58%; iv) $Pd(PPh_3)_4$, $PhSiH_3$, RT, 2h, 91%; v) corresponding Maleimide NHS ester, DIPEA, DMF, RT, 18h, 33-47%.

Phosphate modified Cathepsin B linker

Despite the successful synthesis of the carbonate-linked payloads, concerns remained regarding the potential susceptibility of the carbonate linkage to premature hydrolysis under physiological conditions. In an attempt to further improve linker stability and achieve more controlled intracellular payload release, a phosphate linkage was investigated as an alternative. Unlike carbonate linkages, phosphate groups are relatively stable during systemic circulation but can be selectively cleaved by intracellular

phosphatases (**Figure 12**), providing an additional level of control over payload activation.[94]

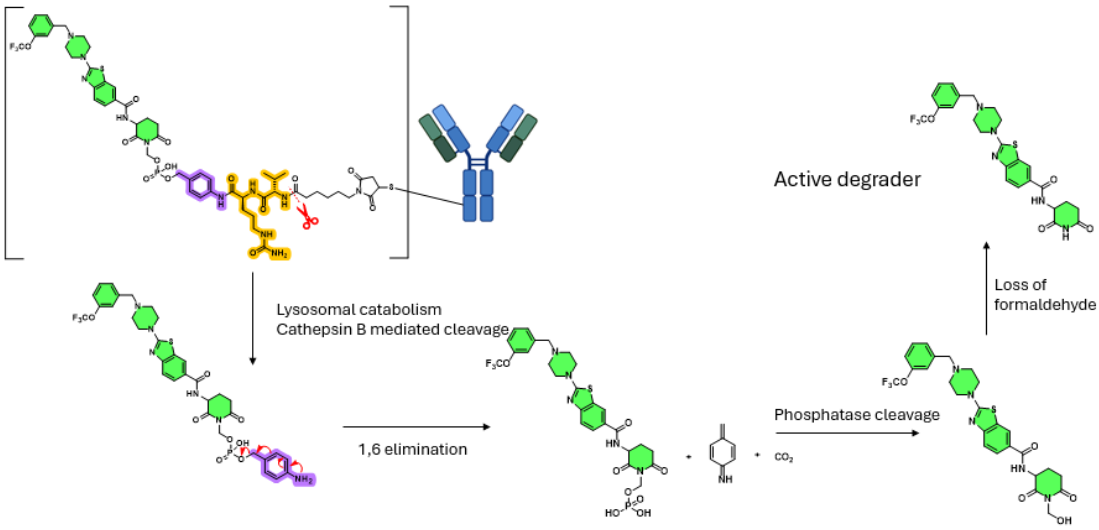
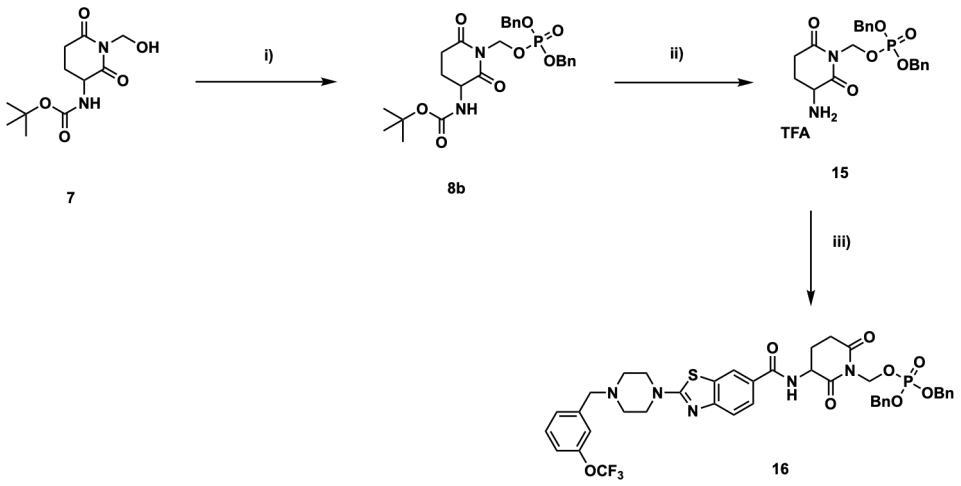


Figure 12. Proposed mechanism of cleavage for the dipeptide linkage. Val-Cit-PAB linker is shown as a representative example, with Val-Ala-PAB undergoing the same release mechanism.

Based on the established literature for a synthesis of monophosphate linkage[95] for a payload with dipeptide Val-Cit linker, the synthesis from the degrader started with the installation of the benzyl protected phosphate group to give **8b** (**Scheme 6**). The capped pan-LMO degrader **16** was then synthesized following the same HATU coupling method as the original pan-LMO degrader.



Scheme 6. The synthesis of pan-LMO degrader with di-benzyl protected phosphate **16.** i) dibenzyl diisopropylphosphoramidite, mCPBA, tetrazole, CH_2Cl_2/MeCN, 0 °C, 1 h; ii) TFA (5 equiv.), CH_2Cl_2, RT, 19h; iii) **5**, HATU, DIPEA, DMF, RT, 20h.

Challenges were encountered during the formation of **15**, during the deprotection of Boc-protected amine using trifluoroacetic acid (TFA). Although the Boc group is known to be readily cleaved under acidic conditions, partial cleavage of the benzyl-protected phosphate was also observed. While benzyl phosphate protecting groups are typically removed *via* Pd-catalysed hydrogenation, they have been reported to undergo deprotection in the presence of TFA[96]. A range of reaction conditions was systematically explored to achieve a balance between efficient removal of the *N*-Boc protecting group while preserving the benzyl-protected phosphate moiety. The extent of benzyl group retention was assessed by comparing the integration of proton signals corresponding to the benzylic position of the benzyl group with those of the hydroxylmethylene environment in the ^{1}H NMR spectrum (**Figure 13**). Following optimisation, the most effective conditions were identified as treatment with 5 equivalents of trifluoroacetic acid (TFA) for 19 hours. These conditions enabled substantial Boc deprotection while minimising cleavage of the benzyl protecting groups.

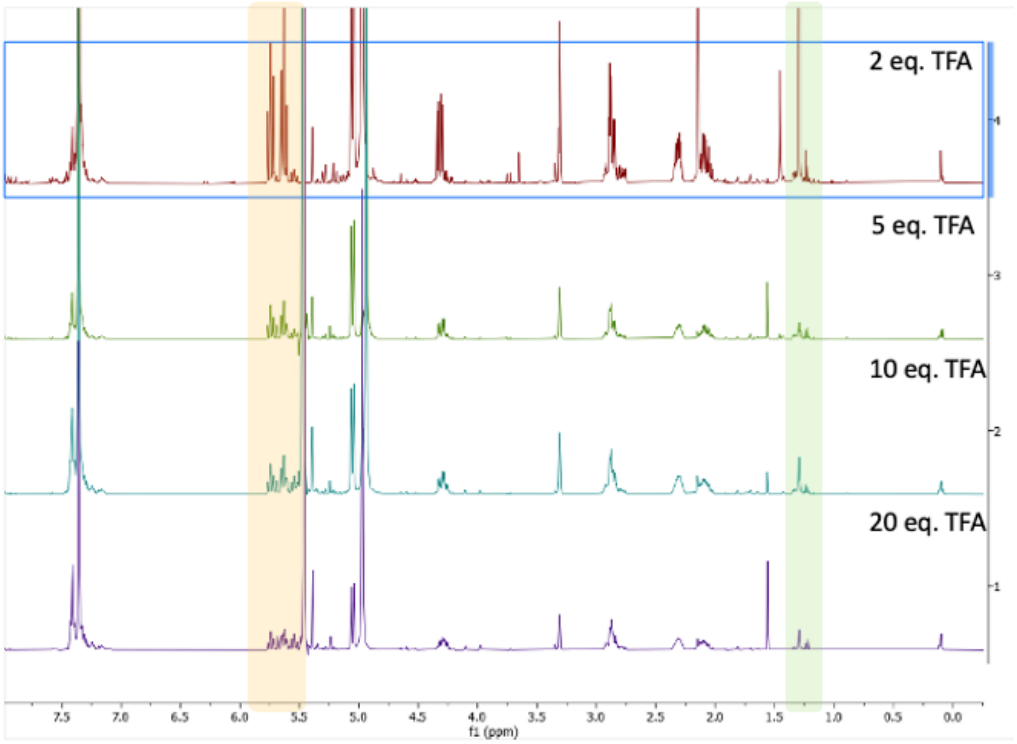


Figure 13. ^{1}H NMR spectra of **8b** following addition of 2, 5, 10, and 20 equivalents of TFA. The yellow region highlights the methylene proton environment of the glutarimide moiety, while the green region highlights the tert-butyl protons of the Boc protecting group. The results showed that increasing amount of TFA leads to a progressive broadening and increased noise in the proton signal corresponding to the methylene group on the glutarimide moiety. This observation suggests the formation of multiple chemical environments at this position, likely due to the presence of closely related species with slightly different chemical shifts, resulting in signal overlap with that of the desired product.

However, partial removal of the benzyl protecting groups presents a significant challenge, particularly when scaling up the reaction. The crude product obtained from the TFA-mediated deprotection was carried forward directly into the amide coupling step without further purification, resulting in a complex mixture of species entering the subsequent reaction. The LC-MS traces of the crude product from amide coupling revealed a heterogeneous composition (**Figure 14**), including unmodified degrader **JDH-06-040**, **16a** (dibenzyl-protected phosphate), **16b** (monobenzyl-protected phosphate group) and **16c** (fully deprotected phosphate). These assignments were further supported by ^{1}H NMR

analysis of fractions isolated by reverse-phase chromatography. The degree of benzyl protection was assessed by comparing the integration of the benzyl proton signals with that of the glutarimide methylene protons. For the dibenzyl-protected species **16a**, an integration ratio of approximately 5:1 (benzyl:methylene) was observed, whereas no benzyl resonances were present for unmodified **JDH-06-040**. Fractions containing a mixture of **16b** and **16c** exhibited lower relative benzyl integration than **16a**, consistent with partial benzyl deprotection. However, **16b** and **16c** could not be readily resolved by reverse-phase chromatography, complicating isolation of the fully deprotected product and limiting further progression of this synthetic route.

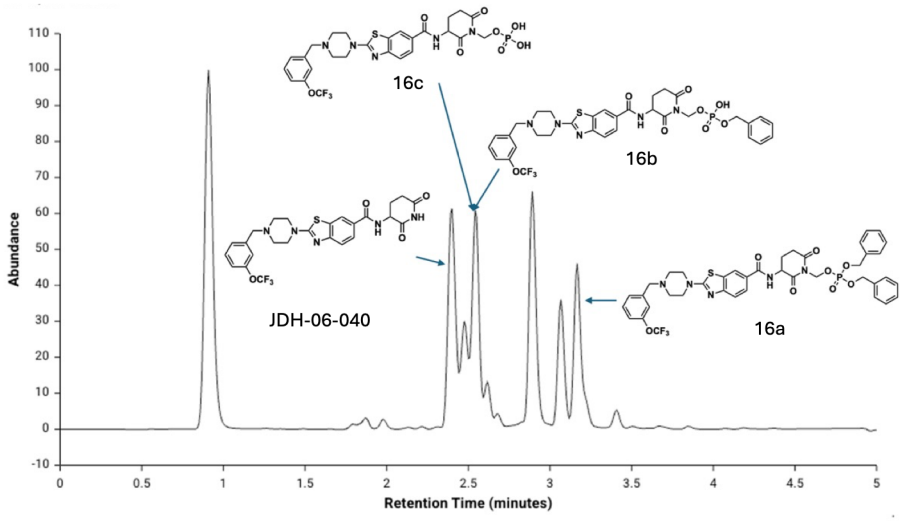
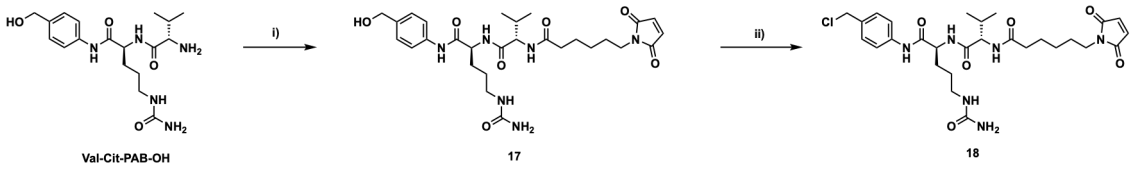


Figure 14. LC-MS trace for amide coupling on large scale.

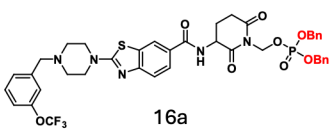
On the linker side of the molecule, the synthesis began with the commercially available Val-Cit-PAB-OH (**Scheme 7**). The C_5 maleimide handle was first introduced, followed by conversion of the hydroxybenzyl group into the corresponding benzyl chloride to enable subsequent coupling with the phosphate-containing degrader. Intermediate **17** was isolated from the crude reaction mixture by recrystallisation and filtration, eliminating the need for further chromatographic purification. However, despite prolonged drying,

residual water remained associated with the isolated solid. During the subsequent chlorination step, this residual moisture consumed a proportion of the thionyl chloride, reducing the efficiency of the reaction and leading to lower isolated yields. To minimise this competing hydrolysis, the reaction was then performed in anhydrous NMP, which significantly improved the conversion to **18**.

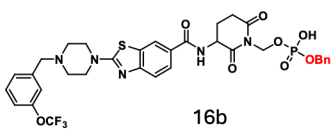


Scheme 7. The synthesis of **18**. i) 2,5-dioxopyrrolidin-1-yl 6-(2,5-dioxo-2,5-dihydro-1H-pyrrol-1-yl)hexanoate, anhydrous NMP, RT, 18h, 83%; ii) $SOCl_2$, DMF, 0 - 20 °C, 1 h, 56%.

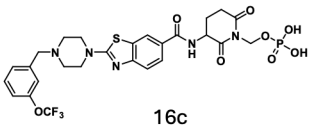
For coupling of benzyl deprotected product of **16** to **18**, prior removal of the benzyl protecting groups was required. However, significant challenges were encountered during attempts to achieve complete deprotection *via* hydrogenation (**Table 1**). Increasing the catalyst loading, as well as the addition of acetic acid, led to improved benzyl removal. However, the reaction produced a mixture of monobenzyl protected and fully deprotected phosphate species. The incomplete hydrogenation may be attributed to catalyst poisoning, as the molecule contains multiple functional groups capable of coordinating to the metal catalyst and inhibiting its activity. Increasing the catalyst loading likely compensates for this effect by providing a greater number of active catalytic sites, thereby enhancing the extent of deprotection at the phosphate (**Table 1, Entry 3,8**).



16a



16b



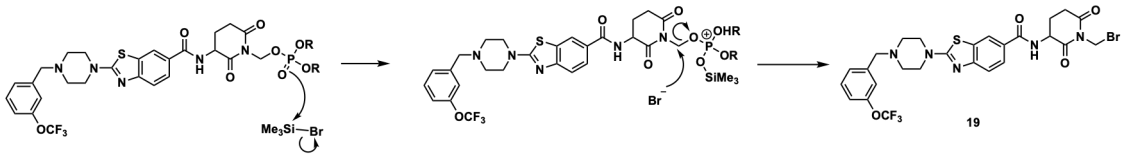
16c

Entry	Catalyst	Loading	Additive	Observation
1	Pd/C	10% wt		No deprotection observed
2	Pd/C	10% wt	2 drops AcOH	**16a**: 68%, **16b**:16%, **16c**: 16%
3	Pd/C	20% wt	2 drops AcOH	**16a**: 0%, **16b**:67%, **16c**: 33%
4	$Pd(OH)_2/C$	10% wt		No further deprotection observed
5	$Pd(OH)_2/C$	10% wt	2 drops AcOH	No further deprotection observed
6	PtO_2	10% wt		all three observed, **16a** being the major peak
7	PtO_2	10% wt	2 drops AcOH	**16a**: 0%, **16b**:60%, **16c**: 40%
8	PtO_2	20% wt		**16a**: 0%, **16b**:40%, **16c**: 20% (20% each of two unknown phosphorous species)

Table 1. Different conditions of hydrogenation tested.

As demonstrated earlier (**Figure 14**), the mono-benzyl-protected **b** and fully deprotected phosphate **c** intermediates exhibited nearly identical retention times on the reverse-phase column, making chromatographic separation extremely challenging. As the mono-benzyl-protected **b** and fully deprotected phosphate **c** intermediates could not be readily separated, an alternative phosphate deprotection strategy was investigated.

Trimethylsilyl bromide (TMSBr)[97] was tested as an alternative deprotection method. Rather than producing the desired deprotected phosphate, LC-MS analysis revealed two molecular-ion peaks at *m/z* = 640.09 and 642.08 in an approximately 1:1 intensity ratio, consistent with the characteristic $^{79}Br/^{81}Br$ isotopic pattern of a monobrominated species. These data support the assignment of the product as **19** (**Scheme 8**).



Scheme 8. The formation of methyl bromide product 19. i) TMSBr, anhydrous $CHCl_3$, 36 °C, 64h.

In summary, four pan-LMO degrader pre-conjugates were successfully synthesised and carried forward for stability assessment and antibody bioconjugation (**Figure 15**). All four constructs incorporate the same pan-LMO degrader warhead and a cysteine-reactive handle for subsequent antibody conjugation, while differing in their linker composition and proposed intracellular release mechanism.

OX05156 incorporated a reduction-cleavable disulfide linker designed to undergo GSH-mediated intracellular cleavage. The remaining three pre-conjugates employed cathepsin-cleavable dipeptide-PAB linkers together with maleimide-based cysteine conjugation. **OX05157** contains a Val-Ala-PAB linker with a C5 maleimide handle, whereas **OX05158** contained a Val-Ala-PAB linker with a PEG8-containing maleimide handle to increase linker hydrophilicity. **OX05159** contained a Val-Cit-PAB linker with a C5 maleimide handle. Together, these four pre-conjugates provide a small panel of linker designs with distinct cleavage and physicochemical properties for subsequent evaluation of stability, solubility, and antibody bioconjugation.

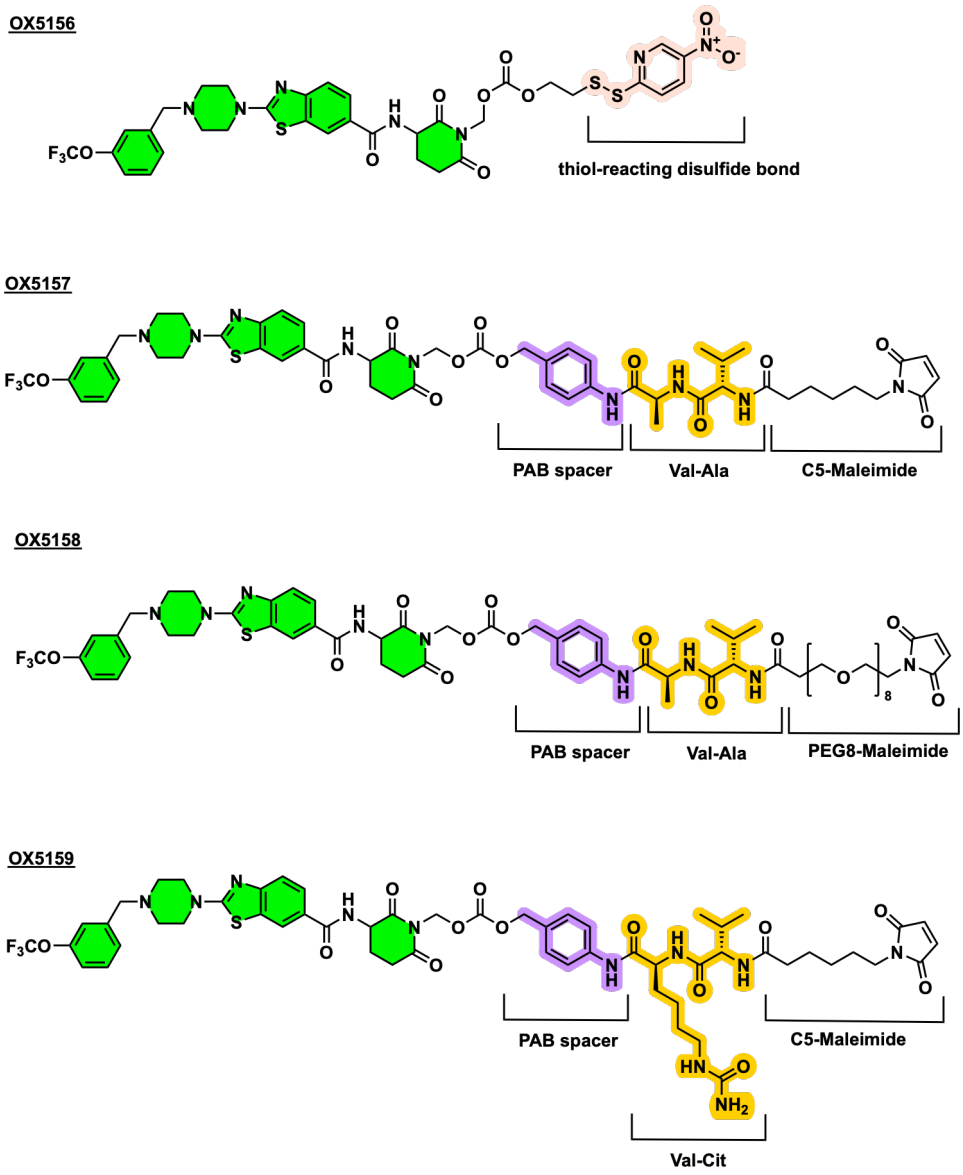


Figure 15. Structures of the four synthesised pre-conjugates.

GSH assay

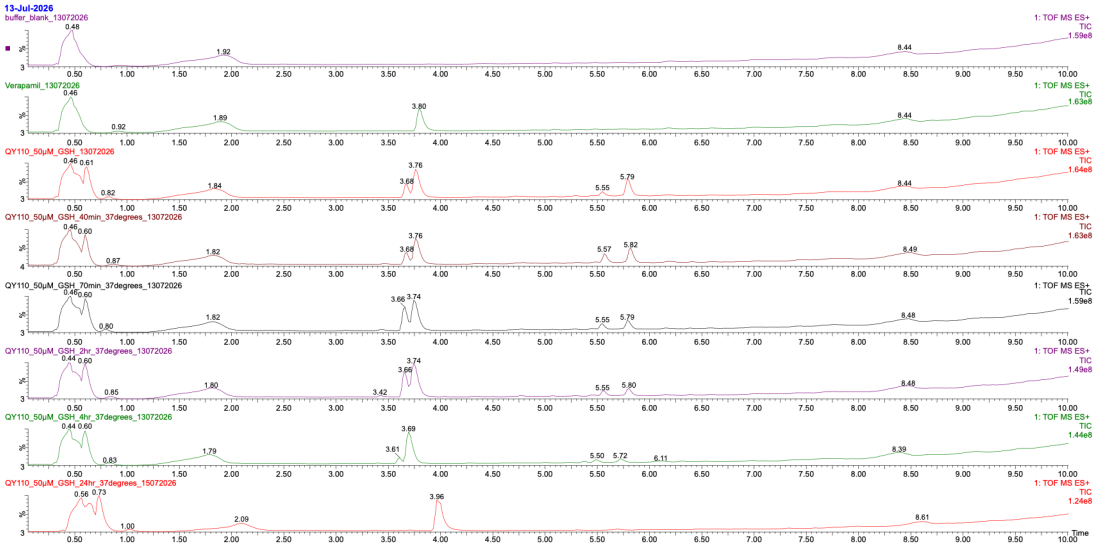
A glutathione (GSH) assay was performed as a preliminary evaluation of the thiol-reacting behaviour of the four synthesised pre-conjugates (**Figure 15**). In parallel, each pre-conjugate was incubated under identical conditions in the absence of GSH to assess its intrinsic behaviour and distinguish GSH-mediated reactivity from changes occurring under the assay conditions alone. Each pre-conjugate was incubated under physiological

conditions in phosphate-buffered saline (PBS) containing 1 mM EDTA at 37 °C, both in the presence and absence of excess GSH. Samples were collected at 10 min, 40 min, 70 min, 2 h, 4 h, and 24 h, and analysed by LC-MS using verapamil as an internal standard.

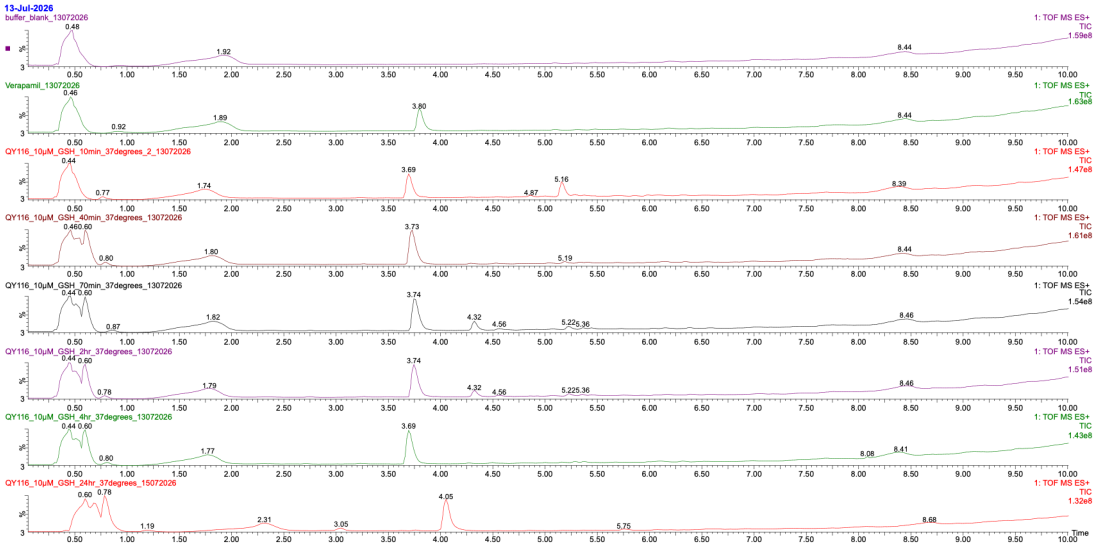
LC–MS analysis of the pre-conjugates incubated in the absence of GSH showed a progressive decrease in the abundance of **OX05156** and **OX05157**, with both exhibiting an approximately 49% reduction in signal after 4 h and becoming undetectable after 24 h. **OX05159** also showed a decrease in abundance after 4 h, however, owing to experimental error, this change could not be reliably quantified. **OX05158** remained relatively unchanged, with a decrease of around 10%. Given the structural similarity of the four pre-conjugates, these differences may reflect differences in their aqueous solubility under the assay conditions. In particular, OX05158, which contains a hydrophilic PEG8 spacer, appeared to remain in solution more effectively than the other pre-conjugates. (**Figure 1-4S**)

In the presence of GSH, all four pre-conjugates reacted readily, as evidenced by the detection of the corresponding GSH adducts by LC-MS after 10 min of incubation. The chromatograms showed a progressive increase in the peak area of the GSH adducts, accompanied by a corresponding decrease in the parent pre-conjugates, confirming efficient reaction of each pre-conjugate with GSH under the assay conditions. (**Figure 16**)

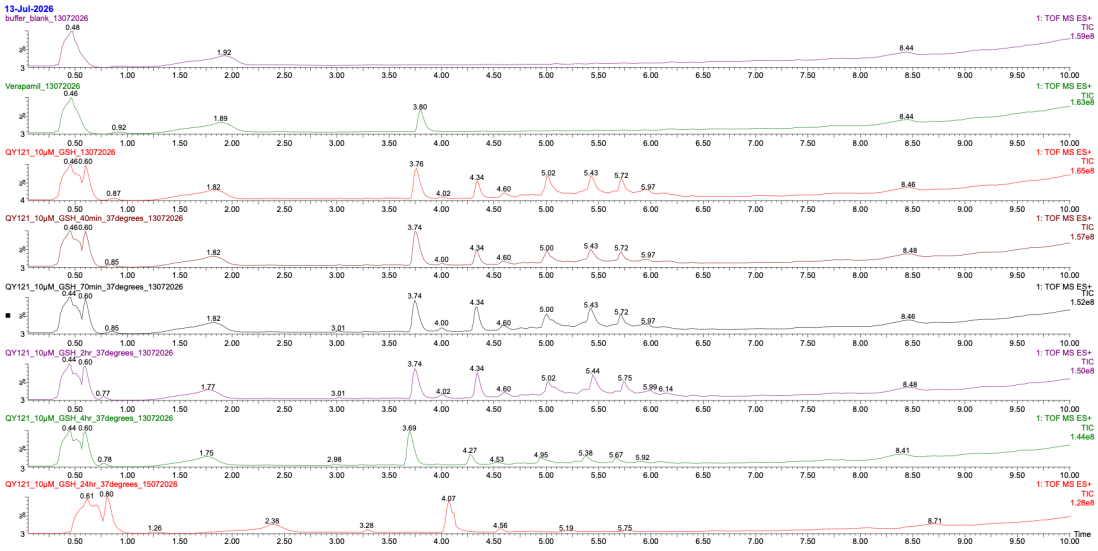
a) OX05156



b) OX05157



c) OX05158



d) OX05159

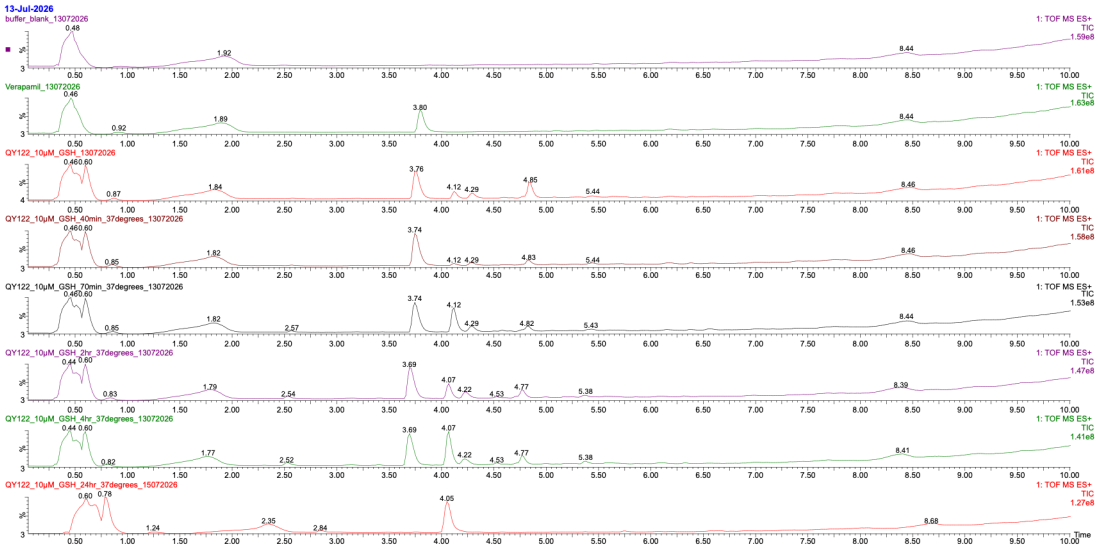


Figure 16. LC-MS for **OX05156** (50 μM), **OX05157** (10 μM), **OX05158** (10 μM), **OX05159** (10 μM) incubated in phosphate-buffered saline (PBS) buffer containing 1 mM EDTA at 37 °C with 4.6 mM GSH at 10 min, 40 min, 70 min, 2 h, 4 h, and 24 h. Verapamil at 3.7 min (around 4.0 min for 24 h). a) OX05156 at 5.8 min, reduced product of OX05156 at 5.55 min, GSH adduct of OX05156 at 3.66 min. b) OX05157 at 5.16 min, GSH adduct of OX05157 at 4.32 min. c) OX05158 across 5.02 to 5.97 min, GSH adduct of OX05158 at 4.34 min. d) OX05159 at 4.85 min, GSH adduct of OX05159 at 4.12 min.

Interestingly, after 4 h of incubation, a substantial decrease in the LC-MS signal for both the parent pre-conjugates and their corresponding GSH adducts was observed. By 24 h,

neither species was detectable, while the verapamil remained unchanged. These observations are consistent with either degradation of the compounds or precipitation during prolonged incubation. Further experiments would be required to distinguish between these possibilities. Although further investigation would be required to confirm the underlying mechanism, these findings indicate that prolonged incubation under the conjugation conditions may result in significant loss of soluble payload. This assay provided insights for the subsequent antibody bioconjugation experiments, where minimising the reaction time was expected to reduce payload loss and maximise conjugation efficiency.

Bioconjugation

The four pre-conjugates were subsequently evaluated for bioconjugation with the human IgG1 monoclonal antibody trastuzumab. Initially, conjugation was performed on a small scale using 8 equivalents of pre-conjugate relative to the antibody, following a reported protocol.[84] However, the concentration of pre-conjugate required for bioconjugation (168 μM) was substantially higher than that used in the previous GSH assay (50 μM for **OX05156** and 10 μM for **OX05157**, **OX05158**, **OX05159**). Therefore, the solubility of each pre-conjugate under the bioconjugation conditions was evaluated (**Figure 17**), as precipitation of the payload would prevent antibody conjugation from happening.

Among the four pre-conjugates, only **OX05158** (degrader-Val-Ala-PEG8-Mc) remained fully soluble under the conjugation conditions. The remaining three pre-conjugates precipitated despite increasing the DMSO content to 10% (v/v), indicating that the high concentration of pre-conjugates was not suitable for bioconjugation. One strategy to overcome this limitation would be to perform the conjugation at a lower payload concentration where the pre-conjugate remains soluble while maintaining the required

molar equivalents. However, owing to the limited timescale of this project, this optimisation was not investigated further, and only **OX05158** was carried forward for antibody conjugation.

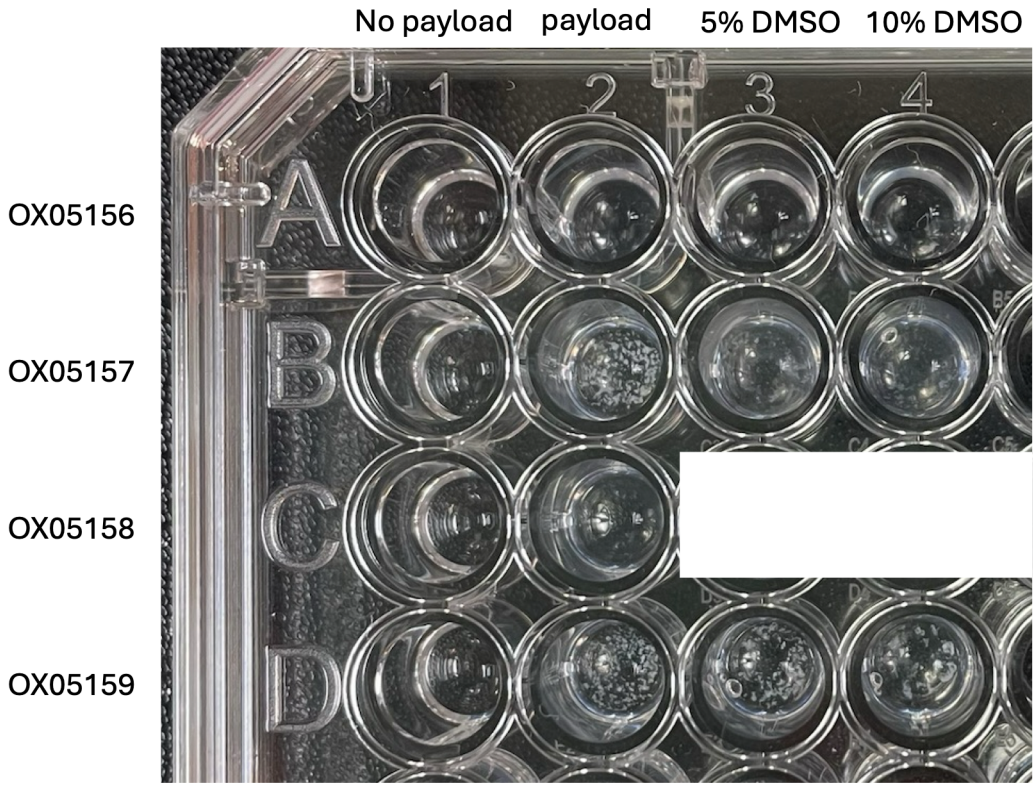


Figure 17. Solubility test with the pre-conjugates. Each well contains 53 µL degassed PBS buffer with 4 mM EDTA. The amount of pre-conjugate added was 1 µL of 10 mM payload in DMSO. Additional 5% or 10% (v/v) DMSO were added to evaluate the effect of DMSO concentration on solubility. For **OX05158**, no visible precipitation was observed under the preceding condition; therefore, testing at the higher DMSO concentrations (5% and 10%) was not performed. These untested wells are obscured by the white box and should not be interpreted as missing data or precipitation results.

Various conjugation conditions were investigated to identify the optimal conditions for conjugating the pre-conjugate **OX05158** to trastuzumab (**Table 2**). The conjugation consists of two steps. First, the interchain disulfide bonds of the antibody are partially reduced by reducing agent TCEP to generate free cysteine thiols. Second, the pre-

conjugate is added to react with these thiol groups via Michael addition. The resulting ADCs were analysed by intact protein LC-MS. During intact protein analysis, the non-covalent interactions between the heavy and light chains are disrupted, while covalent bonds, including disulfide bonds and the thioether (S-C) bonds generated during conjugation, remain intact. Consequently, the different antibody fragments can be separated and identified based on their molecular masses.

conjugation test	Reduction			Conjugation			Fragments detected by LCMS	Conjugation happened
	TCEP eq.	Temperature (°C)	Time (h)	OX05158 eq.	Temperature (°C)	Time (h)		
C1a	3	22	2	8	22	1	Ab full mass	No
C1b	3	22	2	8	22	3	Ab full mass	No
C2a	6	37	2	8	22	1	Ab full mass, LC, HC, HC+LC	No
C2b	6	37	2	24	22	1	LC+payload, HC+LC+2payload, Ab full mass	Yes
C3a	6	37	2	24	37	1	*protein loss*, LC+payload, HC+LC+2payload	Yes
C3b	6	37	2	24	22	3	LC+payload, HC+LC+2payload	Yes
C4a	6	37	2	24	4	1	LC, HC	No
C4b	6	37	2	24	4	22	LC, HC	No

Table 2. Small-scale conjugation conditions for the bioconjugation of OX05158 to trastuzumab.

The initial optimisation focused on the reduction step to generate sufficient free thiols for subsequent conjugation. An initial condition of 3 equivalents of TCEP at 22 °C was selected based on the literature[98] to achieve partial reduction while maintaining antibody stability and antigen-binding activity (**Table 2, C1a**). Although the conjugation time was increased (**Table 2, C1b**), no conjugated products were detected by LC-MS. Instead, only the native antibody (2 heavy-chain (HC) + 2 light-chain (LC)) together with the partially reduced species (2HC + LC and HC + LC) were observed (**Figure 8S**). The appearance of the partially reduced species indicates cleavage of one interchain disulfide bond, resulting in the loss of one light chain or one heavy chain-light chain pair during analysis.

As no purification step was performed following reduction, the free thiols generated during TCEP treatment could undergo reoxidation to reform disulfide bonds in the presence of residual oxygen dissolved in the solvent. To minimise this effect, the number of equivalents of TCEP and reaction temperature were increased in line with previously published optimisation protocols[84] (**Table 2, C2a**). Under these conditions, a greater extent of reduction was observed, as evidenced by the appearance of additional peaks corresponding to HC and LC in the deconvoluted mass spectrum (**Figure 12**).

Following optimisation of the reduction step, attention was shifted to the conjugation reaction. The results from condition C2a indicated that multiple cysteine residues were available for conjugation. Therefore, the equivalents of pre-conjugate **OX05158** were increased (**Table 2, C2b**). Under these conditions, additional peaks with mass increases of approximately 1400 Da and 2800 Da, corresponding to the attachment of one and two **OX05158** molecules, respectively, were observed in the deconvoluted mass spectra (**Figure 18**). These mass shifts are consistent with successful conjugation of the pre-conjugate to the partially reduced antibody, demonstrating that increasing the amount of **OX05158** improved conjugation efficiency.

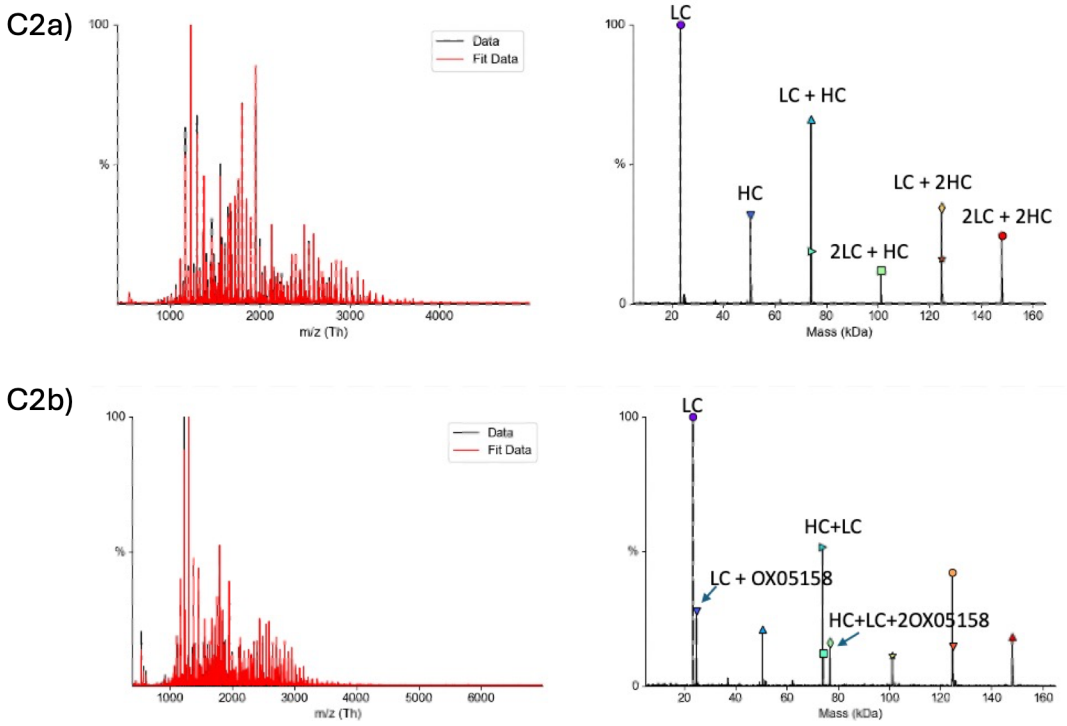


Figure 18. Deconvoluted mass spectrum from the LC-MS for C2a and C2b. The peak corresponding to 2LC + 2HC represents the full antibody mass.

Additional conjugation conditions were investigated to further improve the efficiency of bioconjugation. To increase the reaction rate between the free thiols and the maleimide group of **OX05158**, the conjugation temperature was increased to 37 °C (**Table 2, C3a**). However, substantial protein loss was observed after the conjugation. Based on the initial antibody concentration, the expected protein concentration after the reaction was approximately 0.7 mg/mL, whereas the concentration measured by NanoDrop was only 0.3 mg/mL. This decrease is likely due to protein aggregation or precipitation at the elevated temperature, resulting in loss of soluble antibody during sample handling. The conjugation temperature was then reduced to 4 °C, with conjugation times of 1 hour and 22 hours investigated (**Table 2, C4a and C4b**). Under both conditions, only free heavy chain (HC) and light chain (LC) species were observed in the deconvoluted mass spectra, indicating that conjugation was either minimal or did not occur to a detectable extent in

the solution. One possible explanation is the reduced solubility of **OX05158** at 4 °C. As the solubility of the **OX05158** decreases at lower temperature, precipitation of **OX05158** would reduce the concentration available for conjugation. Furthermore, any payload-conjugated antibody fragments formed may also exhibit reduced solubility and could therefore be lost from the soluble prior to LC-MS analysis. These effects could account for the predominant detection of unmodified HC and LC species. However, further experiments would be required to confirm this mechanism. The effect of extending the conjugation time at room temperature was also investigated (**Table 2, C3b**). Both HC+LC+2**OX05158** conjugate and LC+**OX05158** peaks were observed in the deconvoluted mass spectrum, indicating that conjugation had occurred on both the heavy and light chains. These results demonstrate that **OX05158** can react with cysteine residues present on both chains following partial reduction of the antibody.

Although the deconvoluted mass spectra provided qualitative evidence of successful conjugation, they could not be used to accurately determine the average drug-to-antibody ratio (DAR), as the peak intensities in the deconvoluted spectra do not necessarily reflect the relative abundance of each species due to differences in ionisation efficiency. The average DAR needs to be calculated from the integrated UV chromatographic peak areas corresponding to each DAR species (**Formula 1**). In this calculation, the peak area of each species is weighted by its corresponding DAR value to determine the average DAR. Unfortunately, the only intact protein LC-MS instrument available for open access within the department was the open access BioAccord 1 system, which operates using a fixed chromatographic gradient. Consequently, the antibody fragments were not sufficiently separated, preventing reliable integration of the UV chromatographic peaks and accurate determination of the average DAR.

$$Weighting = Peak\ Area\ (as\ a\ \%)\ \times No.\ Drug\ Molecules\ attached$$

$$DAR = \frac{2 \times (\sum Heavy\ Chain\ weighting + \sum Light\ Chain\ Weighting)}{100}$$

Formula 1. Calculation of the average DAR from intact protein LC-MS chromatograms. The average DAR is calculated as the weighted average of the individual DAR species using their integrated UV peak areas. The calculation is performed separately for the heavy-chain and light-chain species.

MALDI-TOF mass spectrometry was then investigated as an alternative method to detect full ADC mass. Unlike electrospray ionisation, MALDI uses a matrix-assisted laser desorption/ionisation process, allowing detection of the intact antibody as a singly charged molecular ion $(M+H)^+$. ADC samples prepared under conditions C1a, C1b, C2a and C2b were submitted to the departmental MALDI-TOF service for analysis. (**Figure 19**) However, no clear mass shift corresponding to conjugation was observed. The antibody detected with MALDI gives a broad mass distribution, most likely due to its intrinsic heterogeneity arising from glycosylation and other microheterogeneities, together with the limited mass resolution of MALDI for large proteins.

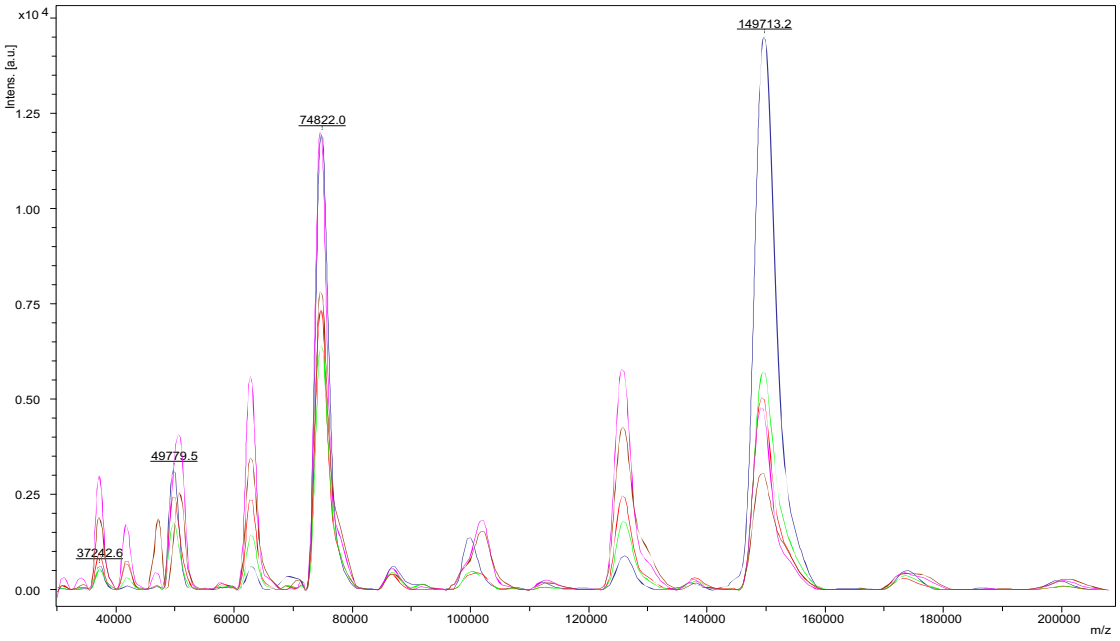


Figure 19. Overlaid MALDI-TOF mass spectra of trastuzumab and the corresponding ADC samples. Unconjugated trastuzumab is shown in dark blue, while ADCs generated under conditions C1a, C1b, C2a, and C2b are shown in red, green, purple, and brown, respectively. Spectra were acquired and processed by the MALDI Mass Spectrometry Service, Department of Chemistry, University of Oxford.

Native mass spectrometry was subsequently explored as an alternative method for estimating the average DAR by comparing the relative peak areas of the ion signals corresponding to different DAR species. Native MS employs soft ionisation conditions that help preserve non-covalent interactions between antibody chains, enabling analysis of the intact antibody complex.

Native trastuzumab, fully reduced trastuzumab, and ADCs prepared under conditions C2b, C3a and C3b were submitted to the departmental native mass spectrometry service for analysis. (**Figure 20**) For the fully reduced antibody, two major species were observed: the intact antibody and a second species with a molecular mass corresponding to 2HC + LC. This is likely the result of partial dissociation of one light chain during ionisation or gas-phase activation within the mass spectrometer.

Interestingly, an additional low-intensity peak was observed in the spectra of samples C2b and C3b that did not belong to the charge-state distribution of the native antibody. The corresponding mass increase was approximately 5280 Da, which is close to the theoretical mass increase expected for conjugation of four **OX05158** molecules (5600 Da). This observation is consistent with the LC-MS results, which indicated conjugation on both the heavy and light chains, corresponding to an overall DAR of approximately 4. The discrepancy between the observed and theoretical mass increase may be due to the relatively low resolution of the native MS spectrum. The ion peaks were broad, which is commonly attributed to residual solvent molecules, buffer adducts, and the inherent heterogeneity of antibodies. Comparison of samples C2b and C3b showed that the relative intensity of the DAR4 species was lower in C3b than in C2b. This suggests that extending the conjugation time reduced the abundance of the conjugated species. Although this decrease may be due to hydrolysis of the maleimide linkage or other degradation processes during the prolonged reaction.

Overall, the native mass spectrometry results indicate that condition C2b produced the highest proportion of conjugated antibody. Based on the relative abundance of the DAR4 peak, the average DAR was estimated to be approximately 0.8, assuming that the DAR4 species represented approximately 20% of the total antibody population and that no other conjugated species were detected.

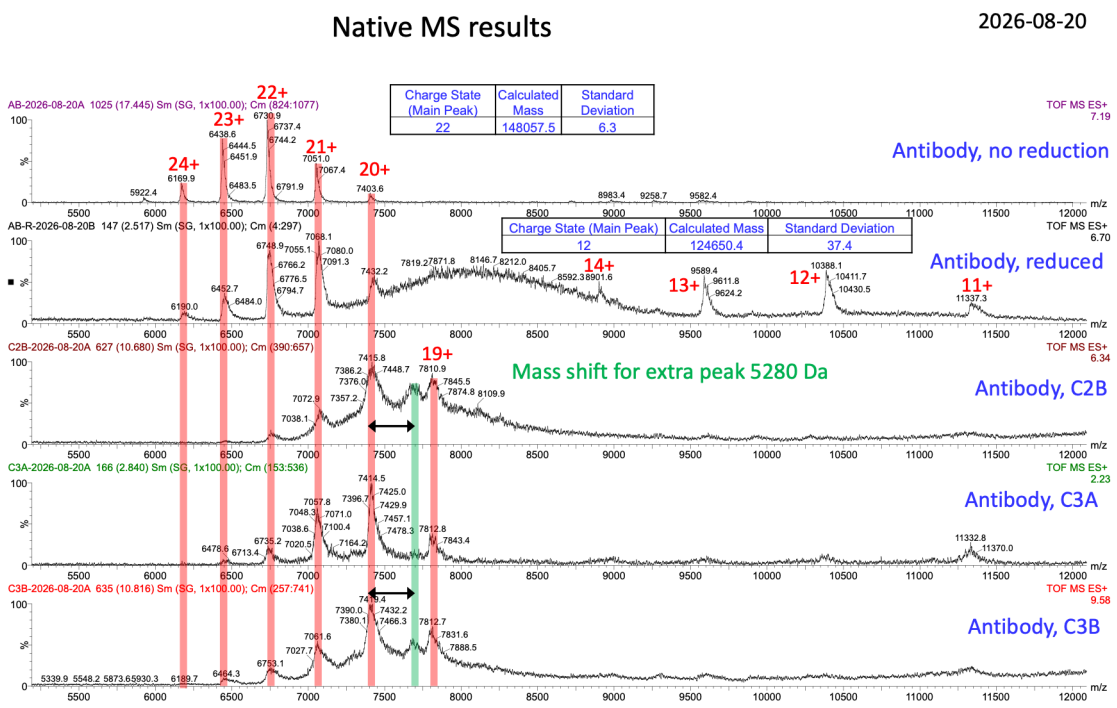


Figure 20. Native MS results from native trastuzumab, fully reduced antibody, ADC from C2b, C3a, C3b.

A larger-scale bioconjugation reaction under C2b conjugation condition was subsequently performed using twice the amount of antibody in order to generate sufficient ADC material for biological testing. Interestingly, the LC-MS analysis showed partial separation of antibody fragments with different degrees of conjugation (**Figure 21a**). Peak A was consistent with the species previously observed under condition C2b, containing LC+**OX05158** and HC+LC+2**OX05158** species. This suggests formation of the same DAR4 species observed in the small-scale reaction. Peak B contained not only species consistent with one **OX05158** modification on the light chain and one modification on the heavy chain, but also a species corresponding to HC+3**OX05158**. This indicates that up to three payload molecules may have been conjugated to a single heavy chain. This could happen as partial reduction of interchain disulfide bonds can generate multiple reactive cysteine residues, and conjugation to these sites is not expected to be fully site selective.

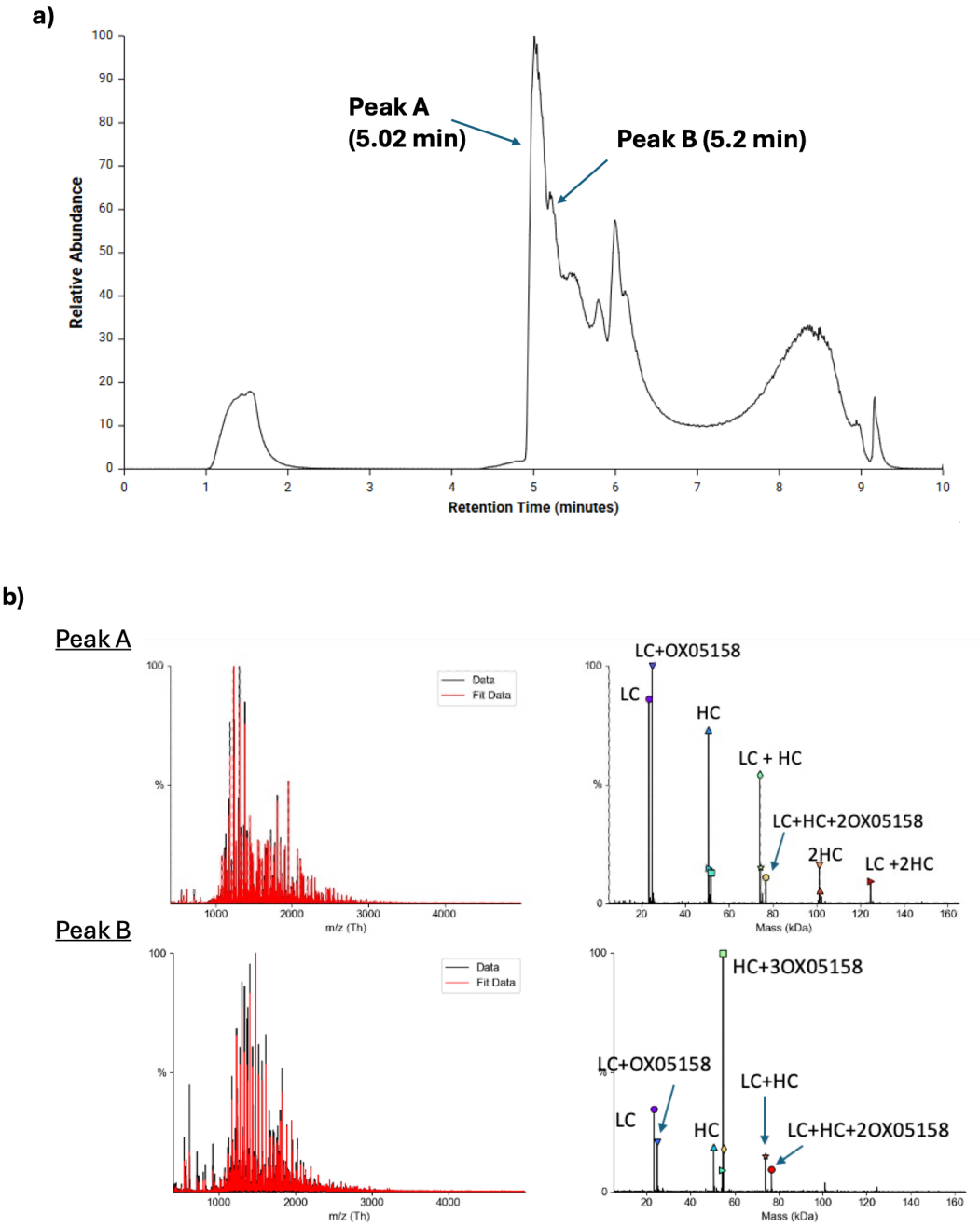


Figure 21. a) LC trace of the large-scale bioconjugation performed under condition C2b. b) Deconvoluted mass spectra of peaks A and B.

The sample was then analysed by native mass spectrometry to estimate the DAR of the resulting ADC (**Figure 22**). In the zoomed-in native mass spectrum, two protein species were observed despite the relatively low resolution. The average mass shift was approximately 5400 Da, which is consistent with the formation of a DAR4 species. Other

lower-DAR species, such as DAR1, DAR2 and DAR3, may also be present but could not be clearly resolved. This is because the mass shift per charge state is relatively small. For example, at a 20+ charge state, a DAR1 species would correspond to a shift of only approximately 70 Da, which may overlap with the broad peak corresponding to unconjugated antibody. Based on the relative intensity of the observed DAR4 peak, the average DAR of the resulting ADC was estimated to be approximately 0.8.

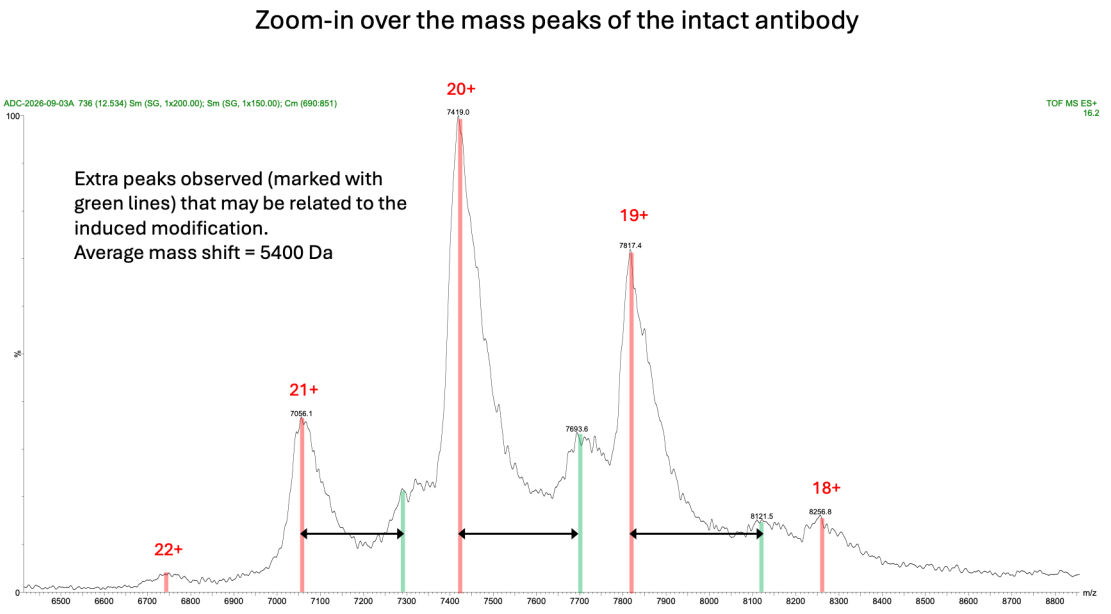


Figure 22. Zoomed-in native mass spectrum of the ADC produced from the large-scale bioconjugation reaction.

During native MS data collection, two aliquots of the same ADC sample were prepared in separate Eppendorf tubes for buffer exchange, labelled A and B. A mass shift consistent with conjugation was observed in sample A, whereas no clear mass shift was observed in sample B (**Figure 16S**). This difference may be related to the high ion activation energy required to promote gas-phase desolvation of antibody ions during native MS analysis. While increased activation can improve desolvation, it can also promote partial dissociation of the reduced antibody complex, for example through loss

of a single light chain. It may also contribute to partial loss of non-covalently retained adducts or labile modifications during analysis. Therefore, the absence of a clear mass shift in sample B may reflect differences in ionisation, desolvation or gas-phase stability rather than a true absence of conjugated species. Further repeat measurements would be required to confirm the estimated DAR 0.8 as there could potentially be more conjugated ADC, but they are cleaved during the ionisation.

Conclusion

In this project, four **JDH-06-040**-based antibody-degrader pre-conjugates were successfully designed and synthesised as proof-of-concept payloads for the targeted delivery of a pan-LMO degrader. To investigate different intracellular release strategies, linker systems based on GSH-mediated reduction and cathepsin B-mediated cleavage were developed. In addition, a PEG8-containing pre-conjugate was synthesised to improve aqueous solubility. An alternative phosphatase-responsive phosphate linker was also investigated. However, incomplete benzyl deprotection of the phosphate intermediate prevented the synthesis from being completed within the scope of this project.

Preliminary evaluation of the pre-conjugates demonstrated rapid reactivity towards glutathione, confirming their ability to undergo intracellular activation under reducing conditions. Among the four constructs, **OX05158** exhibited the greatest stability under physiological conditions together with superior aqueous solubility and was therefore selected for antibody conjugation. Bioconjugation conditions with the human IgG1 monoclonal antibody trastuzumab were successfully established and optimised. LC-MS analysis confirmed conjugation at the intended cysteine residues, while native mass

spectrometry estimated the resulting ADC to possess an average DAR of approximately 0.8.

Collectively, this work establishes a proof-of-concept antibody-drug conjugate platform for the targeted delivery of pan-LMO degraders. More importantly, the modular design enables the targeting antibody to be readily exchanged, allowing the same degrader payload to be redirected towards different tumour-associated antigens and LMO-driven cancers. This platform therefore provides a foundation for future biological evaluation and the development of next-generation targeted protein degradation therapies with improved tumour selectivity and reduced systemic toxicity.

Future work

Bioconjugation optimisation

A major challenge encountered during bioconjugation was the limited aqueous solubility of the pre-conjugates. In the GSH assay, the compounds remained soluble at concentrations of 50 μM for **OX05156** and 10 μM for **OX05157** and **OX05159**. In contrast, bioconjugation required a substantially higher pre-conjugate concentration of 168 μM, at which precipitation was observed. One potential optimisation would be to perform the bioconjugation at a lower pre-conjugate concentration to maintain solubility. However, increased dilution may reduce the reaction rate and require longer conjugation times. Prolonged incubation could potentially result in further loss of soluble pre-conjugate through either degradation or precipitation.

An alternative strategy would be to optimise the pH of the conjugation buffer. Adjustment to a mildly acidic pH (e.g. pH 6.9) could increase protonation of basic centres within the

pre-conjugates and potentially improve their aqueous solubility. The pH would need to remain compatible with both antibody stability and the cysteine-maleimide conjugation chemistry. Following bioconjugation, the resulting ADC could subsequently be exchanged into the PBS buffer at pH 7.4 for storage and further biological evaluation.

Phosphate chemistry optimisation

Complete removal of the benzyl protecting groups from the phosphate intermediate was not achieved during this project, preventing further progression of the phosphate-linker pre-conjugate design. Future work could therefore investigate alternative phosphate protecting groups, such as allyl groups, which can be removed under orthogonal Pd(0)-catalysed conditions in the presence of an allyl scavenger ($PhSiH_3$). However, potential coordination of the palladium catalyst by basic nitrogen centres within the degrader may lead to catalyst deactivation and would require further optimisation.

Alternatively, the synthetic sequence could be redesigned to avoid exposing the complete degrader scaffold to the deprotection conditions. The phosphate functionality could first be installed and deprotected on the dipeptide-linker fragment, followed by coupling to the glutarimide-containing fragment and subsequent late-stage amide coupling with carboxylic acid **5**. This approach would potentially reduce competing interactions during deprotection by avoiding basic centres within the complete degrader scaffold during phosphate deprotection.

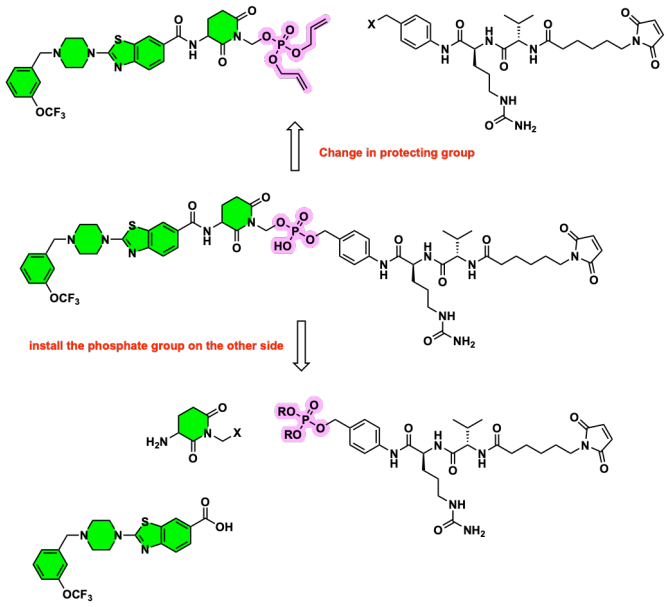


Figure 23. Proposed synthetic strategies for the installation of a phosphate linkage within the pre-conjugate.

Carbonate linkage optimisation

Although the carbonate linkage provided a straightforward synthetic route, they remain relatively underexplored in ADCs, and their *in vivo* stability has not been extensively characterised. In contrast, carbamate linkages are widely employed in clinically approved ADCs owing to their favourable chemical and plasma stability. A potential improvement to the current design would therefore be the introduction of an ethylenediamine as a 'SpacerLinker', enabling replacement of the carbonate linkage with a more stable carbamate group (**Figure 24**).

Following receptor-mediated internalisation and lysosomal processing of the ADC, cleavage of the Val-Cit or Val-Ala dipeptide linker would trigger spontaneous 1,6-elimination of the PAB spacer. The resulting ethylenediamine-containing intermediate is then proposed to undergo intramolecular cyclisation, generating one equivalent of 1,3-

dimethylimidazolidin-2-one. Subsequent spontaneous fragmentation with the release of formaldehyde would regenerate the active pan-LMO degrader.

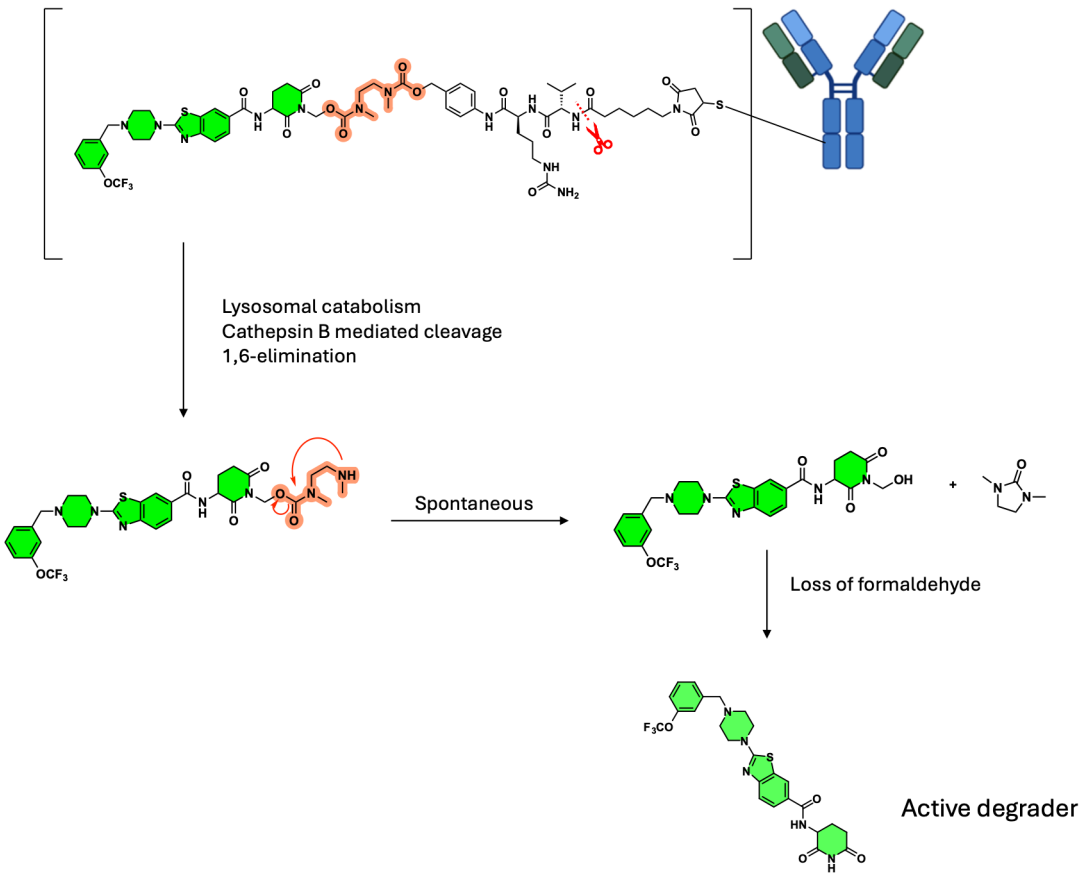


Figure 24. Proposed intracellular release mechanism of the dipeptide-containing ADC incorporating an additional cleavable SpacerLinker. L represents all the linker for maleimide handle and R is the either alanine or citrulline.

Cell testing with breast cancer cells

Due to time constraints, the resulting ADC was not evaluated in cell-based assays as part of this project. However, the Russell group is currently investigating its biological activity in the HER2-positive breast cancer cell lines SKBR3 and BT-474. These cell lines express HER2, which is required for antibody-mediated recognition and internalisation, as well as LMO4, the intended target protein of the degrader payload.

Future *in vitro* studies will assess whether treatment with the ADC leads to degradation of LMO4 in these cell lines. The effect of the ADC will be compared with treatment using trastuzumab alone and the unconjugated degrader alone. This will allow assessment of whether antibody-mediated delivery improves cellular uptake and enhances degradation activity relative to the free degrader. Cells will also be treated with the ADC at a range of concentrations to determine whether LMO4 degradation occurs in a dose-dependent manner.

Overexpression of LMO4 has previously been implicated in promoting trastuzumab resistance in HER2-positive breast cancer cells. Trastuzumab resistance represents a major therapeutic challenge, with *de novo* or acquired resistance reported in at least 70% of HER2-positive breast cancers.[99] More importantly, It has also been reported that downregulation of LMO4 can partially reverse trastuzumab resistance in trastuzumab-resistant breast cancer cell lines.[100] Therefore, in addition to testing the ADC in parental SKBR3 and BT-474 cells, future studies will investigate its activity in trastuzumab-resistant derivatives of these cell lines. This would help determine whether targeted degradation of LMO4 can enhance the response of HER2-positive breast cancer cells to trastuzumab-based therapy.

Bioconjugation with anti-CD7 antibody and testing *in vitro*

More biological evaluation of the constructs can be performed to utilise the pan-LMO degrader in different disease contexts. In addition to the HER2-targeted platform developed in this study, the four synthesised pre-conjugates could also be conjugated to an anti-CD7 monoclonal antibody to target T-cell acute lymphoblastic leukaemia (T-ALL), where LMO2 is a well-established oncogenic driver. This work will be carried out in collaboration with the Rabbitts Group at the Institute of Cancer Research (ICR).

The resulting anti-CD7 ADCs will first be evaluated for their ability to selectively bind and internalise into CD7-positive cells. Internalisation assays, combined with confocal microscopy and time-lapse imaging, will be used to confirm receptor-specific uptake following antibody binding. Following successful internalisation, the biological activity of the degrader payload will be assessed using A549-CD7 cells expressing LMO2-luciferase fusion constructs, enabling degradation efficiency to be quantified through luciferase turnover assays. Degradation of endogenous LMO2 protein will also be confirmed by western blot analysis. Since this is targeting blood cells, the stability of the resulting ADCs in blood stream should also be tested.

Subject to successful *in vitro* evaluation, the therapeutic potential of the ADCs will be further investigated *in vivo* using human CD7 transgenic (hCD7 Tg) mice, which express human CD7 on leukocytes, particularly within the spleen. Finally, efficacy studies in T-ALL cell line-derived xenograft models will determine whether targeted delivery of the pan-LMO degrader can achieve selective LMO degradation and antitumour activity while minimising systemic toxicity.[98]

References

1. H. Sung, J. Ferlay, R. L. Siegel, M. Laversanne, I. Soerjomataram, A. Jemal and F. Bray, *CA: A Cancer Journal for Clinicians*, 2021, **71**, 209-249.
2. B. Liu, H. Zhou, L. Tan, K. T. H. Siu and X.-Y. Guan, *Signal Transduction and Targeted Therapy*, 2024, **9**.
3. X. Sun, Q. Zhang, X. Lin, P. Shu, X. Gao and K. Shen, *Cell Death & Disease*, 2023, **14**.
4. F. Skoulidis, B. T. Li, G. K. Dy, T. J. Price, G. S. Falchook, J. Wolf, A. Italiano, M. Schuler, H. Borghaei, F. Barlesi, T. Kato, A. Curioni-Fontecedro, A. Sacher, A. Spira, S. S. Ramalingam, T. Takahashi, B. Besse, A. Anderson, A. Ang, Q. Tran, O. Mather, H. Henary, G. Ngarmchamnanrith, G. Friberg, V. Velcheti and R. Govindan, *New England Journal of Medicine*, 2021, **384**, 2371-2381.
5. M.-X. Wang, P. Zhu, Y. Shi, Q.-M. Sun and W.-H. Dong, *World Journal of Clinical Cases*, 2024, **12**, 5805-5813.
6. U. S. F. a. D. Administration, FDA approves vepdegestrant for ER-positive, HER2-negative, ESR1-mutated advanced or metastatic breast cancer, https://www.fda.gov/drugs/resources-information-approved-drugs/fda-approves-vepdegestrant-er-positive-her2-negative-esr1-mutated-advanced-or-metastatic-breast).
7. U. Rix and G. Superti-Furga, *Nature Chemical Biology*, 2009, **5**, 616-624.
8. S. M. Swain, M. Shastry and E. Hamilton, *Nature Reviews Drug Discovery*, 2023, **22**, 101-126.
9. Z. Wang, J. Li, J. Guo and P. Wei, *Frontiers in Pharmacology*, 2024, **15**.
10. M. Shastry, A. Gupta, S. Chandarlapaty, M. Young, T. Powles and E. Hamilton, *American Society of Clinical Oncology Educational Book*, 2023, DOI: 10.1200/edbk_390094.
11. G. Zhong, X. Chang, W. Xie and X. Zhou, *Signal Transduction and Targeted Therapy*, 2024, **9**.
12. M. Békés, D. R. Langley and C. M. Crews, *Nature Reviews Drug Discovery*, 2022, **21**, 181-200.
13. A. D. Buhimschi, H. A. Armstrong, M. Toure, S. Jaime-Figueroa, T. L. Chen, A. M. Lehman, J. A. Woyach, A. J. Johnson, J. C. Byrd and C. M. Crews, *Biochemistry*, 2018, **57**, 3564-3575.
14. Y. Shorer Arbel, B.-Z. Katz, R. Gabizon, A. Shraga, Y. Bronstein, T. Kamdjou, A. Globerson Levin, C. Perry, I. Avivi, N. London and Y. Herishanu, *Frontiers in Oncology*, 2021, **11**.
15. L. Zhao, J. Zhao, K. Zhong, A. Tong and D. Jia, *Signal Transduction and Targeted Therapy*, 2022, **7**.
16. N. K. Van Overbeek, T. Aguirre, G. J. Van Der Heden Van Noort, B. Blagoev and A. C. O. Vertegaal, *Frontiers in Molecular Biosciences*, 2024, **10**.
17. L. Deng, T. Meng, L. Chen, W. Wei and P. Wang, *Signal Transduction and Targeted Therapy*, 2020, **5**.
18. Z. Liu, M. Hu, Y. Yang, C. Du, H. Zhou, C. Liu, Y. Chen, L. Fan, H. Ma, Y. Gong and Y. Xie, *Molecular Biomedicine*, 2022, **3**.
19. S. L. Schreiber, *Cell*, 2021, **184**, 3-9.
20. X. Sun, H. Gao, Y. Yang, M. He, Y. Wu, Y. Song, Y. Tong and Y. Rao, *Signal Transduction and Targeted Therapy*, 2019, **4**.

21. M. Girardini, C. Maniaci, S. J. Hughes, A. Testa and A. Ciulli, *Bioorganic & Medicinal Chemistry*, 2019, **27**, 2466-2479.
22. G. Fan, S. Chen, Q. Zhang, N. Yu, Z. Shen, Z. Liu, W. Guo, Z. Tang, J. Yang and M. Liu, *MedComm*, 2025, **6**.
23. M. Pettersson and C. M. Crews, *Drug Discovery Today: Technologies*, 2019, **31**, 15-27.
24. C. A. Lipinski, F. Lombardo, B. W. Dominy and P. J. Feeney, *Advanced Drug Delivery Reviews*, 2001, **46**, 3-26.
25. C. Cecchini, S. Pannilunghi, S. Tardy and L. Scapozza, *Frontiers in Chemistry*, 2021, **9**.
26. J. S. Scott, I. N. Michaelides and M. Schade, *RSC Medicinal Chemistry*, 2025, **16**, 449-456.
27. L. Silvian, *npj Drug Discovery*, 2026, **3**.
28. I. Bach, *Mechanisms of Development*, 2000, **91**, 5-17.
29. M. Sang, L. Ma, M. Sang, X. Zhou, W. Gao and C. Geng, *Molecular Biology Reports*, 2014, **41**, 1067-1073.
30. I. B. Dawid, J. J. Breen and R. Toyama, *Trends in Genetics*, 1998, **14**, 156-162.
31. T. Boehm, L. Foroni, M. Kennedy and T. H. Rabbitts, *Oncogene*, 1990, **5**, 1103-1105.
32. J. Chambers and T. H. Rabbitts, *Open Biology*, 2015, **5**, 150062.
33. M. Aoyama, T. Ozaki, H. Inuzuka, D. Tomotsune, J. Hirato, Y. Okamoto, H. Tokita, M. Ohira and A. Nakagawara, *Cancer Research*, 2005, **65**, 4587-4597.
34. J. E. Visvader, D. Venter, K. Hahm, M. Santamaria, E. Y. M. Sum, L. O'Reilly, D. White, R. Williams, J. Armes and G. J. Lindeman, *Proceedings of the National Academy of Sciences*, 2001, **98**, 14452-14457.
35. E. Y. M. Sum, D. Segara, B. Duscio, M. L. Bath, A. S. Field, R. L. Sutherland, G. J. Lindeman and J. E. Visvader, *Proceedings of the National Academy of Sciences*, 2005, **102**, 7659-7664.
36. V. E. Archer, J. Breton, I. Sanchez-Garcia, H. Osada, A. Forster, A. J. Thomson and T. H. Rabbitts, *Proceedings of the National Academy of Sciences*, 1994, **91**, 316-320.
37. I. A. Wadman, *The EMBO Journal*, 1997, **16**, 3145-3157.
38. E. Lécuyer, S. Larivière, M.-C. Sincennes, A. Haman, R. Lahlil, M. Todorova, M. Tremblay, B. C. Wilkes and T. Hoang, *Journal of Biological Chemistry*, 2007, **282**, 33649-33658.
39. K. El Omari, S. J. Hoosdally, K. Tuladhar, D. Karia, P. Vyas, R. Patient, C. Porcher and E. J. Mancini, *Blood*, 2011, **117**, 2146-2156.
40. Kamel, Sarah, K. Tuladhar, D. Karia, E. Hall-Ponselé, O. Platonova, P. Vyas, R. Patient, C. Porcher and Erika, *Cell Reports*, 2013, **4**, 135-147.
41. H. Sewell, T. Tanaka, K. E. Omari, E. J. Mancini, A. Cruz, N. Fernandez-Fuentes, J. Chambers and T. H. Rabbitts, *Scientific Reports*, 2014, **4**.
42. C. H. Nam, M. N. Lobato, A. Appert, L. F. Drynan, T. Tanaka and T. H. Rabbitts, *Oncogene*, 2008, **27**, 4962-4968.
43. T. Morishima, A.-C. Krahl, M. Nasri, Y. Xu, N. Aghaallaei, B. Findik, M. Klimiankou, M. Ritter, M. D. Hartmann, C. J. Gloeckner, S. Stefanczyk, C. Lindner, B. Oswald, R. Bernhard, K. Hähnel, U. Hermanutz-Klein, M. Ebinger, R. Handgretinger, N. Casadei, K. Welte, M. Andre, P. Müller, B. Bajoghli and J. Skokowa, *Blood*, 2019, **134**, 1159-1175.

44. M. P. McCormack, A. Forster, L. Drynan, R. Pannell and T. H. Rabbitts, *Molecular and Cellular Biology*, 2003, **23**, 9003-9013.
45. S. Herblot, A.-M. Steff, P. Hugo, P. D. Aplan and T. Hoang, *Nature Immunology*, 2000, **1**, 138-144.
46. A. A. Ferrando and A. T. Look, *Seminars in Hematology*, 2003, **40**, 274-280.
47. M. E. Montañez-Wiscovich, D. D. Seachrist, M. D. Landis, J. Visvader, B. Andersen and R. A. Keri, *Oncogene*, 2009, **28**, 3608-3618.
48. X. Zhou, M. Sang, W. Liu, W. Gao, E. Xing, W. Lü, Y. Xu, X. Fan, S. Jing and B. Shan, *Life Sciences*, 2012, **91**, 358-363.
49. Z. Lu, K. S. Lam, N. Wang, X. Xu, M. Cortes and B. Andersen, *Oncogene*, 2006, **25**, 2920-2930.
50. G. Villacampa, T. Pascual, P. Tarantino, J. Cortés, J. Perez-García, A. Llombart-Cussac, P. Conte, M. Mancino, V. Guarneri, M. V. Dieci, A. G. Waks, F. Schettini, F. Brasó-Maristany, G. Griguolo, B. A. De Castro, C. Reboredo, S. Antolín, C. Bueno-Muiño, I. Echavarría, S. López-Tarruella, T. Massarrah, M. Del Monte-Millán, M. Martín, W. Buckingham, J. S. Parker, A. Vivancos, K. Polyak, O. M. Filho, A. C. Wolff, A. Demichele, N. M. Tung, C. M. Perou, L. Paré, P. Villagrasa, A. Prat and S. M. Tolaney, *The Lancet Oncology*, 2025, **26**, 1100-1112.
51. K. Ding, Z. Wu, X. Li, Y. Sheng, X. Wang and S. Tan, *American Journal of Cancer Research*, 2018, **2018;8**, 594-609.
52. A. Zafar, S. Khatoon, M. J. Khan, J. Abu and A. Naeem, *Discover Oncology*, 2025, **16**.
53. P. G. Corrie, *Medicine*, 2008, **36**, 24-28.
54. K. Strebhardt and A. Ullrich, *Nature Reviews Cancer*, 2008, **8**, 473-480.
55. C. Peters and S. Brown, *Bioscience Reports*, 2015, **35**, e00225-e00225.
56. K. Tsuchikama, Y. Anami, S. Y. Y. Ha and C. M. Yamazaki, *Nature Reviews Clinical Oncology*, 2024, **21**, 203-223.
57. M. J. Birrer, K. N. Moore, I. Betella and R. C. Bates, *JNCI: Journal of the National Cancer Institute*, 2019, **111**, 538-549.
58. A. Samantasinghar, N. P. Sunildutt, F. Ahmed, A. M. Soomro, A. R. C. Salih, P. Parihar, F. H. Memon, K. H. Kim, I. S. Kang and K. H. Choi, *Biomedicine & Pharmacotherapy*, 2023, **161**, 114408.
59. A. Yadav, M. K. Mandal and K. K. Dubey, *Indian Journal of Microbiology*, 2020, **60**, 511-517.
60. Y. Matsuda and B. A. Mendelsohn, *Chemical and Pharmaceutical Bulletin*, 2021, **69**, 976-983.
61. A. Sarkar and G. Kellogg, *Current Topics in Medicinal Chemistry*, 2010, **10**, 67-83.
62. A. Falanga, R. Bellavita, S. Braccia and S. Galdiero, *Journal of Peptide Science*, 2024, **30**.
63. F. Giugliano, C. Corti, P. Tarantino, F. Michelini and G. Curigliano, *Current Oncology Reports*, 2022, **24**, 809-817.
64. Y. Wang, X. Cheng, X. Li, W. Chen, X. Zhang and Y. Liu, *Critical Reviews in Oncology/Hematology*, 2025, **216**, 104979.
65. Y. Ogitani, K. Hagihara, M. Oitate, H. Naito and T. Agatsuma, *Cancer Science*, 2016, **107**, 1039-1046.
66. D. Su and D. Zhang, *Frontiers in Pharmacology*, 2021, **12**.
67. K. Tsuchikama and Z. An, *Protein & Cell*, 2018, **9**, 33-46.

68. M. Walles, A. Connor and D. Hainzl, *Current Topics in Medicinal Chemistry*, 2018, **17**, 3463-3475.
69. F. P. Olatunji, J. W. Herman, B. N. Kesic, D. Olabode and C. E. Berkman, *Tetrahedron Letters*, 2020, **61**, 152398.
70. S. Balamkundu and C.-F. Liu, *Biomedicines*, 2023, **11**, 3080.
71. R. Sheyi, B. G. De La Torre and F. Albericio, *Pharmaceutics*, 2022, **14**, 396.
72. Y. Matsuda, J. R. Chang and B. A. Mendelsohn, *ChemBioChem*, 2025, **26**.
73. Y. Ogitani, T. Aida, K. Hagihara, J. Yamaguchi, C. Ishii, N. Harada, M. Soma, H. Okamoto, M. Oitate, S. Arakawa, T. Hirai, R. Atsumi, T. Nakada, I. Hayakawa, Y. Abe and T. Agatsuma, *Clinical Cancer Research*, 2016, **22**, 5097-5108.
74. Y. Anami, C. M. Yamazaki, W. Xiong, X. Gui, N. Zhang, Z. An and K. Tsuchikama, *Nature Communications*, 2018, **9**.
75. S. C. Jeffrey, J. B. Andreyka, S. X. Bernhardt, K. M. Kissler, T. Kline, J. S. Lenox, R. F. Moser, M. T. Nguyen, N. M. Okeley, I. J. Stone, X. Zhang and P. D. Senter, *Bioconjugate Chemistry*, 2006, **17**, 831-840.
76. J. D. Bargh, S. J. Walsh, A. Isidro-Llobet, S. Omarjee, J. S. Carroll and D. R. Spring, *Chemical Science*, 2020, **11**, 2375-2380.
77. J. C. Kern, M. Cancilla, D. Dooney, K. Kwasnjuk, R. Zhang, M. Beaumont, I. Figueroa, S. Hsieh, L. Liang, D. Tomazela, J. Zhang, P. E. Brandish, A. Palmieri, P. Stivers, M. Cheng, G. Feng, P. Geda, S. Shah, A. Beck, D. Bresson, J. Firdos, D. Gately, N. Knudsen, A. Manibusan, P. G. Schultz, Y. Sun and R. M. Garbaccio, *Journal of the American Chemical Society*, 2016, **138**, 1430-1445.
78. H.-G. Lerchen, B. Stelte-Ludwig, A. Sommer, S. Berndt, A.-S. Rebstock, S. Johannes, C. Mahlert, S. Greven, L. Dietz and H. Jörißen, *Bioconjugate Chemistry*, 2020, **31**, 1893-1898.
79. R. V. J. Chari, *Accounts of Chemical Research*, 2007, **41**, 98-107.
80. A. C. Lazar, L. Wang, W. A. Blättler, G. Amphlett, J. M. Lambert and W. Zhang, *Rapid Communications in Mass Spectrometry*, 2005, **19**, 1806-1814.
81. S. O. Doronina, B. E. Toki, M. Y. Torgov, B. A. Mendelsohn, C. G. Cerveny, D. F. Chace, R. L. Deblanc, R. P. Gearing, T. D. Bovee, C. B. Siegall, J. A. Francisco, A. F. Wahl, D. L. Meyer and P. D. Senter, *Nature Biotechnology*, 2003, **21**, 778-784.
82. K. Liu, M. Li, Y. Li, Y. Li, Z. Chen, Y. Tang, M. Yang, G. Deng and H. Liu, *Molecular Cancer*, 2024, **23**.
83. Y. Cheng, J. Lu, C. Zhang, W. Yan, P. Zhu, Q. Qin and L. Gong, *Antibody Therapeutics*, 2025, **8**, 124-144.
84. M. A. Maneiro, N. Forte, M. M. Shchepinova, C. S. Kounde, V. Chudasama, J. R. Baker and E. W. Tate, *ACS Chemical Biology*, 2020, **15**, 1306-1312.
85. Y. Gu, C. Li, Y. Zhao, T. Xu, Y. Zhu, D. Wang, X. Wang, J. Chen, J. Li and X. Guan, *Cell Reports Medicine*, 2026, **7**, 102948.
86. N. Bery, C. J. R. Bataille, A. Russell, A. Hayes, F. Raynaud, S. Milhas, S. Anand, H. Tulmin, A. Miller and T. H. Rabbitts, *Science Advances*, 2021, **7**, eabg1950.
87. N. Sereesongsaeng, C. Bataille, A. Russell, N. Bery, F. J. Sialana, J. Choudhary, A. Miller and T. Rabbitts, *eLife*, 2025, **14**, RP106699.
88. M. H. Lee, Z. Yang, C. W. Lim, Y. H. Lee, S. Dongbang, C. Kang and J. S. Kim, *Chemical Reviews*, 2013, **113**, 5071-5109.

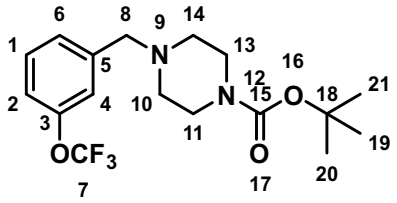
89. T. H. Pillow, J. D. Sadowsky, D. Zhang, S.-F. Yu, G. Del Rosario, K. Xu, J. He, S. Bhakta, R. Ohri, K. R. Kozak, E. Ha, J. R. Junutula and J. A. Flygare, *Chemical Science*, 2017, **8**, 366-370.
90. K. Chan, P. S. Sathyamurthi, M. A. Queisser, M. Mullin, H. Shrives, D. M. Coe and G. A. Burley, *Bioconjugate Chemistry*, 2023, **34**, 2049-2054.
91. S. Li, Y. Guo, J. Che, H. Dai and X. Dong, *Journal of Medicinal Chemistry*, 2025, **68**, 19871-19892.
92. J. M. J. M. Ravasco, H. Faustino, A. Trindade and P. M. P. Gois, *Chemistry – A European Journal*, 2019, **25**, 43-59.
93. P. G. M. Wuts and T. W. Greene, in *Greene's Protective Groups in Organic Synthesis*, 2006, DOI: https://doi.org/10.1002/9780470053485.ch7, pp. 696-926.
94. J. C. Kern, D. Dooney, R. Zhang, L. Liang, P. E. Brandish, M. Cheng, G. Feng, A. Beck, D. Bresson, J. Firdos, D. Gately, N. Knudsen, A. Manibusan, Y. Sun and R. M. Garbaccio, *Bioconjugate Chemistry*, 2016, **27**, 2081-2088.
95. A. Zhang, K. Seiss, L. Laborde, S. Palacio-Ramirez, D. Guthy, M. Lanter, J. Lorber, A. Vulpetti, L. Arista, T. Zoller, T. Radimerski, C. Thoma, C. Hebach, W. R. Tschantz, A. Karpov, G. J. Hollingworth, J. A. D'Alessio, S. Ferretti and M. T. Burger, *Bioconjugate Chemistry*, 2024, **35**, 140-146.
96. P. G. M. Wuts and T. W. Greene, in *Greene's Protective Groups in Organic Synthesis*, 2014, DOI: https://doi.org/10.1002/9781118905074.ch09, pp. 1203-1262.
97. T. Tanaka, T. Sakata, K. Fujimoto and M. Ikehara, *Nucleic Acids Research*, 1987, **15**, 6209-6224.
98. J. Zhang, A. Jain, S. Milhas, D. J. Williamson, J. Mysliwy, A. Lodge, J. Thirlway, M. Al Nakeeb, A. Miller and T. H. Rabbitts, *Leukemia Research*, 2021, **108**, 106626.
99. H. Korkaya, G.-I. Kim, A. Davis, F. Malik, N, S. Ithimakin, Ahmed, N. Tawakkol, R. D'Angelo, A. K. Paulson, S. Chung, T. Luther, Hayley, S. Liu, K. A. Hassan, Q. Zen, Shawn and Max, *Molecular Cell*, 2012, **47**, 570-584.
100. K. Ding, Z. Wu, X. Li, Y. Sheng, X. Wang and S. Tan, *Am J Cancer Res*, 2018, **8**, 594-609.
101. L. R. Staben, S. G. Koenig, S. M. Lehar, R. Vandlen, D. Zhang, J. Chuh, S.-F. Yu, C. Ng, J. Guo, Y. Liu, A. Fourie-O'Donohue, M. Go, X. Linghu, N. L. Segraves, T. Wang, J. Chen, B. Wei, G. D. L. Phillips, K. Xu, K. R. Kozak, S. Mariathasan, J. A. Flygare and T. H. Pillow, *Nature Chemistry*, 2016, **8**, 1112-1119.
102. C. Wu, Z. Cheng, D. Lu, K. Liu, Y. Cheng, P. Wang, Y. Zhou, M. Li, X. Shao, H. Li, W. Su and L. Fang, *Journal of Medicinal Chemistry*, 2021, **64**, 991-1000.

Experimental

All reactions involving moisture-sensitive reagents were carried out under a nitrogen atmosphere. Water was purified by a Suez® Select Fusion System. All solvents and reagents were purchased from commercial sources (analytical or HPLC grade) and used without prior purification. Brine refers to a sat. aq. solution of NaCl. *In vacuo* refers to the use of a rotary evaporator attached to a diaphragm pump. All reactions were carried out using an oven-dried flask under a nitrogen atmosphere or in a sealed Biotage® microwave vial unless otherwise stated. Mixtures of solvents were used; ratios are reported by volume. TLC was performed on Merck aluminium plates coated with 60 F254 silica and was visualised using UV light (254 or 364nm), or by KMnO4 and ninhydrin staining. Flash column chromatography was performed on Biotage® isolera system using prepacked columns. Melting points were recorded on Gallenkamp Hot Stage apparatus and are uncorrected. Infrared spectra were recorded on a Bruker Tensor 27 FT-IR spectrometer, as thin films. Selected characteristic peaks are reported in wavenumbers v (cm'). NMR spectra were recorded on Bruker Avance II HD nanobay NMR equipped with a 9.4T magnet (AVG400 and AVH400) or Bruker NEO 600 with broadband helium cryoprobe equipped with a 14.1T magnet (NEO600) in the deuterated solvent stated. Data were analysed using MestReNova software and reported as follows: chemical shift (in ppm), multiplicity (s= singlet, d = doublet, t = triplet, q = quartet and m = multiplet), integration, coupling constant (J in Hz), and assignment. Accurate mass measurements were performed on an ACQUITY I-Class PLUS UPLC System (Waters) coupled to an ACQUITY RDa mass spectrometer (Waters) equipped with an ESI probe, from solutions of MeOH. m/z values are given in Daltons (Da). High resolution mass spectra were run on a Bruker micro TOF (ESI) by the mass spectrometry department of the Chemistry Research Laboratory, University of Oxford.

Synthesis of Intermediates

tert-Butyl 4-(3-(trifluoromethoxy)benzyl)piperazine-1-carboxylate (2)



Chemical Formula: $C_{17}H_{23}F_3N_2O_3$
Exact Mass: 360.1661
Molecular Weight: 360.3772

To a solution of 1-(bromomethyl)-3-(trifluoromethoxy)benzene **1** (3.96 mL, 24.2 mmol, 1 eq.) and K_2CO_3 (1.7 g, 62 mmol) in acetonitrile (25 mL), *tert*-butyl piperazine-1-carboxylate (5.0 g, 27 mmol, 1.1 eq.) was added dropwise. The reaction was stirred at room temperature for 19 hours. The reaction was quenched with 50% brine in water, extract with EtOAc. The combined organic layer was dried with $MgSO_4$ and concentrated *in vacuo*. The crude product was purified by flash column chromatography (50% EtOAc in pentane) to afford the title product as a colourless oil (6.90 g, 78%).

^{1}H NMR (400 MHz, $CDCl_3$) δ 7.33 (t, *J* = 7.8 Hz, 1H, C_1-H), 7.25 – 7.20 (m, 2H, $C_{2,4}$-H), 7.10 (ddt, *J* = 8.1, 2.5, 1.2 Hz, 1H, C_6-H), 3.51 (s, 2H, C_8-H), 3.43 (t, *J* = 5.1 Hz, 4H, $C_{11,13}$-H), 2.38 (t, *J* = 5.1 Hz, 4H, $C_{10,14}$-H), 1.45 (s, 9H, $C_{19,20,21}$-H).

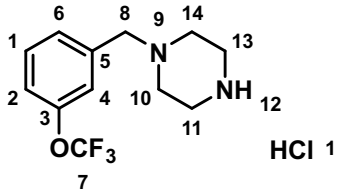
^{13}C NMR (101 MHz, $CDCl_3$) δ 154.92 (C_{15}), 149.55 (C_3), 140.73 (C_5), 129.70 (C_1), 127.33 ($C_{2\text{ or }4}$), 121.90(C_7), 121.42 ($C_{2\text{ or }4}$), 119.69 (C_6), 119.34 (C_7), 79.75 (C_{18}), 62.42 (C_8), 52.98 ($C_{10,14}$), 28.55 ($C_{19,20,21}$).

^{19}F NMR (377 MHz, $CDCl_3$) δ -57.75.

HRMS (ESI): m/z $[M + H]^+$ calcd. for $C_{17}H_{24}F_3N_2O_3$: 361.1734 Found: 361.1747

IR (vmax/cm^{-1}) 1696 (carbamate C=O), 1246 (C-O), 1216 (C-F), 1165 (C-N)

1-(3-(Trifluoromethoxy)benzyl)piperazine hydrochloride (3)



Chemical Formula: $C_{12}H_{16}ClF_3N_2O$
Exact Mass: 296.0903
Molecular Weight: 296.7182

To a solution of **2** (6.88 g, 19.1 mmol) in MeOH (20 mL) under nitrogen, 2 M HCl in 1,4-dioxane (20 mL) was added under nitrogen. The reaction was stirred for 18 hours. The reaction mixture was concentrated *in vacuo* to afford the title product as white solids (5.61 g, 99%). The crude product was carried to next step without further purification.

^{1}H NMR (400 MHz, MeOD) δ 7.72 – 7.59 (m, 3H, $C_{1,2,4}$-H), 7.45 (ddt, *J* = 8.2, 2.3, 1.1 Hz, 1H, C_6-H), 4.59 (s, 2H, C_8-H), 3.66 (s, 8H, $C_{10,11,13,14}$-H).

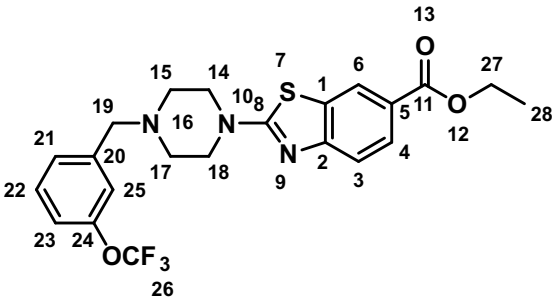
^{13}C NMR (101 MHz, MeOD) δ 149.92 (C_3), 130.92 (C_1), 130.07 (C_6), 123.76 ($C_{2\text{ or }4}$), 122.47($C_{2\text{ or }4}$), 59.40 (C_8), 48.11 ($C_{10,14}$), 40.79 ($C_{11,13}$)

^{19}F NMR (376 MHz, MeOD) δ -59.36

HRMS (ESI): m/z $[M + Na]^+$ calcd. for $C_{12}H_{16}ClF_3N_2ONa$: 319.0795 Found: 319.0807

IR (vmax/cm^{-1}) 1223 (C-O), 1154 (C-N)

Ethyl 2-(4-(3-(trifluoromethoxy)benzyl)piperazin-1-yl)benzo[*d*]thiazole-6-carboxylate (4)



Chemical Formula: $C_{22}H_{22}F_3N_3O_3S$
Exact Mass: 465.1334
Molecular Weight: 465.4912

To a solution of **3** (5.0 g, 15 mmol, 1.2 eq.), ethyl 2-chlorobenzo[*d*]thiazole-6-carboxylate (2.67 g, 12.5 mol, 1 eq.) and DIPEA (8.7 mL) in 1,4-dioxane (80 mL). The reaction was stirred at 100 °C for 18 hours. The reaction mixture was concentrated *in vacuo*. The crude was purified by flash column chromatography (10 % MeOH in CH_2Cl_2) to afford the titled product as a brown solid (4.05 g, 70%).

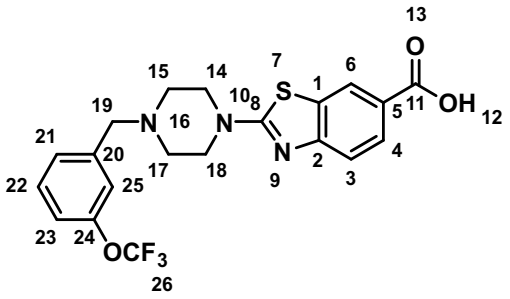
^{1}H NMR (400 MHz, MeOD) δ 8.33 (d, *J* = 1.7 Hz, 1H, C_6-H), 7.95 (dd, *J* = 8.5, 1.7 Hz, 1H, C_4-H), 7.51 – 7.31 (m, 4H, $C_{3,21,23,25}$-H), 7.23 – 7.16 (m, 1H, C_{22}-H), 4.36 (q, *J* = 7.1 Hz, 2H, C_{27}-H), 3.75 – 3.68 (m, 4H, $C_{14,18}$-H), 3.65 (s, 2H, C_{19}-H), 2.63 (m, 4H, $C_{15,17}$-H), 1.39 (t, *J* = 7.2 Hz, 3H, C_{28}-H).

^{19}F NMR (377 MHz, MeOD) δ -59.39.

HRMS (ESI): m/z $[M + H]^+$ calcd. for $C_{22}H_{22}F_3N_3O_3S$: 466.1407 Found: 466.1414

IR (vmax/cm^{-1}) 1698 (C=O),1438 (C-H),1263 (C-F), 1227 (C-N), 1157 (C-O)

2-(4-(3-(Trifluoromethoxy)benzyl)piperazin-1-yl)benzo[*d*]thiazole-6-carboxylic acid (5)



Chemical Formula: $C_{20}H_{18}F_3N_3O_3S$
Exact Mass: 437.1021
Molecular Weight: 437.4372

To a solution of **4** (4.1 g, 8.8 mmol, 1 eq.) in THF/EtOH/H2O (3:1:1, 80 mL). Add LiOH · H_2O(1.85 g, 44 mmol, 5 eq.) and stir for 18 hours at room temperature. The reaction mixture was concentrated *in vacuo* and acidified with 1M HCl to pH 5. The aqueous layer was extracted with EtOAc. The combined organic layer was dried with $MgSO_4$ and concentrated *in vacuo* to afford the titled product as a yellow solid (3.86 g, 99%).

^{1}H NMR (400 MHz, MeOD) δ 8.32 (d, *J* = 1.7 Hz, 1H, C_6-H), 7.96 (dd, *J* = 8.5, 1.8 Hz, 1H, C_4-H), 7.45 (dd, *J* = 16.1, 8.2 Hz, 2H, $C_{3,23}$-H), 7.38 (d, *J* = 7.7 Hz, 1H, C_{21}-H), 7.33 (s, 1H, C_{25}-H), 7.20 (d, *J* = 8.0 Hz, 1H, C_{22}-H), 3.71 (t, *J* = 5.1 Hz, 4H, $C_{14,18}$-H), 3.65 (s, 2H, C_{19}-H), 2.63 (t, *J* = 5.1 Hz, 4H, $C_{15,17}$-H).

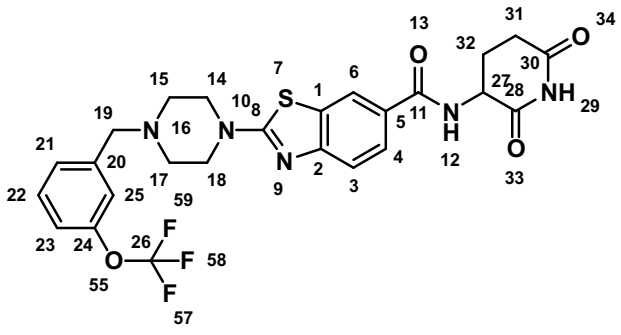
^{13}C NMR (101 MHz, MeOD) δ 171.22 (C_{11}), 156.12 (C_5), 149.32 (C_{24}), 140.34 (C_{20}), 130.27 ($C_{3\text{ or }22}$), 129.68 (C_4), 127.78 ($C_{1\text{ or }2}$), 127.63 (C_4), 122.71 (C_{25}), 121.20 (C_6), 119.53 (C_{23}), 117.53 ($C_{3\text{ or }22}$), 61.40 (C_{19}), 51.85 ($C_{15,17}$), 48.07 ($C_{14,18}$)

^{19}F NMR (376 MHz, MeOD) δ -59.39.

HRMS (ESI): m/z $[M + H]^+$ calcd. for $C_{20}H_{19}F_3N_3O_3S$: 438.1094 Found: 438.1100

IR (vmax/cm^{-1}) 1662 (C=O), 1525 (C=N), 1439 (O-H), 1215 (C-F)

***N*-(2,6-Dioxopiperidin-3-yl)-2-(4-(3-(trifluoromethoxy)benzyl)piperazin-1-yl)benzo[*d*]thiazole-6-carboxamide (JDH-06-040)**



Chemical Formula: $C_{25}H_{24}F_3N_5O_4S$
Exact Mass: 547.1501
Molecular Weight: 547.5532

To a solution of **5** (500 mg, 1.14 mmol, 1 eq.) in anhydrous DMF (1.5 mL), HATU (565 mg, 1.48 mmol) and DIPEA (0.2 mL, 1.15 mmol) was added. The solution was stirred for 30 minutes at room temperature. The activated **5** solution was added to 3-aminopiperidine-2,6-dione hydrochloride (282 mg, 1.72 mmol, 1.5 eq.) in DIPEA (1 mL, 5.72 mmol) and anhydrous DMF (1.5 mL). The reaction was stirred for 20 hours at room temperature. The rection mixture was directly purified with C18 reverse phase column chromatography (0-100% MeCN/H_2O gradient with 0.1% formic acid modifier) to afford the titled product as a yellow oil (0.23 g, 37%).

^{1}H NMR (400 MHz, DMSO) δ 10.85 (s, 1H, C_{29}-H), 8.68 (d, *J* = 8.3 Hz, 1H, C_{12}-H), 8.29 (d, *J* = 1.8 Hz, 1H, C_6-H), 7.82 (dd, *J* = 8.4, 1.8 Hz, 1H, C_4-H), 7.49 (dt, *J* = 7.9, 3.6 Hz, 2H, $C_{22,3}$-H), 7.38 (d, *J* = 7.7 Hz, 1H, C_{21}-H), 7.33 (s, 1H, C_{25}-H), 7.30 – 7.23 (m, 1H, C_{23}-H), 4.79 (ddd, *J* = 12.9, 8.3, 5.3 Hz, 1H, C_{27}-H), 3.65 – 3.59 (m, 6H, $C_{15,17,19}$-H), 2.80 (ddd, *J* = 18.0, 13.2, 5.5 Hz, 1H, C_{31}-H), 2.57 (d, *J* = 3.9 Hz, 1H, C_{31}-H), 2.53 (t, *J* = 5.0 Hz, 4H, $C_{14,18}$-H), 2.20 – 2.03 (m, 1H, C_{32}-H), 1.98 (ddq, *J* = 8.6, 5.6, 2.9 Hz, 1H, C_{32}-H).

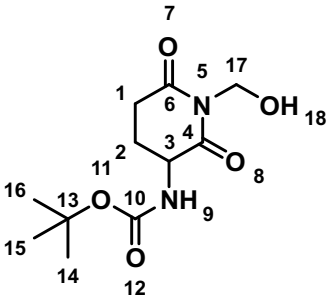
^{13}C NMR (101 MHz, DMSO) δ 170.19 (C_{11}), 166.18 (C_8), 165.36 (C_{28}), 161.54 (C_{30}), 155.50 (C_5), 148.97 (C_{24}), 141.40 (C_{20}), 130.82 ($C_{1\text{ or }2}$), 130.69 ($C_{3\text{ or }22}$), 128.29 (C_{21}), 127.15 ($C_{1\text{ or }2}$), 126.11(C_4), 121.86 (C_{26}), 121.39 (C_{25}), 121.27 (C_6), 120.01 (C_{23}), 119.31 (C_{26}), 118.16 ($C_{3\text{ or }22}$), 61.25 (C_{19}), 52.17 ($C_{14,18}$), 50.03 (C_{27}), 48.49 ($C_{15,17}$), 31.48 (C_{32}), 24.76 (C_{31}).

^{19}F NMR (377 MHz, DMSO) δ -56.63.

HRMS (ESI): m/z $[M + H]^+$ calcd. for $C_{25}H_{25}F_3N_5O_4S$: 548.1574 Found: 5448.1593

IR (vmax/cm^{-1}) 3277 (aromatic C-H), 1641 (C=O), 1536 (N-H), 1253 (C-N)

***tert*-Butyl (1-(hydroxymethyl)-2,6-dioxopiperidin-3-yl)carbamate (7)**



Chemical Formula: $C_{11}H_{18}N_2O_5$
Exact Mass: 258.1216
Molecular Weight: 258.2740

tert-butyl (2,6-dioxopiperidin-3-yl)carbamate (7.10 g, 31.1 mmol, 1 eq.) was dissolved in 37% formaldehyde in water (37.2 mL, 50.0 mmol, 1.6 eq.). The reaction was heated under reflux at 100 °C for 2 hours. The mixture was then cooled down and white precipitate formed. The reaction mixture was filtered and washed with petroleum ether.

The solid was dried under vacuum overnight to afford the titled product as a white solid (4.31 g, 54%). The crude product was carried to the next step without further purification.

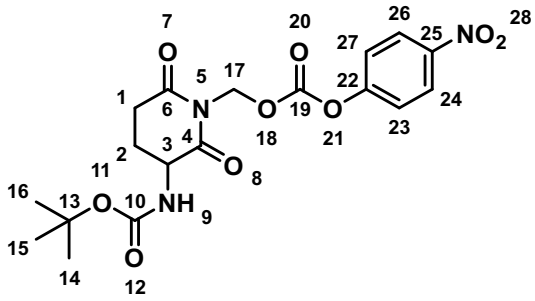
^{1}H NMR (400 MHz, DMSO) δ 7.22 (d, *J* = 8.9 Hz, 1H, C_{18}-H), 6.06 (t, *J* = 7.3 Hz, 1H, C_9-H), 5.13 – 4.93 (m, 2H, C_{17}-H), 4.31 (q, *J* = 8.9 Hz, 1H, C_3-H), 2.85 (ddd, *J* = 18.4, 11.6, 7.3 Hz, 1H, $C_{1\text{ or }2}$-H), 2.65 (dt, *J* = 17.3, 3.7 Hz, 1H, $C_{1\text{ or }2}$-H), 1.91 (tt, *J* = 8.3, 4.2 Hz, 2H, $C_{1\text{ or }2}$-H), 1.41 (s, 9H, $C_{14,15,16}$-H).

^{13}C NMR (101 MHz, DMSO) δ 172.37 ($C_{4\text{ or }6}$), 172.15 ($C_{4\text{ or }6}$), 155.97 (C_{10}), 78.65 (C_{13}), 62.81 (C_{17}), 51.43 (C_3), 31.82 (C_2), 28.65 ($C_{14,15,16}$), 23.76 (C_1).

HRMS (ESI): m/z $[M + Na]^+$ calcd. for $C_{11}H_{18}N_2O_5Na$: 281.1108 Found: 281.1140; m/z $[M + K]^+$ calcd. for $C_{11}H_{18}N_2O_5K$: 297.0847 Found: 297.0856

IR (vmax/cm^{-1}) 3372 (O-H), 1698 (carbamate C=O), 1527 (C-N), 1674 (C=O)

tert-Butyl (1-((((4-nitrophenoxy)carbonyl)oxy)methyl)-2,6-dioxopiperidin-3-yl)carbamate (8a)



Chemical Formula: $C_{18}H_{21}N_3O_9$
Exact Mass: 423.1278
Molecular Weight: 423.3780

To a solution of **7** (100 mg, 0.39 mmol) in DMF (1 mL), was added DIPEA (0.12 mL, 0.66 mmol) and bis(4-nitrophenyl) carbonate (307 mg, 1.01 mmol). The reaction was stirred at room temperature for 4 hours. The reaction mixture was extracted with EtOAc and washed with water. The organic layer was dried with $MgSO_4$ and concentrated *in vacuo*. The crude product was purified by flash column chromatography (30-55% EtOAc in pentane) to afford the titled product as a colourless oil (0.13 g, 82%).

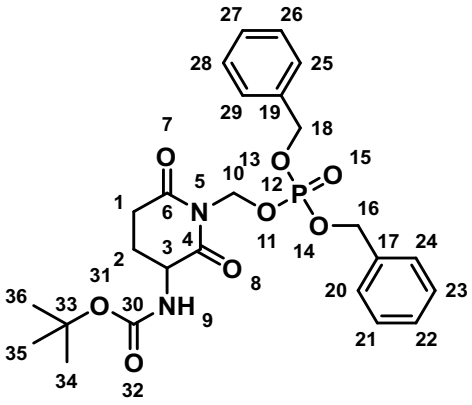
^{1}H NMR (400 MHz, CDCl3) δ 8.29 – 8.20 (m, 2H, $C_{23,27}$-H), 7.43 – 7.32 (m, 2H, $C_{24,25}$-H), 5.98 (d, *J* = 9.3 Hz, 1H, C_{17}-H), 5.87 (d, *J* = 9.3 Hz, 1H, C_{17}-H), 5.40 (d, *J* = 6.4 Hz, 1H, C_9-H), 4.41 (t, *J* = 8.5 Hz, 1H, C_3-H), 2.94 (ddd, *J* = 18.2, 4.7, 2.4 Hz, 1H, C_1-H), 2.81 (ddd, *J* = 18.4, 13.5, 5.4 Hz, 1H, C_1-H), 2.53 – 2.36 (m, 1H, C_2-H), 1.95 (qd, *J* = 13.5, 4.8 Hz, 1H, C_2-H), 1.44 (s, 9H, $C_{14,15,16}$-H).

^{13}C NMR (101 MHz, $CDCl_3$) δ 171.39 (C_4), 170.43 (C_6), 155.48 (C_{10}), 155.14 ($C_{22\text{ or }25}$), 150.97 (C_{19}), 145.55 ($C_{22\text{ or }25}$), 125.35 ($C_{23,27}$), 121.75 ($C_{24,25}$), 80.71 (C_{13}), 66.58 (C_{17}), 52.36 (C_3), 31.63 (C_1), 28.27 ($C_{14,15,16}$), 24.25 ($C_{24,25}$), 21.04 (C_2).

HRMS (ESI): m/z $[M + Na]^+$ calcd. for $C_{18}H_{21}N_3O_9Na$: 446.1170 Found: 446.1182; m/z $[M + K]^+$ calcd. for $C_{18}H_{21}N_3O_9K$: 462.0909 Found: 462.0924

IR (vmax/cm^{-1}) 1774 (carbonate C=O, C=O), 1698 (carbamate C=O), 1216 (N-O)

***tert*-Butyl (1-(((bis(benzyloxy)phosphoryl)oxy)methyl)-2,6-dioxopiperidin-3-yl)carbamate (8b)**



Chemical Formula: $C_{25}H_{31}N_2O_8P$
Exact Mass: 518.1818
Molecular Weight: 518.5028

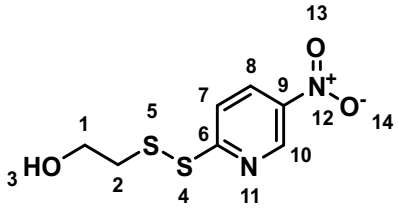
To a solution of **7** (1.0 g, 3.9 mmol, 1 eq.), tetrazole (0.35 mg, 5.0 mmol, 1.3 eq.) in dissolved in CH_2Cl_2 (15 mL) and MeCN (15 mL) at 0 °C, dibenzyl diisopropylphosphoramidite (1.56 mL, 4.64 mmol, 1.2 eq.) was added dropwise. The reaction mixture was stirred for 1 hour. Then *m*CPBA (800 mg, 4.64 mmol, 1.2 eq.) was added into the reaction mixture and stirred for 10 minutes. The reaction mixture was dilute with CH_2Cl_2, then wash with saturated $NaHCO_3$ and saturated NH_4Cl. The combined organic layer was dried with $MgSO_4$ and concentrated *in vacuo*. The crude product was purified by flash column chromatography (10% MeOH in CH_2Cl_2) to afford a colourless oil (1.52 g, 76%)

^{1}H NMR (400 MHz, MeOD) δ 7.38 – 7.34 (m, 10H, $C_{20,21,22,23,24,25,26,27,28,29}$-H), 5.68 (dt, J = 31.1, 9.0 Hz, 2H, C_{10}-H), 5.05 (d, J = 8.2 Hz, 4H, $C_{16,18}$-H), 4.35 (dd, J = 12.2, 5.0 Hz, 1H, C_3-H), 2.78 (dd, J = 8.9, 4.3 Hz, 2H, C_2-H), 2.14 – 1.91 (m, 2H, C_1-H), 1.46 (s, 10H, $C_{34,35,36}$-H).

^{31}P NMR (162 MHz, MeOD) δ -3.64.

HRMS (ESI): m/z $[M + H]^+$ calcd. For $C_{25}H_{32}N_2O_8P$: 519.1891 Found: 519.1909

2-((5-Nitropyridin-2-yl)disulfaneyl)ethan-1-ol (9a)



Chemical Formula: $C_7H_8N_2O_3S_2$
Exact Mass: 231.9976
Molecular Weight: 232.2720

To a solution of 5,5'-dinitro-2,2'-dipyridyl disulfide (1.99 g, 6.40 mol) in MeOH/DMF (1:1, 2 mL), a solution of 2-mercaptoethanol (0.5 g, 6.4 mol) in DCM/MeOH (10 mL, 95/5 (v/v)) was added dropwise under nitrogen at room temperature and stirred for 24 hours. The reaction mixture was concentrated *in vacuo*. The orange crude was purified with flash column chromatography (0-30 % EtOAc in dichloromethane) and an orange solid was obtained. The orange solid was then dissolved in dichloromethane and the suspension was filtered. The filtrate collected was concentrated in vacuo to afford the titled product as an orange solid. (776 mg, 52%)

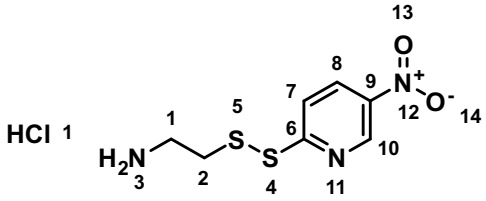
^{1}H NMR (400 MHz, $CDCl_3$) δ 9.33 – 9.31 (m, 1H, C_{10}-H), 8.37 (dd, J = 8.8, 2.5 Hz, 1H, C_8-H), 7.71 – 7.64 (m, 1H, C_7-H), 3.82 – 3.75 (m, 2H, C_1-H), 3.01 (dd, J = 5.7, 4.8 Hz, 2H, C_2-H).

^{13}C NMR (101 MHz, $CDCl_3$) δ 167.64 (C_6), 145.39 (C_{10}), 142.59 (C_9), 131.48 (C_8), 120.85 (C_7), 58.75 (C_1), 42.56 (C_2).

HRMS (ESI): m/z $[M + H]^+$ calcd. for $C_7H_9N_2O_3S_2$: 233.0049 Found: 233.0054

IR (vmax/cm^{-1}) 3306 (alcohol O-H)

2-((5-Nitropyridin-2-yl)disulfaneyl)ethan-1-ol (9b)



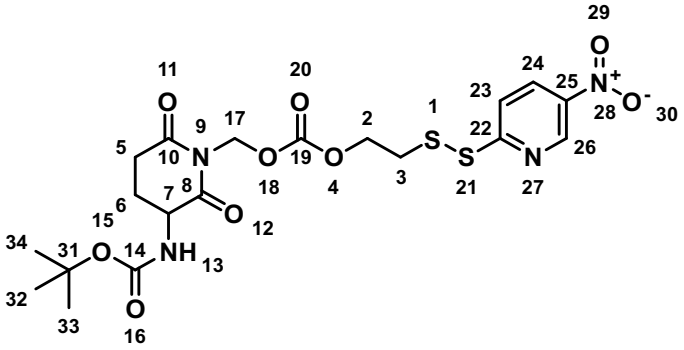
Chemical Formula: $C_7H_{10}ClN_3O_2S_2$
Exact Mass: 266.9903
Molecular Weight: 267.7460

To a solution of 5,5'-dinitro-2,2'-dipyridyl disulfide (136 mg, 0.44 mmol) in MeOH/DMF (1:1, 2 mL), a solution of 2-mercaptoethanol (50 mg, 0.44 mmol) with AcOH (0.1 mL) in DCM/MeOH (10 mL, 50/50 (v/v)) was added dropwise under nitrogen at room temperature and stirred for 24 hours. An orange solid was collected by filtration (82 mg, 70%).

^{1}H NMR (400 MHz, DMSO) δ 8.57 (d, J = 2.7 Hz, 1H, C_{10}-H), 8.25 (s, 3H, N_3-H), 7.98 (dd, J = 9.6, 2.7 Hz, 1H, C_8-H), 7.32 (d, J = 9.6 Hz, 1H, C_7-H), 3.10 (t, J = 7.0 Hz, 2H, C_1-H), 3.00 (t, J = 7.0 Hz, 2H, C_2-H).

^{13}C NMR (101 MHz, DMSO) δ 183.65 (C_6), 138.20 (C_{10}), 136.14 (C_9), 133.43 (C_8), 129.56 (C_7), 38.25 (C_1), 34.39 (C_2).

***tert*-Butyl (1-((((2-((5-nitropyridin-2-yl)disulfaneyl)ethoxy)carbonyl)oxy)methyl)-2,6-dioxopiperidin-3-yl)carbamate (10)**



Chemical Formula: $C_{19}H_{24}N_4O_9S_2$
Exact Mass: 516.0985
Molecular Weight: 516.5400

To a solution of **9a** (160 mg, 0.68 mmol) in dichloromethane (5 mL), **8a** (291 mg, 0.68 mmol) and DMAP (84 mg, 0.68 mmol) were added under nitrogen at room temperature. The reaction mixture was stirred at room temperature for 18 hours. The reaction mixture was diluted with EtOAc and washed with water. The organic layer was dried with $MgSO_4$ and concentrated *in vacuo*. The crude was purified with flash column chromatography (0-50 % EtOAc in pentane) to afford the titled product as a pale-yellow oil (114 mg, 32%).

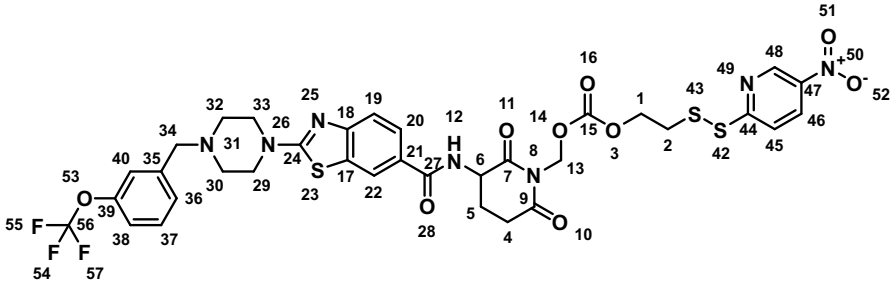
^{1}H NMR (400 MHz, $CDCl_3$) δ 9.29 (d, J = 2.6 Hz, 1H, C_{26}-H), 8.44 (dd, J = 8.9, 2.6 Hz, 1H, C_{24}-H), 7.87 (d, J = 8.8 Hz, 1H, C_{23}-H), 5.91 – 5.72 (m, 2H, C_{17}-H), 4.43 – 4.26 (m, 2H, $C_{2,7}$-H), 3.11 (t, J = 6.2 Hz, 2H, C_3-H), 3.00 – 2.63 (m, 2H, C_5-H), 2.55 – 2.46 (m, 1H ,C_6-H), 1.96 – 1.81 (m, 1H, C_6-H), 1.47 (s, 11H, $C_{32,33,34}$-H).

^{13}C NMR (151 MHz, $CDCl_3$) δ 171.11 (C_{14}), 170.26 ($C_{8,10}$), 167.86 (C_{22}), 153.15 (C_{19}), 145.21 (26), 142.29 (C_{25}), 131.81 (C_{24}), 119.47 (C_{23}), 80.71 (C_{31}), 65.91 (C_{17}), 65.49 (C_2), 52.45 (C_7), 37.26 (C_3), 31.64 (C_5), 28.29 ($C_{32,33,24}$), 24.38 (C_6).

HRMS (ESI): m/z $[M + H]^+$ calcd. for $C_{19}H_{25}N_4O_9S_2$: 517.1058 Found: 517.1060

IR (vmax/cm^{-1}) 1755 (carbonate C=O, C=O)

(2,6-Dioxo-3-(2-(4-(3-(trifluoromethoxy)benzyl)piperazin-1-yl)benzo[*d*]thiazole-6-carboxamido)piperidin-1-yl)methyl (2-((5-nitropyridin-2-yl)disulfaneyl)ethyl) carbonate (OX05156)



Chemical Formula: $C_{34}H_{32}F_3N_7O_9S_3$
Exact Mass: 835.1376
Molecular Weight: 835.8452

To a solution of **10** (100 mg, 0.20 mmol) in dichloromethane (5 mL) was added TFA (15 mL). The reaction solution was stirred at room temperature for 5 minutes then concentrated *in vacuo* to remove the solvent and provide the crude TFA salt (not shown, 99 mg, 99%) as a purple oil. **HRMS (ESI):** m/z $[M + Na]^+$ calcd. for $C_{14}H_{16}N_4O_7S_2Na$: 439.0353 Found: 439.0363.

To a solution of **5** (56 mg, 0.13 mmol, 1 eq.) in anhydrous DMF (1 mL), HATU (64 mg, 0.17 mmol) and DIPEA (0.12 mL, 0.65 mmol) was added. The solution was stirred for 30 minutes at room temperature. The activated **5** solution was added to (**3-amino-2,6-dioxopiperidin-1-yl)methyl (2-((5-nitropyridin-2-yl)disulfaneyl)ethyl) carbonate-2,2,2-trifluoroacetaldehyde** (99 mg, 0.20 mmol, 1.5 eq.) in DIPEA (0.12 mL, 0.65 mmol) and anhydrous DMF (1 mL). The reaction was stirred for 20 hours at room temperature. The rection mixture was diluted with EtOAc and washed with water and then brine. The organic layer was dried with $MgSO_4$ and concentrated *in vacuo*. The crude was purified with flash column chromatography (60-80 % EtOAc in pentane) to afford a green solid. The product was then purified with C18 reverse phase column chromatography (0-100% MeCN/H_2O gradient with 0.1% formic acid modifier) to afford the titled product as an off-white solid. (32 mg, 30%)

^{1}H NMR (400 MHz, DMSO) δ 9.26 (d, *J* = 2.6 Hz, 1H, C_{48}-H), 8.84 (d, *J* = 8.3 Hz, 1H, N_{12}-H), 8.59 (dd, *J* = 8.9, 2.7 Hz, 1H, C_{46}-H), 8.30 (d, *J* = 1.7 Hz, 1H, C_{22}-H), 8.02 (d, *J* = 8.9 Hz, 1H, C_{45}-H), 7.83 (dd, *J* = 8.5, 1.8 Hz, 1H, C_{20}-H), 7.54 – 7.46 (m, 2H, $C_{19,37}$-H), 7.40 (d, *J* = 7.7 Hz, 1H, C_{36}-H), 7.34 (s, 1H, C_{40}-H), 7.28 (d, *J* = 8.1 Hz, 1H, C_{38}-H), 5.68 (q, *J* = 9.3 Hz, 2H, C_{13}-H), 4.97 (ddd, *J* = 13.1, 8.0, 5.2 Hz, 1H, C_6-H), 4.34 (t, *J* = 5.9 Hz, 2H, C_1-H), 3.64 (d, *J* = 4.2 Hz, 6H, $C_{30,32,34}$-H), 3.22 (t, *J* = 5.9 Hz, 2H, C_2-H), 3.01 (ddd, *J* = 18.1, 13.0, 5.5 Hz, 1H, C_4-H), 2.85 – 2.75 (m, 1H, C_4-H), 2.54 (t, *J* = 5.0 Hz, 4H, $C_{29,33}$-H), 2.28 – 2.14 (m, 1H, C_5-H), 2.07 – 1.99 (m, 1H, C_5-H).

^{13}C NMR (151 MHz, DMSO) δ 171.96 ($C_{7 \text{ or } 9}$), 171.94 ($C_{7 \text{ or } 9}$), 170.22 (C_{24}), 166.25 (C_{27}), 155.57 (C_{21}), 153.33 (C_{15}), 148.96 (C_{39}), 145.39 (C_{48}), 141.41 (C_{35}), 133.09 (C_{46}), 130.69 ($C_{19 \text{ or } 37}$), 128.30 (C_{36}), 126.95 ($C_{17,18}$), 126.14 (C_{20}), 121.43 ($C_{22 \text{ or } 40}$), 121.39

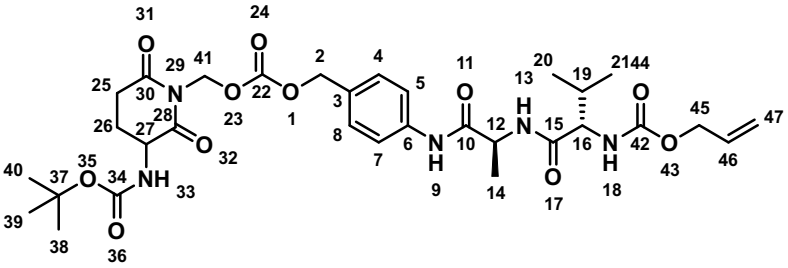
($C_{22\ or\ 40}$), 120.09 (C_{45}), 120.02 (C_{38}), 118.17 ($C_{19\ or\ 37}$), 66.26 (C_{13}), 65.82 (C_1), 61.25 (C_{34}), 52.17 ($C_{29,33}$), 50.49 (C_6), 48.49 ($C_{30,32}$), 37.23 (C_2), 31.56 (C_4), 23.39 (C_5).

^{19}F NMR (377 MHz, DMSO) δ -56.62.

HRMS (ESI): m/z $[M + Na]^+$ calcd. for $C_{34}H_{32}F_3N_7O_9S_3Na$: 858.1268 Found: 858.1274

IR (vmax/cm^{-1}) 1660 (amide C=O)

***tert*-Butyl (1-(((((4-((*S*)-2-((*S*)-2-(((allyloxy)carbonyl)amino)-3-methylbutanamido)propanamido)benzyl)oxy)carbonyl)oxy)methyl)-(*RS*)-2,6-dioxopiperidin-3-yl)carbamate (12a)**



Chemical Formula: $C_{31}H_{43}N_5O_{11}$
Exact Mass: 661.2959
Molecular Weight: 661.7090

To a solution of **8a** (300 mg, 0.71 mmol) in DMF (3 mL), Alloc-Val-Ala-PAB-OH (267 mg, 0.71 mmol) and DMAP (86 mg, 0.71 mmol) were added. The reaction was stirred under room temperature for 24 hours. The reaction mixture was purified directly with C18 reverse phase column chromatography (0-100% MeCN/H_2O gradient with 0.1% formic acid modifier) to afford the titled product as a white solid. (413 mg, 88%)

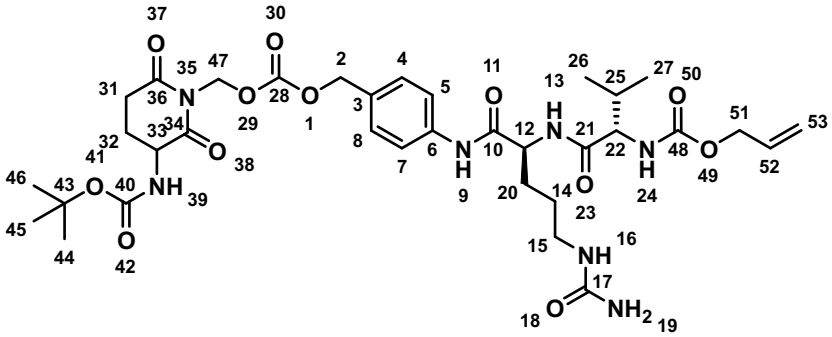
^{1}H NMR (600 MHz, DMSO) δ 10.03 (s, 1H, N_9-H), 8.17 (d, J = 7.0 Hz, 1H, N_{13}-H), 7.63 – 7.56 (m, 2H, $C_{4,8}$-H), 7.36 – 7.31 (m, 2H, $C_{5,7}$-H), 7.28 (d, J = 8.8 Hz, 1H, N_{33}-H), 7.24 (d, J = 8.8 Hz, 1H, N_{18}-H), 5.91 (ddt, J = 17.2, 10.5, 5.3 Hz, 1H, C_{46}-H), 5.68 (d, J = 9.2 Hz, 1H, C_{41}-H), 5.63 (d, J = 9.3 Hz, 1H, C_{41}-H), 5.30 (dt, J = 17.2, 1.8 Hz, 1H, C_{47}-H), 5.17 (dt, J = 10.5, 1.6 Hz, 1H, C_{47}-H), 5.09 (s, 2H, C_2-H), 4.48 (ddt, J = 4.9, 3.2, 1.6 Hz, 2H, C_{45}-H), 4.47 – 4.38 (m, 2H, $C_{12,27}$-H), 3.90 (dd, J = 8.8, 6.8 Hz, 1H, C_{16}-H), 2.91 (ddd, J = 18.3, 13.0, 5.9 Hz, 1H, C_{25}-H), 2.71 (ddd, J = 17.6, 4.4, 2.9 Hz, 1H, C_{25}-H), 2.02 – 1.92 (m, 2H, C_{26}-H), 1.94 – 1.87 (m, 1H, C_{19}-H), 1.41 (s, 8H, $C_{38,39,40}$-H), 1.31 (d, J = 7.1 Hz, 3H, $C_{20\ or\ 21}$-H), 0.89 (d, J = 6.7 Hz, 3H, $C_{20\ or\ 21}$-H), 0.84 (d, J = 6.8 Hz, 3H, $C_{20\ or\ 21}$-H).

^{13}C NMR (151 MHz, DMSO) δ 172.25 ($C_{28\ or\ 30}$), 171.86 ($C_{28\ or\ 30}$), 171.66 (C_{10}), 171.49 (C_{15}), 156.46 (C_{42}), 155.90 (C_{34}), 153.55 (C_{22}), 139.69 (C_6), 134.11 (C_{46}), 130.25 (C_3), 129.67 ($C_{5,7}$), 119.44 ($C_{4,8}$), 117.40 (C_{47}), 78.79 (C_{37}), 69.54 (C_2), 66.15 (C_{41}), 64.89 (C_{45}), 60.35 (C_{16}), 51.32 ($C_{12\ or\ 27}$), 49.50 ($C_{12\ or\ 27}$), 31.55 (C_{25}), 30.81 (C_{19}), 28.63 ($C_{38,39,40}$), 23.46 ($C_{20\ or\ 21}$), 19.64 (C_{26}), 18.56 ($C_{20\ or\ 21}$), 18.48 (C_{14}).

HRMS (ESI): m/z $[M + H]^+$ calcd. for $C_{31}H_{43}N_5O_{11}$: 662.3032 Found: 662.3052

IR (vmax/cm^{-1}) 1750 (carbonate C=O), 1695 (amide C=O), 1644 (C=C)

***tert*-Butyl (1-(((((4-((*S*)-2-((*S*)-2-(((allyloxy)carbonyl)amino)-3-methylbutanamido)-5-ureidopentanamido)benzyl)oxy)carbonyl)oxy)methyl)-(*RS*)-2,6-dioxopiperidin-3-yl)carbamate (12b)**



Chemical Formula: $C_{34}H_{49}N_7O_{12}$
Exact Mass: 747.3439
Molecular Weight: 747.8030

To a solution of **8a** (42.7 mg, 0.010 mmol) in DMF (1 mL), Alloc-Val-Cit-PAB-OH (70.0 mg, 0.015 mmol) and DMAP (12.4 mg, 0.010 mmol) were added. The reaction was stirred under room temperature for 24 hours. The reaction mixture was purified directly with C18 reverse phase column chromatography (0-100% MeCN/H_2O gradient with 0.1% formic acid modifier) to afford the titled product as a white solid. (31 mg, 41%)

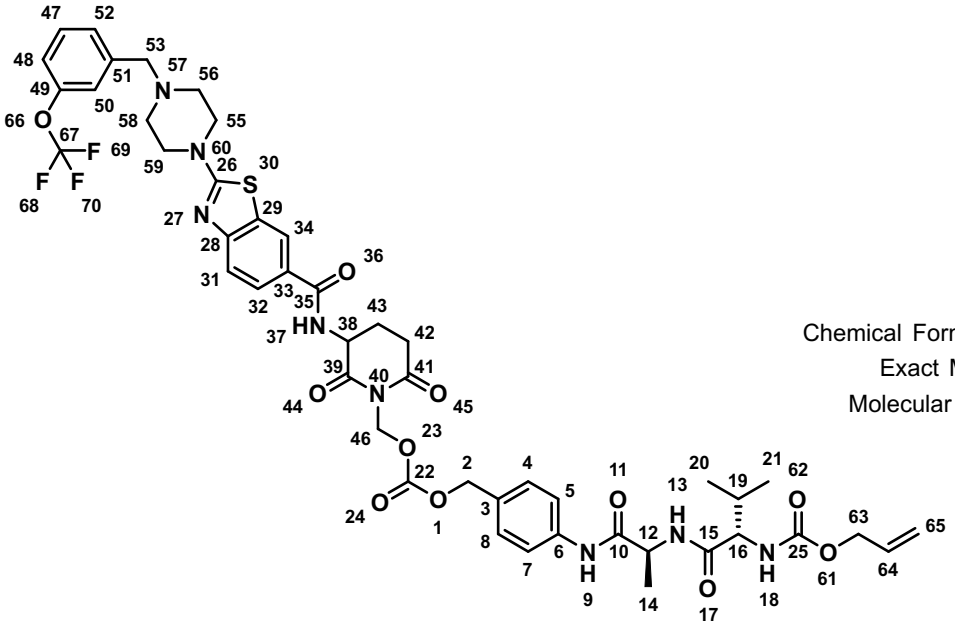
^{1}H NMR (400 MHz, DMSO) δ 10.20 (s, 1H, N_9-H), 8.18 (d, J = 7.6 Hz, 1H, N_{13}-H), 7.65 – 7.58 (m, 2H, $C_{4,8}$-H), 7.36 – 7.19 (m, 4H, $C_{5,7}$-H and $N_{16,39}$-H), 6.13 (s, 1H, N_{24}-H), 5.91 (ddt, J = 16.2, 10.5, 5.3 Hz, 1H, C_{52}-H), 5.71 – 5.59 (m, 2H, C_{47}-H), 5.46 (s, 2H, C_{19}-H), 5.36 – 5.12 (m, 2H, C_{53}-H), 5.08 (s, 2H, C_2-H), 4.48 (dd, J = 5.4, 1.6 Hz, 2H, C_{51}-H), 4.45 – 4.36 (m, 2H, $C_{12,33}$-H), 3.90 (dd, J = 8.9, 6.8 Hz, 1H, C_{22}-H), 2.94 (dtt, J = 32.2, 12.8, 6.3 Hz, 3H, $C_{15,31}$-H), 2.70 (dt, J = 17.3, 3.7 Hz, 1H, C_{31}-H), 2.03 – 1.89 (m, 2H, $C_{25,32}$-H), 1.76 – 1.53 (m, 1H, C_{20}-H), 1.49 – 1.29 (m, 9H, $C_{44,45,46,14}$-H), 0.85 (dd, J = 16.6, 6.7 Hz, 7H, $C_{26,27,32}$-H).

^{13}C NMR (151 MHz, DMSO) δ 172.25 ($C_{34\text{ or }36}$), 171.86 ($C_{34\text{ or }36}$), 171.73 (C_{21}), 171.15 (C_{17}),159.34 ($C_{10\text{ or }40}$), 156.43 (C_{48}), 155.90 ($C_{10\text{ or }40}$), 153.55 (C_{28}), 139.62 (C_6), 134.11 (C_{52}), 130.28 (C_3), 129.67 ($C_{5,7}$), 119.43 ($C_{4,8}$), 117.41 (C_{53}), 78.80 (C_{43}), 69.54 (C_2), 66.15 (C_{47}), 64.90 (C_{51}), 60.46 (C_{22}), 53.56 ($C_{33\text{ or }12}$), 51.32 ($C_{33\text{ or }12}$), 39.03 (C_{15}), 31.55 (C_{31}), 30.83 (C_{25}), 29.88 (C_{20}), 28.63 ($C_{45,46,47}$), 27.25 (C_{14}), 23.46 (C_{32}), 19.67 ($C_{26\text{ or }27}$), 18.60 ($C_{26\text{ or }27}$).

HRMS (ESI): m/z $[M + H]^+$ calcd. for $C_{34}H_{50}N_7O_{12}$: 748.3512 Found: 748.3512

IR (vmax/cm^{-1}) 1752 (carbonate C=O, C=O), 1693 (carbamate C=O)

Allyl ((2*S*)-1-(((2*S*)-1-((4-((((((*RS*)-2,6-dioxo-3-(2-(4-(3-(trifluoromethoxy)benzyl)piperazin-1-yl)benzo[*d*]thiazole-6-carboxamido)piperidin-1-yl)methoxy)carbonyl)oxy)methyl)phenyl)amino)-1-oxopropan-2-yl)amino)-3-methyl-1-oxobutan-2-yl)carbamate (13a)



Chemical Formula: $C_{46}H_{51}F_3N_8O_{11}S$
Exact Mass: 980.3350
Molecular Weight: 981.0142

To a solution of **12a** (200 mg, 0.302 mmol) in 1,4-dioxane (5 mL) was added 2.68 M HCl in 1,4-dioxane(1.2 mL, 3.1 mmol). The reaction solution was stirred at room temperature for 3.5 hours then concentrated *in vacuo* to remove the solvent and provide the crude HCl salt (not shown, 190 mg, 99%) as a pale-yellow oil.

To a solution of **5** (87 mg, 0.20 mmol, 1 eq.) in anhydrous DMF (1 mL), HATU (494 mg, 0.26 mmol) and DIPEA (0.17 mL, 1.0 mmol) was added. The solution was stirred for 30 minutes at room temperature. The activated **5** solution was added to allyl ((2S)-1-(((2S)-1-((4-((((((*RS*)-3-amino-2,6-dioxopiperidin-1-yl)methoxy)carbonyl)oxy)methyl)phenyl)amino)-1-oxopropan-2-yl)amino)-3-methyl-1-oxobutan-2-yl)carbamate hydrochloride (190 mg, 0.302 mmol, 1.5 eq.) in DIPEA (0.17 mL, 1.0 mmol) and anhydrous DMF (1 mL). The reaction was stirred for 20 hours at room temperature. The rection mixture was purified with C18 reverse phase column chromatography (0-100% MeCN/H_2O gradient with 0.1% formic acid modifier) to afford the title product as a white solid. (113 mg, 58%)

^{1}H NMR (400 MHz, DMSO) δ 10.03 (s, 1H, N_9-H), 8.82 (d, J = 8.3 Hz, 1H, N_{37}-H), 8.29 (d, J = 1.9 Hz, 1H, C_{34}-H), 8.16 (d, J = 6.9 Hz, 1H, N_{13}-H), 7.82 (dd, J = 8.5, 1.8 Hz, 1H, C_{32}-H), 7.60 (d, J = 8.4 Hz, 2H, $C_{4,8}$-H), 7.48 (dd, J = 8.2, 2.8 Hz, 2H, $C_{31,47}$-H), 7.42 – 7.20 (m, 6H, $C_{5,7,48,50,52}$-H, N_{18}-H), 5.90 (ddd, J = 16.0, 9.0, 3.8 Hz, 1H, C_{64}-H), 5.71 (dt, J = 18.1, 8.5 Hz, 2H, C_{46}-H), 5.29 (dd, J = 17.1, 2.0 Hz, 1H, C_{65}-H), 5.20 – 5.13 (m, 1H, C_{65}-H), 5.09 (s, 2H, C_2-H), 4.96 (dq, J = 13.0, 6.2 Hz, 1H, C_{38}-H), 4.48 (dt, J = 5.4, 1.6 Hz, 2H, C_{63}-H), 4.45 – 4.37 (m, 1H, C_{12}-H), 3.93 – 3.85 (m, 1H, C_{16}-H), 3.63 (d,

J = 4.8 Hz, 6H, $C_{53,56,58}$-H), 3.05 – 2.92 (m, 1H, C_{42}-H), 2.82 – 2.71 (m, 1H, C_{42}-H), 2.54 (d, *J* = 5.7 Hz, 4H, $C_{55,59}$-H), 2.26 – 2.12 (m, 1H, C_{43}-H), 2.04 – 1.93 (m, 2H, $C_{19,43}$-H), 1.30 (d, *J* = 7.1 Hz, 3H, C_{14}-H), 0.86 (dd, *J* = 18.8, 6.7 Hz, 6H, $C_{20,21}$-H).

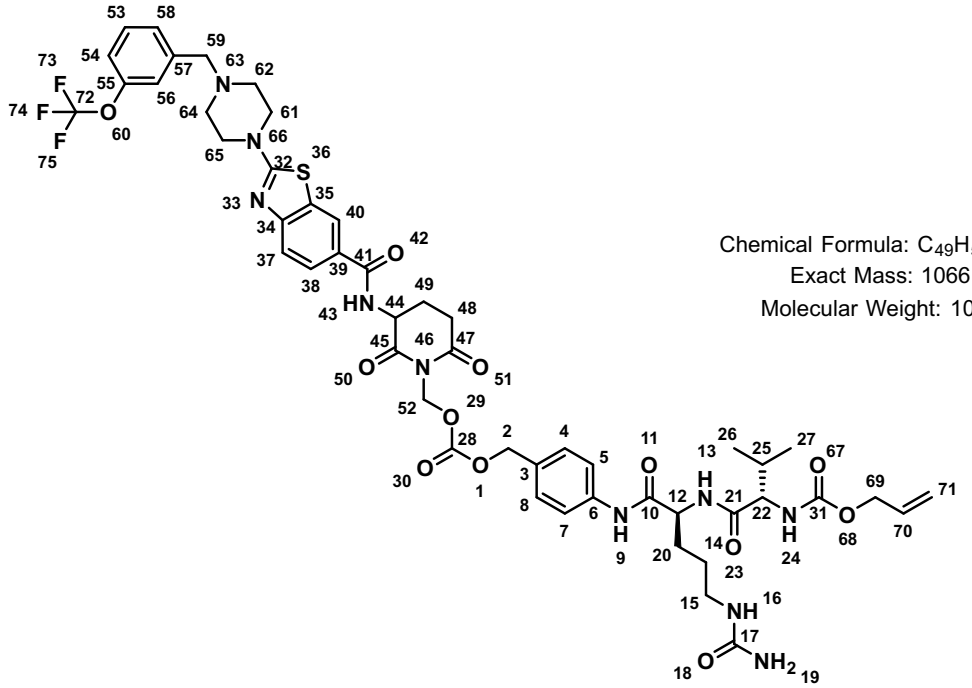
^{13}C NMR (151 MHz, DMSO) δ 171.94 ($C_{39.41}$), 171.66 (C_{10}), 170.23 (C_{26}), 166.24 (C_{35}), 156.46 (C_{25}), 155.57 (C_{33}), 153.56 (C_{22}), 148.96 (C_{49}), 141.41 (C_{51}), 139.69 (C_{6}), 134.10 (C_{64}), 130.84 ($C_{28\text{ or }29}$), 130.69 ($C_{31\text{ or }47}$), 130.25 (C_{3}), 129.69 ($C_{5,7}$), 128.29 ($C_{48\text{ or }50\text{ or }52}$), 126.95 ($C_{28\text{ or }29}$), 126.14 ($C_{32}$), 121.39 ($C_{48\text{ or }50\text{ or }52}$), 121.33 ($C_{34}$), 120.02 ($C_{48\text{ or }50\text{ or }52}$), 119.45 ($C_{4,8}$), 118.17 ($C_{31\text{ or }47}$), 69.55 ($C_{2}$), 66.16 ($C_{46}$), 64.89 ($C_{63}$), 61.25 ($C_{53}$), 60.35 ($C_{16}$), 52.16 ($C_{55,\ 59}$), 50.46 ($C_{38}$), 49.50 ($C_{12}$), 48.49 ($C_{56,\ 58}$), 31.56 ($C_{42}$), 31.16 ($C_{19\text{ or }43}$), 30.81 ($C_{19\text{ or }43}$), 23.4 ($C_{19\text{ or }43}$), 19.63 ($C_{20\text{ or }21}$), 18.56 ($C_{20\text{ or }21}$), 18.48 ($C_{14}$).

^{19}F NMR (376 MHz, DMSO) δ -56.63.

HRMS (ESI): m/z $[M + Na]^+$ calcd. for $C_{46}H_{51}F_3N_8O_{11}SNa$: 1003.3242 Found: 1003.3251

IR (vmax/cm^{-1}) 3287 (N-H), 1750 (carbonate C=O), 1693 (amide C=O), 1256 (C-F)

Allyl ((2*S*)-1-(((2*S*)-1-((4-((((((*RS*)-2,6-dioxo-3-(2-(4-(3-(trifluoromethoxy)benzyl)piperazin-1-yl)benzo[*d*]thiazole-6-carboxamido)piperidin-1-yl)methoxy)carbonyl)oxy)methyl)phenyl)amino)-1-oxo-5-ureidopentan-2-yl)amino)-3-methyl-1-oxobutan-2-yl)carbamate (13b)



Chemical Formula: $C_{49}H_{57}F_3N_{10}O_{12}S$
Exact Mass: 1066.3830
Molecular Weight: 1067.1082

To a solution of **12b** (115 mg, 0.154 mmol) in 1,4-dioxane (1 mL) was added 2.68 M HCl in 1,4-dioxane (1.2 mL, 3.1 mmol). The reaction solution was stirred at room temperature for 3.5 hours then concentrated *in vacuo* to remove the solvent and provide the crude HCl salt (not shown, 105 mg, 99%) as a pale-yellow oil.

To a solution of **5** (45 mg, 0.10 mmol, 1 eq.) in anhydrous DMF (1 mL), HATU (50 mg, 0.133 mmol) and DIPEA (0.1 mL, 0.51 mmol) was added. The solution was stirred for 30 minutes at room temperature. The activated **5** solution was added to allyl ((2*S*)-1-(((2*S*)-1-((4-((((((*RS*)-3-amino-2,6-dioxopiperidin-1-yl)methoxy)carbonyl)oxy)methyl)phenyl)amino)-1-oxo-5-ureidopentan-2-yl)amino)-3-methyl-1-oxobutan-2-yl)carbamate hydrochloride (105 mg, 0.154 mmol, 1.5 eq.) in DIPEA (0.1 mL, 0.5 mmol) and anhydrous DMF (1 mL). The reaction was stirred for 20 hours at room temperature. The rection mixture was purified with C18 reverse phase column chromatography (0-100% MeCN/H_2O gradient with 0.1% formic acid modifier) to afford the titled product as a white solid. (48 mg, 43%)

^{1}H NMR (600 MHz, DMSO) δ 10.10 (s, 1H, N_9-H), 8.33 – 8.28 (m, 1H, C_{40}-H), 8.13 – 8.05 (m, 1H, N_{13}-H), 7.78 (d, *J* = 1.7 Hz, 1H, C_{38}-H), 7.63 – 7.58 (m, 2H, $C_{4,8}$-H), 7.54 – 7.38 (m, 2H, $C_{37,53}$-H), 7.35 – 7.23 (m, 5H, $C_{5,7,54,56,58}$-H), 6.00 (t, *J* = 5.9 Hz, 1H, N_{24}-H), 5.96 – 5.87 (m, 1H, C_{70}-H), 5.71 – 5.60 (m, 2H, C_{52}-H), 5.41 (s, 2H, N_{19}-H), 5.30 (dt, *J* = 17.2, 1.9 Hz, 1H, C_{71}-H), 5.17 (dt, *J* = 10.5, 1.6 Hz, 1H, C_{71}-H), 5.09 (s, 2H, C_2-H), 4.48 (tq, *J* = 3.2, 1.5 Hz, 2H, C_{69}-H), 4.46 – 4.38 (m, 2H, C_{12}-H), 3.91 (dd, *J* = 8.9, 6.8

Hz, 1H, C_{22}-H), 3.71 – 3.55 (m, 6H, $C_{59,62,64}$-H), 3.09 – 2.84 (m, 2H, $C_{15,48}$-H), 2.74 – 2.67 (m, 1H, C_{48}-H), 2.58 – 2.51 (m, 4H, $C_{61,65}$-H), 2.04 – 1.89 (m, 3H, $C_{25,49}$-H), 1.73 – 1.65 (m, 1H, C_{20}-H), 1.62 – 1.57 (m, 1H, C_{20}-H), 1.48 – 1.31 (m, 1H, C_{14}-H), 0.90 – 0.82 (m, 8H, $C_{26,27}$-H).

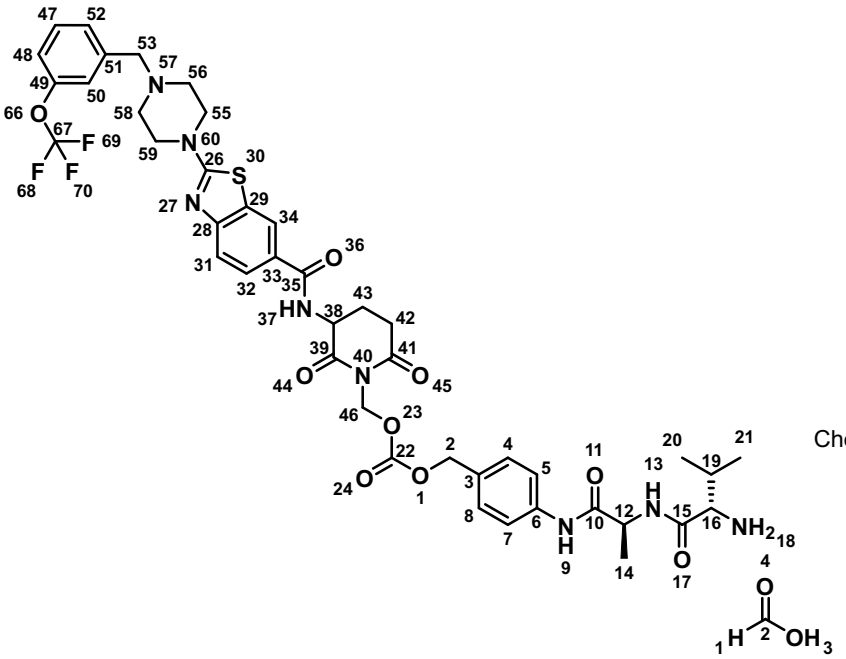
^{13}C NMR (151 MHz, $CDCl_3$) δ 171.76 (C_{28}), 171.38 (C_{21}), 171.24 (C_{31}), 170.67 (C_{32}), 158.86 (C_{17}), 155.94 (C_{41}), 155.41 (C_{22}), 153.06 (C_3), 148.47 (C_{55}), 139.15 (C_{57}), 133.62 (C_{70}), 130.21 ($C_{37 \text{ or } 53}$), 129.18 ($C_{5,7 \text{ or } 54 \text{ or } 56 \text{ or } 58}$), 127.82 ($C_{37 \text{ or } 53}$), 120.91 ($C_{5,7 \text{ or } 54 \text{ or } 56 \text{ or } 58}$), 119.53 ($C_{38}$), 118.95 ($C_{4,8}$), 116.92 ($C_{71}$), 69.05 ($C_2$), 65.66 ($C_{52}$), 64.41 ($C_{69}$), 60.79 ($C_{25}$), 59.98 ($C_{22}$), 53.07 ($C_{12}$), 51.68 ($C_{61,65}$), 48.04 ($C_{62,64}$), 31.06 ($C_{48}$), 30.34 ($C_{25}$), 29.38($C_{20}$), 26.75 ($C_{14}$), 22.97 ($C_{15}$), 20.65 ($C_{49}$), 19.19 ($C_{26 \text{ or } 27}$), 18.11 ($C_{26 \text{ or } 27}$).

^{19}F NMR (376 MHz, DMSO) δ -56.62.

HRMS (ESI): m/z $[M + H]^+$ calcd. for $C_{29}H_{42}N_7O_{10}$: 648.2988 Found: 648.2983

IR (vmax/cm^{-1}) 3286 (N-H), 1744 (carbonate C=O, C=O), 1692 (amide C=O), 1246 (C-F)

4-((*S*)-2-((*S*)-2-Amino-3-methylbutanamido)propanamido)benzyl (((*RS*)-2,6-dioxo-3-(2-(4-(3-(trifluoromethoxy)benzyl)piperazin-1-yl)benzo[*d*]thiazole-6-carboxamido)piperidin-1-yl)methyl) carbonate formate (14a)



Chemical Formula: $C_{43}H_{49}F_3N_8O_{11}S$
Exact Mass: 942.32
Molecular Weight: 942.97

To a solution of **13a** (86 mg, 0.088 mmol) in MeOH (3 mL) was added $PhSiH_3$ (28 mg, 0.26 mmol). The reaction mixture was degassed with a nitrogen balloon for 10 minutes. $Pd(PPh_3)_4$ (20 mg, 0.017 mmol) was added. The reaction mixture was further degassed with a nitrogen balloon for 10 minutes. After the reaction was stirred under nitrogen for

2 hours, the mixture was filtered and the filtrate was collected and concentrated *in vacuo*. The residue was dissolved in DMSO (1 mL) and purified with C18 reverse phase column chromatography (0-100% MeCN/H_2O gradient with 0.1% formic acid modifier) to afford the title product as a white solid. (72 mg, 91%)

^{1}H NMR (400 MHz, DMSO) δ 10.22 (s, 1H), 8.84 (d, *J* = 8.3 Hz, 1H, N_9-H), 8.56 (s, 1H, N_{37}-H), 8.33 – 8.22 (m, 3H, N_{18}-H, C_{34}-H), 7.87 – 7.79 (m, 1H, C_{32}-H), 7.61 (d, *J* = 8.3 Hz, 2H, $C_{4,8}$-H), 7.58 – 7.43 (m, 2H, $C_{31,47}$-H), 7.42 – 7.21 (m, 5H, $C_{5,7,48,50,52}$-H), 5.70 (q, *J* = 9.3 Hz, 2H, C_{46}-H), 5.09 (s, 2H, C_2-H), 4.96 (ddd, *J* = 13.1, 8.2, 5.3 Hz, 1H, C_{38}-H), 4.54 – 4.40 (m, 1H, C_{12}-H), 3.66 – 3.60 (m, 6H, $C_{53,56,58}$-H), 3.40 – 3.29 (m, 1H, C_{16}-H), 2.99 (ddd, *J* = 18.1, 13.2, 5.6 Hz, 1H, C_{42}-H), 2.82 – 2.72 (m, 1H, C_{42}-H), 2.57 – 2.51 (m, 4H, $C_{55,59}$-H), 2.19 (ddt, *J* = 17.2, 13.1, 5.6 Hz, 1H, C_{43}-H), 2.05 – 1.96 (m, 2H, $C_{19,43}$-H), 1.33 (d, *J* = 7.0 Hz, 3H, C_{14}-H), 0.89 (dd, *J* = 18.8, 6.7 Hz, 6H, $C_{20,21}$-H).

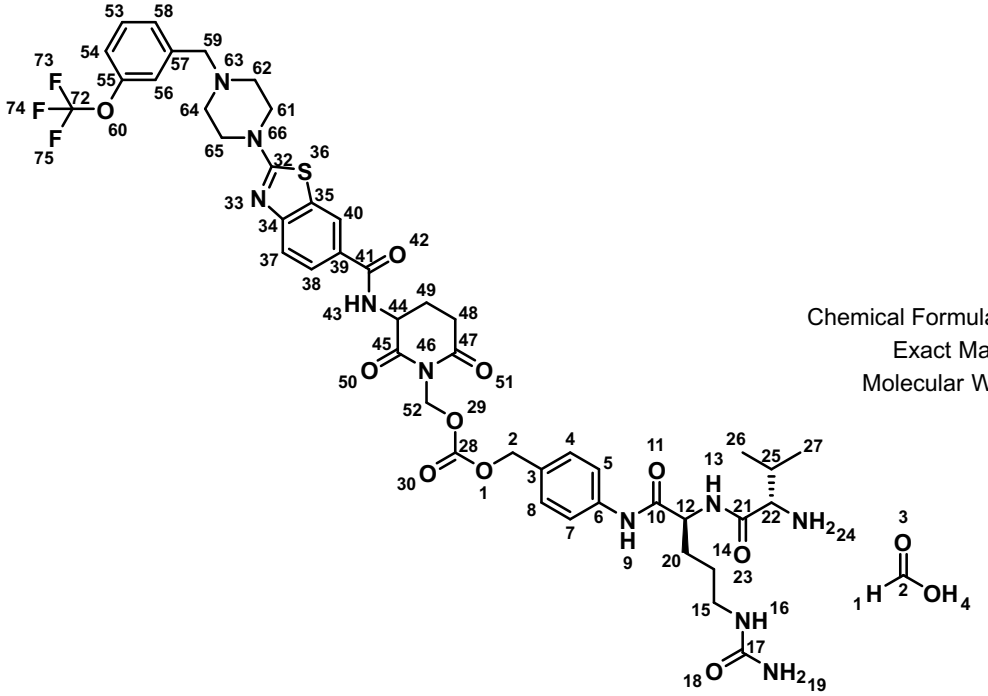
^{13}C NMR (151 MHz, DMSO) δ 171.94 ($C_{39,41}$), 171.50 (C_{10}), 170.23 (C_{26}), 166.25 (C_{35}), 155.57 (C_{33}), 153.57 (C_{22}), 148.96 (C_{49}), 141.40 (C_{51}), 139.64 (C_6), 130.84 ($C_{28\text{ or }29}$), 130.68 ($C_{31\text{ or }47}$), 130.34 (C_3), 129.68 ($C_{5,7}$), 128.29 ($C_{48\text{ or }50\text{ or }52}$), 126.95 ($C_{28\text{ or }29}$), 126.15 ($C_{32}$), 121.39 ($C_{48\text{ or }50\text{ or }52}$), 121.33 ($C_{34}$), 120.01 ($C_{48\text{ or }50\text{ or }52}$), 119.55 ($C_{4,8}$), 118.17 ($C_{31\text{ or }47}$), 69.54 ($C_2$), 66.17 ($C_{46}$), 61.25 ($C_{53}$), 58.73 ($C_{16}$), 52.16 ($C_{55,59}$), 50.47 ($C_{38}$), 49.49 ($C_{12}$), 48.49 ($C_{56,58}$), 31.56 ($C_{42}$), 31.05 ($C_{19}$), 23.40 ($C_{43}$), 19.31 ($C_{20\text{ or }21}$), 18.72 ($C_{14}$), 17.85 ($C_{20\text{ or }21}$).

^{19}F NMR (376 MHz, DMSO) δ -56.63.

HRMS (ESI): m/z $[M + H]^+$ calcd. for $C_{42}H_{47}F_3N_8O_9S$: 897.3212 Found: 897.3201

IR (vmax/cm^{-1}) 3417 (amine N-H), 1749 (carbonate C=O), 1698 (amide C=O), 1256 (C-F)

4-((*S*)-2-((*S*)-2-Amino-3-methylbutanamido)-5-ureidopentanamido)benzyl (((*RS*)-2,6-dioxo-3-(2-(4-(3-(trifluoromethoxy)benzyl)piperazin-1-yl)benzo[*d*]thiazole-6-carboxamido)piperidin-1-yl)methyl) carbonate formate (14b)



Chemical Formula: $C_{46}H_{55}F_3N_{10}O_{12}S$
Exact Mass: 1028.37
Molecular Weight: 1029.06

To a solution of **13b** (37 mg, 0.035 mmol) in MeOH (3 mL) was added $PhSiH_3$ (11 mg, 0.10 mmol). The reaction mixture was degassed with a nitrogen balloon for 10 minutes. $Pd(PPh_3)_4$ (8 mg, 0.007 mmol) was added. The reaction mixture was further degassed with a nitrogen balloon for 10 minutes. After the reaction was stirred under nitrogen at room temperature for 2 hours, the mixture was filtered through celite and the filtrate was collected and concentrated *in vacuo*. The residue was dissolved in DMSO (1 mL) and purified with C18 reverse phase column chromatography (0-100% $MeCN/H_2O$ gradient with 0.1% formic acid modifier) to afford the formate salt of the titled product as a white solid (16 mg, 47%).

^{1}H NMR (400 MHz, DMSO) δ 10.23 (s, 1H, N-H), 8.83 (d, *J* = 8.2 Hz, 1H, N-H),), 8.39 (d, *J* = 7.7 Hz, 1H, N_{43}-H), 8.29 (d, *J* = 1.9 Hz, 1H, C_{40}-H), 8.27 (s, 1H, N_{19}-H), 7.82 (dd, *J* = 8.5, 1.9 Hz, 1H, C_{38}-H), 7.61 (d, *J* = 8.1 Hz, 2H, $C_{4,8}$-H), 7.48 (dd, *J* = 8.1, 2.0 Hz, 2H, $C_{53,57}$-H), 7.42 – 7.26 (m, 5H, $C_{5,7,54,56,58}$-H), 6.06 (s, 1H, N-H), 5.78 – 5.58 (m, 2H, C_{52}-H), 5.45 (s, 2H, C_{52}-H), 5.09 (s, 2H, C_2-H), 4.96 (dt, *J* = 13.2, 7.1 Hz, 1H, C_{44}-H), 4.50 – 4.45 (m, 1H, C_{12}-H), 3.63 (d, *J* = 7.3 Hz, 5H, $C_{59,62,64}$-H), 3.26 (d, *J* = 5.2 Hz, 1H, C_{22}-H), 2.98 (dh, *J* = 27.2, 7.0 Hz, 3H, $C_{15,48}$-H), 2.82 – 2.66 (m, 1H, C_{48}-H), 2.54 (d, *J* = 1.1 Hz, 9H, $C_{61,65}$-H), 2.24 – 2.12 (m, 1H, C_{49}-H), 1.97 (dt, *J* = 20.4, 10.1 Hz, 2H, $C_{25,49}$-H), 1.78 – 1.51 (m, 2H, C_{20}-H), 1.50 – 1.28 (m, 3H, C_{14}-H), 0.87 (dd, *J* = 25.2, 6.9 Hz, 6H, $C_{26,27}$-H).

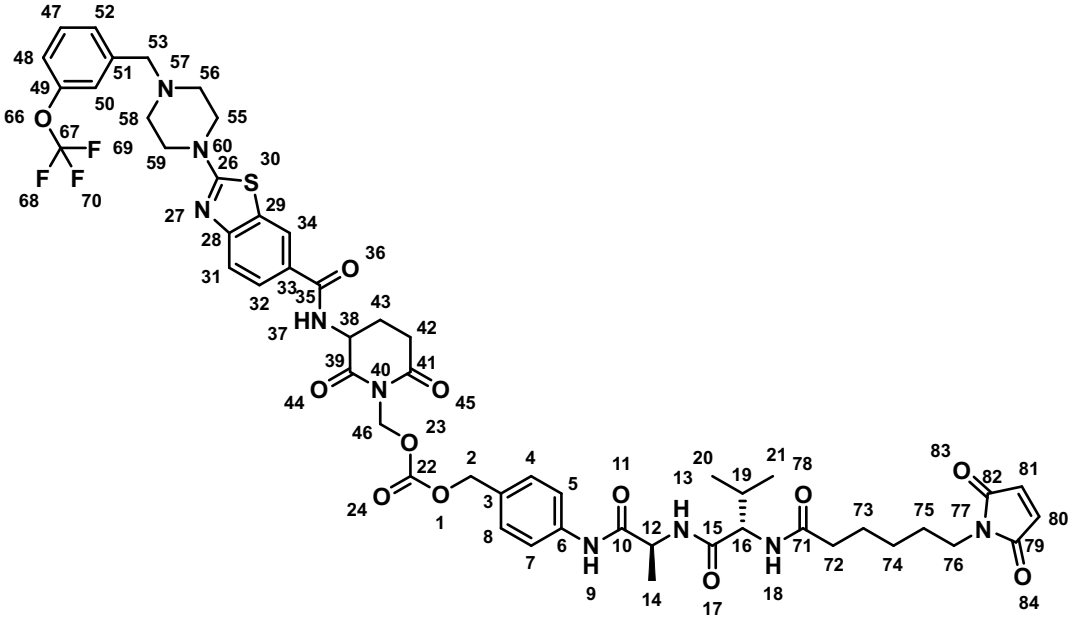
^{13}C NMR (151 MHz, DMSO) δ 172.42 (C_{21}), 171.94 ($C_{45,47}$), 171.09 (C_{10}), 170.23 (C_{17}), 166.24 (C_{41}), 155.90 (C_{39}), 153.57 (C_{28}), 148.96 (C_{55}), 141.41 (C_{57}), 139.58 (C_{6}), 130.84 ($C_{34\ or\ 35}$), 130.69 ($C_{37\ or\ 53}$), 130.36 (C_{3}), 129.69 ($C_{5,7}$), 128.30 ($C_{54\ or\ 56\ or\ 58}$), 126.95 ($C_{34\ or\ 35}$), 126.15 (C_{38}), 121.39 ($C_{54\ or\ 56\ or\ 58}$), 121.33 (C_{40}), 120.02 ($C_{54\ or\ 56\ or\ 58}$), 119.53 ($C_{4,8}$), 118.17 ($C_{37\ or\ 53}$), 69.55 (C_{2}), 66.17 (C_{52}), 61.25 (C_{59}), 59.15 (C_{22}), 53.26 (C_{12}), 52.17 ($C_{61,65}$), 50.47 (C_{44}), 48.49 ($C_{62,64}$), 31.55 (C_{48}), 31.27 (C_{25}), 30.17 (C_{20}), 28.63 (C_{15}), 27.17 (C_{14}), 23.40 (C_{49}), 19.53 ($C_{26\ or\ 27}$), 17.73 ($C_{26\ or\ 27}$).

^{19}F NMR (377 MHz, DMSO) δ -56.62.

HRMS (ESI): m/z $[M + Na]^+$ calcd. for $C_{45}H_{53}F_3N_{10}O_{10}SNa$: 1005.3511 Found: 1005.3520

IR (vmax/cm^{-1}) 3227 (amine N-H), 1751 (carbonate C=O), 1698 (amide C=O), 1256 (C-F)

4-((*S*)-2-((*S*)-2-(6-(2,5-Dioxo-2,5-dihydro-1H-pyrrol-1-yl)hexanamido)-3-methylbutanamido)propanamido)benzyl (((*RS*)-2,6-dioxo-3-(2-(4-(3-(trifluoromethoxy)benzyl)piperazin-1-yl)benzo[*d*]thiazole-6-carboxamido)piperidin-1-yl)methyl) carbonate (OX05157)



Chemical Formula: $C_{52}H_{58}F_3N_9O_{12}S$
Exact Mass: 1089.3878
Molecular Weight: 1090.1422

To **14a** (37 mg, 0.04 mmol) in DMF (1 mL) was added 2,5-dioxopyrrolidin-1-yl 6-(2,5-dioxo-2,5-dihydro-1H-pyrrol-1-yl)hexanoate (19 mg, 0.06 mmol) and DIPEA (26 mg,

0.2 mmol). The reaction was left stirred under nitrogen at room temperature for 18 hours. The reaction was then purified directly with C18 reverse phase column chromatography (0-100% MeCN/H_2O gradient with 0.1% formic acid modifier) to afford the titled product as a white solid. (14 mg, 33%)

^{1}H NMR (400 MHz, DMSO) δ 9.98 (s, 1H), 8.82 (d, *J* = 8.3 Hz, 1H, N_9-H), 8.29 (d, *J* = 1.8 Hz, 1H, C_{34}-H), 8.16 (d, *J* = 6.9 Hz, 1H, N_{13}-H), 7.84 – 7.79 (m, 2H, C_{32}-H, N_{18}-H), 7.60 (d, *J* = 8.5 Hz, 2H, $C_{4,8}$-H), 7.49 (dd, *J* = 8.4, 6.7 Hz, 2H, $C_{31,47}$-H), 7.43 – 7.22 (m, 5H, $C_{5,7,48,50,52}$-H), 6.99 (s, 2H, $C_{80,81}$-H), 5.70 (q, *J* = 9.3 Hz, 2H, C_{46}-H), 5.08 (s, 2H, C_2-H), 5.01 – 4.90 (m, 1H, C_{38}-H), 4.43 – 4.33 (m, 1H, C_{12}-H), 4.21 – 4.12 (m, 1H, C_{16}-H), 3.67 – 3.59 (m, 6H, $C_{53,56,58}$-H), 3.36 (t, *J* = 7.1 Hz, 2H, C_{76}-H), 3.06 – 2.85 (m, 1H, C_{42}-H), 2.83 – 2.67 (m, 1H, C_{42}-H), 2.54 (t, *J* = 5.0 Hz, 4H, $C_{55,59}$-H), 2.26 – 2.05 (m, 3H, $C_{43,72}$-H), 2.03 – 1.90 (m, 2H, $C_{19,43}$-H), 1.48 (q, *J* = 7.5 Hz, 4H, $C_{73,75}$-H), 1.30 (d, *J* = 7.0 Hz, 3H, C_{14}-H), 1.19 (dt, *J* = 15.2, 7.8 Hz, 2H, C_{74}-H), 0.84 (dd, *J* = 15.7, 6.7 Hz, 6H, $C_{20,21}$-H).

^{13}C NMR (151 MHz, DMSO) δ 172.73 (C_{71}), 171.94 ($C_{39,41}$), 171.68 (C_{10}), 171.52 (C_{15}), 171.50 ($C_{79,82}$), 170.23 (C_{26}), 166.24 (C_{35}), 155.56 (C_{33}), 153.56 (C_{22}), 148.96 (C_{49}), 141.41 (C_{51}), 139.72 (C_6), 134.91($C_{80,81}$), 130.84 ($C_{28\text{ or }29}$), 130.69 ($C_{31\text{ or }47}$), 130.20 (C_3), 129.67 ($C_{5,7}$), 128.30($C_{48\text{ or }50\text{ or }52}$), 126.95 ($C_{28\text{ or }29}$), 126.14 ($C_{32}$), 121.39 ($C_{48\text{ or }50\text{ or }52}$), 121.33 ($C_{34}$), 120.02 ($C_{48\text{ or }50\text{ or }52}$), 119.42 ($C_{4,8}$), 118.17 ($C_{31\text{ or }47}$), 69.56 ($C_2$), 66.16 ($C_{46}$), 61.25 ($C_{53}$), 57.95 ($C_{16}$), 52.17 ($C_{55,59}$), 50.46 ($C_{38}$), 49.52 ($C_{12}$), 48.49 ($C_{56,58}$), 37.47 ($C_{76}$), 35.36 ($C_{72}$), 31.56 ($C_{42}$), 30.86 ($C_{19}$), 28.23 ($C_{73\text{ or }75}$), 26.25 ($C_{74}$), 25.36 ($C_{73\text{ or }75}$), 23.40 ($C_{43}$), 19.67 ($C_{20\text{ or }21}$), 18.65 ($C_{20\text{ or }21}$), 18.36 ($C_{14}$).

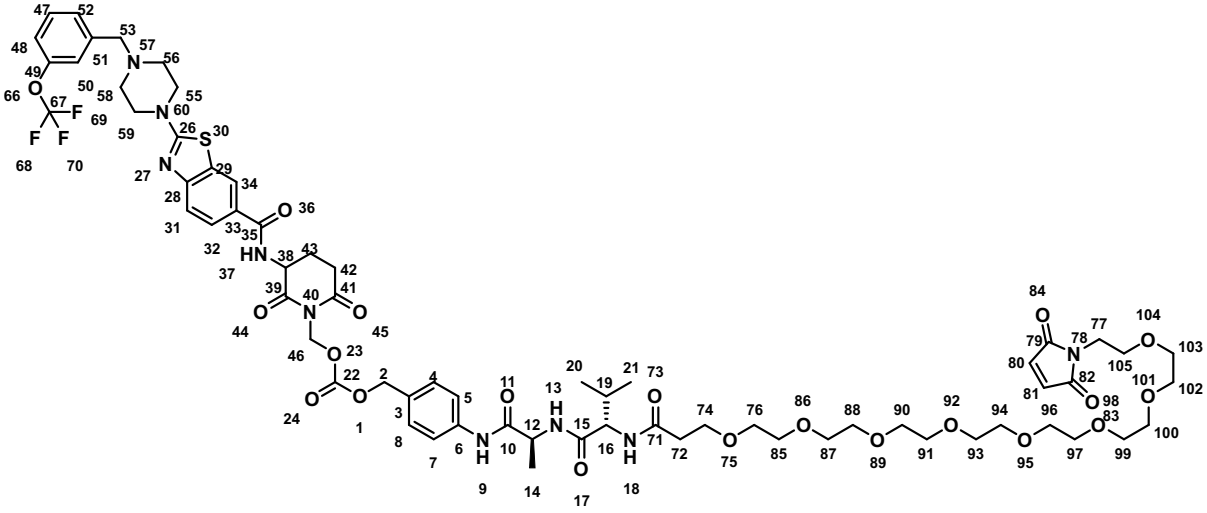
^{19}F NMR (376 MHz, DMSO) δ -56.62.

IR (vmax/cm^{-1}) 1662 (carbonate C=O)

HRMS (ESI): m/z $[M + Na]^+$ calcd. for $C_{52}H_{58}F_3N_9O_{12}SNa$: 1112.3770 Found: 1112.3813

IR (vmax/cm^{-1}) 1662 (carbonate C=O), 1256 (C-F)

4-((29*S*,32*S*)-1-(2,5-Dioxo-2,5-dihydro-1H-pyrrol-1-yl)-29-isopropyl-32-methyl-27,30-dioxo-3,6,9,12,15,18,21,24-octaoxa-28,31-diazatritriacontan-33-amido)benzyl (((*RS*)-2,6-dioxo-3-(2-(4-(3-(trifluoromethoxy)benzyl)piperazin-1-yl)benzo[*d*]thiazole-6-carboxamido)piperidin-1-yl)methyl) carbonate (OX05158)



Chemical Formula: $C_{65}H_{84}F_3N_9O_{20}S$
Exact Mass: 1399.5505
Molecular Weight: 1400.4852

To **14a** (35 mg, 0.037 mmol) in DMF (1 mL) was added Mal-PEG8-NHS ester (34 mg, 0.056 mmol) and DIPEA (24 mg, 0.19 mmol). The reaction was left stirred under nitrogen at room temperature for 18 hours. The reaction was then purified directly with C18 reverse phase column chromatography (0-100% MeCN/H_2O gradient with 0.1% formic acid modifier) to afford the title product as a white solid. (20 mg, 34%).

^{1}H NMR (600 MHz, DMSO) δ 9.97 (s, 1H, N_9-H), 8.82 (d, *J* = 8.3 Hz, 1H, N_{37}-H), 8.30 (d, *J* = 1.8 Hz, 1H, C_{34}-H), 8.19 (d, *J* = 6.5 Hz, 1H, N_{13}-H), 7.88 (d, *J* = 8.7 Hz, 1H, N_{18}-H), 7.82 (dd, *J* = 8.5, 1.9 Hz, 1H, C_{32}-H), 7.65 – 7.58 (m, 2H, $C_{4,8}$-H), 7.52 – 7.47 (m, 2H, $C_{31,47}$-H), 7.42 – 7.25 (m, 5H, $C_{5,7,48,50,52}$-H), 7.02 (s, 1H, $C_{80,81}$-H), 5.76 – 5.64 (m, 2H, C_{46}-H), 5.09 (s, 2H, C_2-H), 4.96 (ddd, *J* = 13.2, 8.2, 5.4 Hz, 1H, C_{38}-H), 4.39 (td, *J* = 15.3, 8.3 Hz, 1H, C_{12}-H), 4.21 (dd, *J* = 8.7, 6.7 Hz, 1H, C_{16}-H), 3.66 – 3.60 (m, 6H, $C_{53,56,58}$-H), 3.53 – 3.44 (m, 38H, PEG8 chain), 2.99 (ddd, *J* = 18.0, 13.2, 5.5 Hz, 1H, C_{42}-H), 2.78 (dt, *J* = 17.4, 3.7 Hz, 1H, C_{42}-H), 2.54 (t, *J* = 5.2 Hz, 4H, $C_{55,59}$-H), 2.18 (dt, *J* = 12.8, 6.4 Hz, 1H, C_{43}-H), 2.04 – 1.92 (m, 2H, $C_{19,43}$-H), 1.31 (d, *J* = 7.1 Hz, 3H, C_{14}-H), 0.91 – 0.79 (m, 6H, $C_{20,21}$-H).

^{13}C NMR (151 MHz, DMSO) δ 171.93 ($C_{39,41}$), 171.66 (C_{10}), 171.37 (C_{71}), 171.35 ($C_{79,82}$), 170.23 (C_{26}), 166.23 (C_{35}), 155.57 (C_{33}), 153.57 (C_{22}), 148.96 (C_{49}), 141.41 (C_{51}), 139.72 (C_6), 135.02 ($C_{80,81}$), 130.84 ($C_{28\text{ or }29}$), 130.69 ($C_{31\text{ or }47}$), 130.21 (C_3), 129.68 ($C_{5,7}$), 128.30 ($C_{48\text{ or }50\text{ or }52}$), 126.95 ($C_{28\text{ or }29}$), 126.14 ($C_{32}$), 121.39 ($C_{48\text{ or }50\text{ or }52}$), 121.33 ($C_{34}$), 120.02 ($C_{48\text{ or }50\text{ or }52}$), 119.73 ($C_{4,8}$), 118.17 ($C_{31\text{ or }47}$), 70.24 ($C_{PEG8}$), 69.56 ($C_2$), 67.39 ($C_{PEG8}$), 66.15 ($C_{46}$), 61.25 ($C_{53}$), 57.89 ($C_{16}$), 52.17 ($C_{55,59}$), 50.46 ($C_{38}$), 49.52 ($C_{12}$),

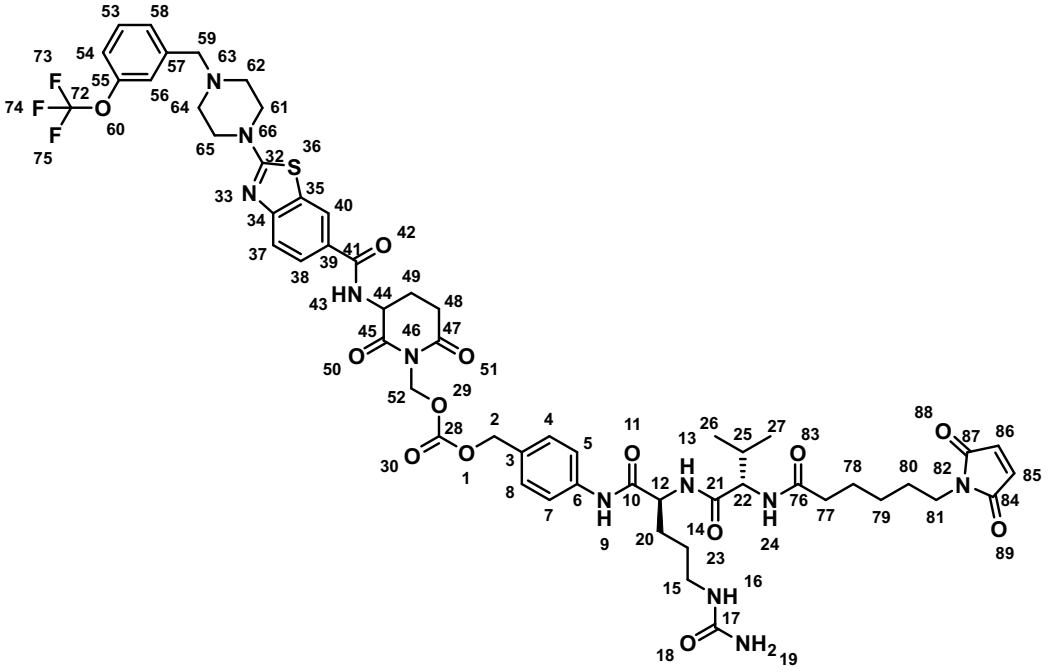
48.49 ($C_{56,58}$), 31.56 (C_{42}), 31.06 (C_{19}), 23.41 (C_{43}), 19.61 ($C_{20\text{ or }21}$), 18.58 ($C_{20\text{ or }21}$), 18.34 (C_{14}).

^{19}F NMR (377 MHz, DMSO) δ -56.62.

HRMS (ESI): m/z $[M + H]^+$ calcd. for $C_{65}H_{85}F_3N_9O_{20}S$: 1400.5578 Found: 1400.5588

IR (vmax/cm^{-1}) 1655 (carbonate C=O)

4-((*S*)-2-((*S*)-2-(6-(2,5-Dioxo-2,5-dihydro-1H-pyrrol-1-yl)hexanamido)-3-methylbutanamido)-5-ureidopentanamido)benzyl (((*RS*)-2,6-dioxo-3-(2-(4-(3-(trifluoromethoxy)benzyl)piperazin-1-yl)benzo[*d*]thiazole-6-carboxamido)piperidin-1-yl)methyl) carbonate (OX05159)



Chemical Formula: $C_{55}H_{64}F_3N_{11}O_{13}S$
Exact Mass: 1175.4358
Molecular Weight: 1176.2362

To **14b** (15 mg, 0.015 mmol) in DMF (1 mL) was added 2,5-dioxopyrrolidin-1-yl 6-(2,5-dioxo-2,5-dihydro-1H-pyrrol-1-yl)hexanoate (7 mg, 0.02 mmol) and DIPEA (10 mg, 0.076 mmol). The reaction was left stirred under nitrogen at room temperature for 18 hours. The reaction was then purified directly with C18 reverse phase column chromatography (0-100% MeCN/H_2O gradient with 0.1% formic acid modifier) to afford the title product as a white solid. (6 mg, 36%).

^{1}H NMR (400 MHz, DMSO) δ 10.04 (s, 1H, N_9-H), 8.82 (d, J = 8.3 Hz, 1H, N_{43}-H), 8.29 (s, 1H, C_{40}-H), 8.09 (d, J = 7.4 Hz, 1H, N_{13}-H), 7.85 – 7.77 (m, 2H, C_{38}-H, N_{24}-H),

7.61 (d, J = 8.2 Hz, 2H, $C_{4,8}$-H), 7.53 – 7.45 (m, 2H, $C_{37,53}$-H), 7.42 – 7.24 (m, 5H, $C_{5,7,54,56,58}$-H), 6.99 (s, 2H, $C_{85,86}$-H), 6.00 – 5.96 (m, 1H, N_{16}-H), 5.70 (q, J = 9.3 Hz, 2H, C_{52}-H), 5.40 (s, 2H, N_{19}-H), 5.08 (s, 2H, C_2-H), 5.01 – 4.90 (m, 1H, C_{44}-H), 4.40 – 4.34 (m, 1H, C_{12}-H), 4.19 (t, J = 7.7 Hz, 1H, C_{22}-H), 3.66 – 3.60 (m, 6H, $C_{59,62,64}$-H), 3.36 (t, J = 7.0 Hz, 2H, C_{81}-H), 3.05 – 2.90 (m, 3H, $C_{15,48}$-H), 2.82 – 2.71 (m, 1H, C_{48}-H), 2.56 – 2.50 (m, 4H, $C_{61,65}$-H), 2.22 – 2.05 (m, 3H, $C_{49,77}$-H), 2.03 – 1.91 (m, 2H, $C_{25,49}$-H), 1.71 – 1.66 (m, 1H, C_{20}-H), 1.62 – 1.55 (m, 1H, C_{20}-H), 1.53 – 1.31 (m, 6H, $C_{14,78,80}$-H), 1.26 – 1.14 (m, 2H, C_{79}-H), 0.83 (dd, J = 12.8, 6.7 Hz, 6H, $C_{26,27}$-H).

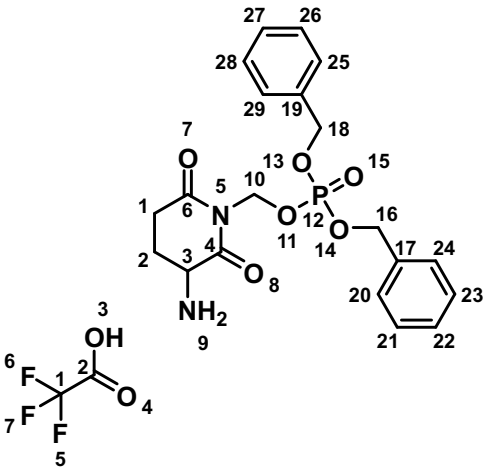
^{13}C NMR (151 MHz, DMSO) δ 172.72 (C_{76}), 171.94 ($C_{45,47}$), 171.76 (C_{21}), 171.53 ($C_{84,87}$), 171.16 (C_{10}), 166.24 (C_{41}), 159.34 (C_{17}), 155.57 (C_{32}), 153.57 (C_{28}), 148.97 (C_{55}), 141.41 (C_{57}), 139.66 (C_6), 134.91 ($C_{85,86}$), 130.84 (C_{39}), 130.69 ($C_{37\text{ or }53}$), 130.23 (C_3), 129.67 ($C_{5,7}$), 128.30 ($C_{54\text{ or }56\text{ or }58}$), 126.95 ($C_{34,35}$), 126.14 ($C_{38}$), 121.39 ($C_{54\text{ or }56\text{ or }58}$), 121.33 ($C_{40}$), 120.02 ($C_{54\text{ or }56\text{ or }58}$), 119.43 ($C_{4,8}$), 118.17 ($C_{37\text{ or }53}$), 69.56 ($C_2$), 66.16 ($C_{52}$), 61.25 ($C_{59}$), 58.01 ($C_{22}$), 53.59 ($C_{12}$), 52.17 ($C_{61,65}$), 50.46 ($C_{44}$), 48.49 ($C_{62,64}$), 39.01 ($C_{15}$), 37.47 ($C_{81}$), 35.40 ($C_{77}$), 31.56 ($C_{48}$), 30.85 ($C_{25}$), 29.72 ($C_{20}$), 28.23 ($C_{14\text{ or }78\text{ or }80}$), 27.27 ($C_{14\text{ or }78\text{ or }80}$), 26.25 ($C_{79}$), 25.38 ($C_{14\text{ or }78\text{ or }80}$), 23.41 ($C_{49}$), 19.71 ($C_{26\text{ or }27}$), 18.66 ($C_{26\text{ or }27}$).

^{19}F NMR (377 MHz, DMSO) δ -56.62.

HRMS (ESI): m/z $[M + H]^+$ calcd. for $C_{55}H_{64}F_3N_{11}O_{13}S$: 1176.4431 Found: 1176.4426

IR (vmax/cm^{-1}) 1669 (carbonate C=O, 1393 (C-F)

(3-Amino-2,6-dioxopiperidin-1-yl)methyl dibenzyl phosphate 2,2,2-trifluoroacetate (15)



Chemical Formula: $C_{22}H_{24}F_3N_2O_8P$
Exact Mass: 532.12
Molecular Weight: 532.41

To a solution of **8b** (730 mg, 1.41 mmol, 1 eq.) in CH_2Cl_2 (1 mL), TFA (0.54 mL, 5 eq.) was added dropwise at room temperature. The reaction was stirred for 19 hours. The

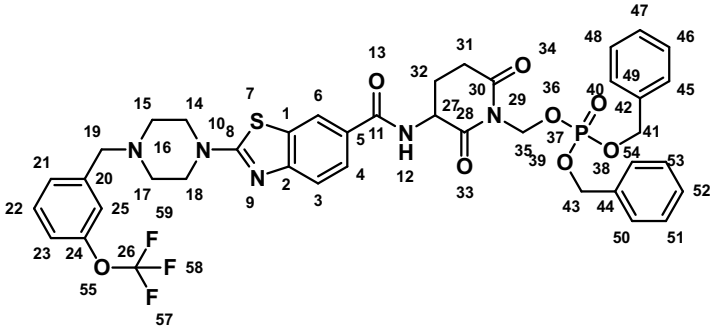
reaction mixture was concentrated *in vacuo* to afford the titled product as a purple oil (0.61 g, 99%). The crude product was carried to the next step without further purification.

^{1}H NMR (400 MHz, MeOD) δ 7.46 – 7.28 (m, 10H, $C_{20,21,22,23,24,25,26,27,28,29}$-H), 5.80 – 5.59 (m, 2H, C_{10}-H), 5.06 (dd, *J* = 8.5, 1.8 Hz, 4H, $C_{16,18}$-H), 4.39 – 4.27 (m, 1H, C_3-H), 2.99 – 2.77 (m, 2H, C_2-H), 2.40 – 2.23 (m, 1H, C_1-H), 2.15 – 1.99 (m, 1H, C_1-H).

^{31}P NMR (162 MHz, MeOD) δ -3.76.

IR (vmax/cm^{-1}) 2519 (N-H), 1703 (C=O), 1454 (C=C), 1206 (P=O), 1000 (P-O)

Dibenzyl ((2,6-dioxo-3-(2-(4-(3-(trifluoromethoxy)benzyl)piperazin-1-yl)benzo[*d*]thiazole-6-carboxamido)piperidin-1-yl)methyl) phosphate (16)



Chemical Formula: $C_{40}H_{39}F_3N_5O_8PS$
Exact Mass: 837.2209
Molecular Weight: 837.8080

To a solution of **5** (100 mg, 0.229 mmol, 1 eq.) in anhydrous DMF (1 mL), HATU (113 mg, 0.297 mmol) and DIPEA (0.20 mL, 1.2 mmol) was added. The solution was stirred for 30 minutes at room temperature. The activated **5** solution was added to **9** (56.6 mg, 0.344 mmol, 1.5 eq.) in DIPEA (0.20 mL, 1.2 mmol) and anhydrous DMF (1 mL). The reaction was stirred for 20 hours at room temperature. The reaction mixture was directly purified with C18 reverse phase column chromatography (0-100% MeCN/H_2O gradient with 0.1% formic acid modifier) to afford the titled product as a yellow oil (88 mg, 57%).

^{1}H NMR (400 MHz, DMSO) δ 8.85 (d, *J* = 8.2 Hz, 1H, C_{12}-H), 8.29 (d, *J* = 1.7 Hz, 1H, C_6-H), 7.83 (dd, *J* = 8.5, 1.8 Hz, 1H, C_4-H), 7.49 (dt, *J* = 8.0, 3.7 Hz, 2H, $C_{3,22}$-H), 7.42 – 7.31 (m, 12H, $C_{45\text{-}54,21,25}$-H), 7.27 (d, *J* = 8.2 Hz, 1H, C_{23}-H), 5.67 – 5.50 (m, 2H, C_{35}-H), 5.04 (d, *J* = 7.6 Hz, 4H, $C_{41,43}$-H), 4.94 (ddd, *J* = 13.0, 8.2, 5.2 Hz, 1H, C_{27}-H), 3.67 – 3.60 (m, 6H, $C_{15,17,19}$-H), 2.97 (ddd, *J* = 18.2, 13.2, 5.5 Hz, 1H, C_{31}-H), 2.77 (dt, *J* = 17.5, 3.8 Hz, 1H, C_{31}-H), 2.54 (t, *J* = 5.0 Hz, 4H, $C_{14,18}$-H), 2.19 (qd, *J* = 13.0, 4.5 Hz, 1H, C_{32}-H), 2.05 – 1.96 (m, 1H, C_{32}-H).

^{13}C NMR (101 MHz, DMSO) δ 171.80 (C_{11}),170.23 (C_8), 166.30 ($C_{28,30}$),155.58 (C_5), 148.96 (C_{24}), 141.38 (C_{20}), 130.85 ($C_{1\text{ or }2}$), 130.69 ($C_{3\text{ or }22}$), 128.94 ($C_{42,44}$), 128.87 ($C_{49,45,50,54\text{ or }46,47,48,51,52,53}$), 128.36($C_{21}$), 128.30 ($C_{49,45,50,54\text{ or }46,47,48,51,52,53}$), 126.98 ($C_{1\text{ or }2}$), 126.17 ($C_4$), 121.40 ($C_{25}$), 121.33 ($C_6$), 120.02 ($C_{23}$), 118.17 ($C_{3\text{ or }22}$), 69.21 ($C_{41\text{ or }43}$),

69.16 ($C_{41\text{ or }43}$), 65.78 (C_{35}), 61.25 (C_{19}), 52.17 ($C_{14,18}$), 50.57 (C_{27}), 48.49 ($C_{15,17}$), 31.61 (C_{32}), 23.33 (C_{31}).

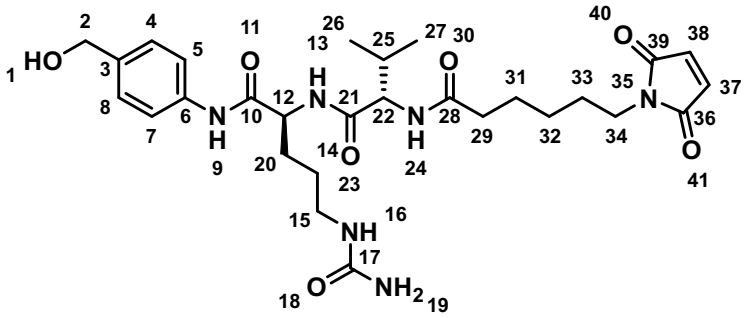
^{19}F NMR (377 MHz, DMSO) δ -56.63.

^{31}P NMR (162 MHz, DMSO) δ -3.24.

HRMS (ESI): m/z $[M + H]^+$ calcd. for $C_{40}H_{40}F_3N_5O_8PS$: 838.2282 Found: 828.2301

IR (vmax/cm^{-1}) 3272 (aromatic C-H), 1702 (C=O), 1632 (C=C), 1254 (P=O)

6-(2,5-Dioxo-2,5-dihydro-1*H*-pyrrol-1-yl)-*N*-((*S*)-1-(((*S*)-1-((4-(hydroxymethyl)phenyl)amino)-1-oxo-5-ureidopentan-2-yl)amino)-3-methyl-1-oxobutan-2-yl)hexanamide (17)



Chemical Formula: $C_{28}H_{40}N_6O_7$
Exact Mass: 572.2958
Molecular Weight: 572.6630

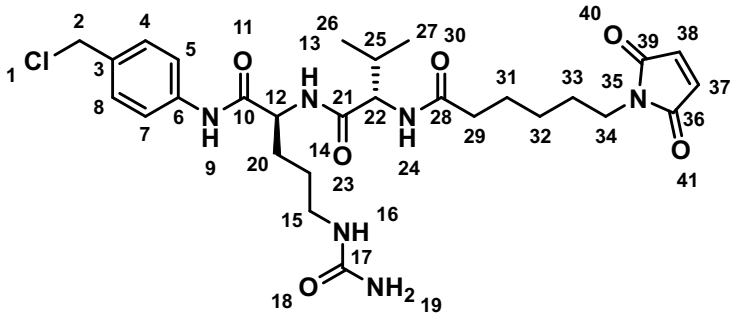
To a solution of Val-Cit-PAB-OH (200 mg, 0.527 mmol, 1 eq.) in NMP (20 mL), 2,5-dioxopyrrolidin-1-yl 6-(2,5-dioxo-2,5-dihydro-1*H*-pyrrol-1-yl)hexanoate (178 mg, 0.579 mmol, 1.1 eq.) was added. The reaction was stirred at room temperature for 18 hours. The product was precipitated out by the addition of diethyl ether. A yellow solid was collected by filtration (27 mg, 83%). The ^{1}H NMR and ^{13}C spectra were consistent with the literature.[101]

^{1}H NMR (400 MHz, DMSO) δ 9.90 (s, 1H, O_1-H), 8.06 (d, J = 7.5 Hz, 1H, N_{13}-H), 7.82 (d, J = 8.6 Hz, 1H, N_{24}-H), 7.58 – 7.51 (d, *J* = 8.2 Hz, 2H, $C_{5,7}$-H), 7.23 (d, J = 8.2 Hz, 2H, $C_{4,8}$-H), 7.00 (s, 2H, $C_{37,38}$-H), 4.43 (s, 2H, C_2-H), 4.43 – 4.34 (m, 1H, C_{12}-H), 4.18 (dd, J = 8.6, 6.7 Hz, 1H, C_{22}-H), 3.36 (d, J = 14.1 Hz, 1H, C_{34}-H), 2.98 (d, *J* = 22.8 Hz, C_{15}-H), 2.25 – 2.05 (m, 2H, C_{29}-H), 1.97 (h, J = 6.8 Hz, 1H, C_{25}-H), 1.75 – 1.54 (m, 2H, C_{20}-H), 1.53 – 1.31 (m, 5H, $C_{14,33,31}$-H), 1.18 (p, J = 7.5 Hz, 2H, C_{32}-H), 0.83 (dd, J = 12.3, 6.7 Hz, 6H, $C_{26,27}$-H).

^{13}C NMR (101 MHz, DMSO) δ 172.78 (C_{28}), 171.73 (C_{21}), 171.54 ($C_{36,39}$), 170.85 (C_3), 159.37 (C_{17}), 137.99 ($C_{6\text{ or }10}$), 137.87 ($C_{6\text{ or }10}$), 134.91 ($C_{37,38}$), 127.38 ($C_{4,8}$), 119.31 ($C_{5,7}$), 63.06 (C_2), 58.08 (C_{22}), 53.54 (C_{12}), 39.07 (C_{15}), 37.48 (C_{34}), 35.41 (C_{29}), 30.83 (C_{25}), 29.83 (C_{20}), 28.23 ($C_{14\text{ or }31\text{ or }33}$), 27.26 ($C_{14\text{ or }31\text{ or }33}$), 26.25 ($C_{32}$), 25.38 ($C_{14\text{ or }31\text{ or }33}$), 19.72 ($C_{26\text{ or }27}$), 18.66 ($C_{26\text{ or }27}$).

IR (vmax/cm^{-1}) 3272 (N-H), 2939 (aliphatic C-H), 1632 (C=O), 1537 (C-N)

***N*-((*S*)-1-(((*S*)-1-((4-(Chloromethyl)phenyl)amino)-1-oxo-5-ureidopentan-2-yl)amino)-3-methyl-1-oxobutan-2-yl)-6-(2,5-dioxo-2,5-dihydro-1*H*-pyrrol-1-yl)hexanamide (18)**



Chemical Formula: $C_{28}H_{39}ClN_6O_6$
Exact Mass: 590.2620
Molecular Weight: 591.1060

To a solution of **11** (315 mg, 0.55 mmol, 1 eq.) in anhydrous DMF (5 mL) was added dropwise a solution of thionyl chloride in DCM (1 mol/L, 0.61 mL, 0.61 mmol) at 0 °C. The reaction mixture was held at 0 °C for 30 min and then increased to room temperature. The reaction was monitored by LC-MS. Another 1.1 equivalence of thionyl chloride was added to push the reaction to completion. After successive stirring for 30 minutes, the mixture was concentrated under reduced pressure and purified by silica gel chromatography (DCM/MeOH = 5:1) to afford a yellow solid (0.182 g, 56%). The ^{1}H NMR spectrum was consistent with the literature.[102]

^{1}H NMR (400 MHz, DMSO) δ 10.04 (s, 1H), 8.09 (d, *J* = 7.6 Hz, 1H, N_{13}-H), 7.80 (d, *J* = 8.5 Hz, 1H, N_{24}-H), 7.60 (d, *J* = 8.4 Hz, 2H, $C_{5,7}$-H), 7.36 (d, *J* = 8.7 Hz, 2H $C_{4,8}$-H), 7.00 (s, 2H, $C_{37,38}$-H), 4.71 (s, 2H, C_2-H), 4.37 (dt, *J* = 15.2, 8.6 Hz, 1H, C_{12}-H), 4.19 (t, *J* = 7.7 Hz, 1H, C_{22}-H), 3.36 (t, *J* = 7.0 Hz, 2H, C_{34}-H), 3.05 – 2.91 (m, 2H, C_{15}-H), 2.15 (ddq, *J* = 21.3, 14.3, 7.4 Hz, 2H, C_{29}-H), 1.96 (dq, *J* = 14.0, 7.1 Hz, 1H, C_{25}-H), 1.75 – 1.47 (m, 6H, $C_{14,33,31}$-H), 1.19 (h, *J* = 7.1 Hz, 2H, C_{32}-H), 0.83 (dd, *J* = 12.7, 6.7 Hz, 6H, $C_{26,27}$-H).

Biological testing

Glutathione assay procedure

The reactivity of the payloads is tested by measuring the disappearance of parent compound and the formation of the GSH adduct over time. Compounds are incubated at 50 µM for **OX05156** and 10 µM concentration for **OX05157**, **OX05158**, **OX05159** at 37 °C. Each run contains one compound and 10 µM verapamil. DMSO concentration was kept below 0.1%.

Molecular masses were measured using a Waters Xevo G2-XS QTOF system (Waters, UK). Waters Acquity UPLC system was equipped with a Waters ACQUITY Premier CSH C18 Column 1.7 µm, 2.1 x 50 mm, 1/pk. 5 µL of sample was injected on the column using mobile phase A (water-0.1% formic acid) and B (acetonitrile-0.1% formic acid) with an eluting gradient (Table 1) at the flow rate of 0.3 mL/min. The oven temperature was maintained at 20 °C.

Time (min)	Solvent A (%)	Solvent B (%)
1.0	95.0	5.0
7.0	5.0	95.0
8.0	5.0	95.0
8.10	95.0	5.0
10.00	95.0	5.0

Table 1. LC-MS mobile phase A/B gradient elution.

Waters Xevo G2-XS QTOF mass spectrometer operated in a positive mode, coupled with ESI ion source. The data was analysed by Masslynx.

Materials and methods – Bioconjugation

Conjugation experiments were carried out in standard polypropylene Eppendorf safe-lock tubes (0.5 mL) at atmospheric pressure with mixing the temperature stated. Reagents and solvents were purchased from commercial sources and used as supplied. All buffer solutions were degassed prior to use, where the term ‘degassed’ refers to the process of removing oxygen from the solution by bubbling nitrogen through it. Phosphate-buffered saline (PBS) was by adding 4 mM EDTA to commercially available PBS (pluriSelect). Ultrafiltration was carried out in Amicon® Ultra-0.5 Centrifugal Filter Units with a molecular weight cut-off (MWCO) of 10 kDa. Centrifugation was carried out at 14G at 19 °C. Trastuzumab was purchased from Cambridge Bioscience Ltd.

Analysis of trastuzumab conjugate by LC-MS

Trastuzumab samples after the conjugation were diluted to 5 µM with PBS buffer with 4 mM EDTA (pH 7.4) and analysed by LC-MS. Molecular masses were measured using an ACQUITY I-Class PLUS UPLC System (Waters, Milford, MA, USA) coupled to an ACQUITY RDa mass spectrometer (Waters, Milford, MA, USA) equipped with an ESI probe, in positive ion mode. A ProSwift™ RP-2H Analytical column (4.6 x 50 mm SS; Thermo Fisher Scientific, Sunnyvale, CA, USA) at 40 °C, was used with mobile phase A: water + 0.1 % formic acid, and mobile phase B: acetonitrile + 0.1 % formic acid. The linear gradient used was: 0.00 min, 5.0 % B; 2.00 min, 5.0 % B; 7.0 min 95.0 % B; 7.50 min, 95.0 % B; 7.60 min, 5.0 % B; and 10.0 min, 5.0 % B. The flow rate was 0.300 mL / min and the total analysed time was 10.0 min. Scan parameters were set as follows: analyser mode, full scan; scan range, 400-7000 *m/z*; scan rate, 2 Hz; cone voltage, 30 V; capillary voltage, 1.5 kV; desolvation temperature, 550 °C; and *intelligent data capture*, on. The data was then analysed by deconvoluting the spectrum to a zero-charge mass spectrum using Bayesian deconvolution algorithm within the UniDec GUI software version 8.2.1.

Synthesis of trastuzumab-OX05158 conjugate

To trastuzumab (106.9 µL, 0.0023 µmol, 21.5 µM, 3.13 mg/mL) in PBS buffer with 4 mM EDTA (pH 7.4) was added TCEP-HCl (1.38 µL, 0.0138 µmol, 10 mM in H_2O, 6 eq.). After 2 hours at 37 °C, OX05158 (5.52 µL, 0.0552 µmol, 10 mM in DMSO, 24 eq.) was added in the conjugation and the resultant mixture was incubated for 1 hour at 22 °C. The excess reagents were then removed via ultrafiltration (10 KDa MWCO) into PBS buffer with 4 mM EDTA (pH 7.4). The concentration was determined to be 4.65 mg/mL by NanoDrop™.

Analysis of trastuzumab conjugate by MALDI-QTOF

Matrix Preparation

The matrix solution was prepared as follows: Sinapinic acid (SA, 10 mg) was dissolved in 1000 µL of a solvent mixture comprising (50% water**,** 50% acetonitrile**,** 0.3% trifluoroacetic acid (TFA))**.**

The resulting suspension underwent:

- Vortex mixing (≥1 minute)
- Sonication (15 minutes)

- Additional vortex mixing (1 minute)

Sample-Matrix Mixing and Spotting

1. The sample solution (3 µL) was mixed with an equal volume of SA matrix solution (3 µL).
2. The resulting mixture (1.5 µL) was spotted on a 384-spot ground steel target plate.
3. The Spotted matrix/analyte mixture was allowed to air-dry at ambient temperature.

Calibration

The samples were analysed using the MALDI Autoflex Speed system (Bruker Daltonics, Bremen, Germany), equipped with an Nd: YAG @ 355 nm laser with a variable repetition rate of up to 2 kHz. The instrument parameters were set: mass range: 30,000 to 200,000 Da, sample rate: 0.16 GS/s, laser shots: 1000, laser power: 73%, laser frequency: 200 Hz, and detector gain: 3kV. The spectra were obtained in linear mode positive ion mode, and no peaks were observed below 30kDa. The data obtained from the Bruker time-of-flight mass spectrometer was processed using the FlexAnalysis software.

Analysis of trastuzumab conjugate by Native Mass Spectrometry

Non-denaturing MS measurements were carried out on Waters Synapt HD MS Q-TOF mass spectrometer interfaced with a Triversa Nanomate (Advion) chip-based nESI source. Antibody solutions in ammonium acetate at uM concentration were pipetted in the wells on a Nanomate sample plate. Nanomate chip was operated at a spray voltage of 1.85 kV, backing gas pressure 0.75 psi. Synapt inlet pressure was 3.5 mbar. Sample and extractor cone voltages were adjusted to facilitate gas-phase ion desolvation (cone voltage 100-200 V, extractor voltage 10 V). Trap voltage was also elevated to 145 V to facilitate the desolvation, however, this could also lead to limited dissociation of the light chain from the intact reduced antibody. Data collection and analysis were carried out using Waters MassLynx software. Mass spectra were calibrated externally using CsI solution.